Study of the speciation of Tc and its homologous Mn and Re in concentrated carbonate solution under γ and He2+ irradiation

Mohammad Ghalei

Thèse de Doctorat

Mohammad Ghalei

Mémoire présenté en vue de l'obtention du
grade de Docteur de l'École des Mines de Nantes
sous le label de L'Université Nantes Angers Le Mans

École doctorale : 3MPL

Discipline : *211 – Milieux denses, Matériaux et Composants*
Spécialité : Radiochimie et Chimie sous Irradiation
Unité de recherche : *Laboratoire SUBATECH, UMR 6457*

Soutenue le *16 Novembre 2015*
Thèse N° : *2015EMNA0226*

Study of the speciation of Tc and its homologous Mn and Re in concentrated carbonate solutions under γ and He^{2+} irradiation

JURY

Rapporteurs : **Philippe MOISY**, Directeur de recherche, CEA Marcoule
James WISHART, Professeur, Brookhaven National Lab

Examinateurs : **Mehran MOSTAFAVI,** Professeur, Université Paris SUD XI
Abdelouas ABDESSELAM, Professeur, Ecole de Mines de Nantes
Pier-Lorenzo SOLARI, Docteur, Synchrotron SOLEIL
Ferid HADDAD, Enseignant Chercheur, Cyclotron ARRONAX

Directeur de Thèse : **Massoud FATTAHI**, Professeur, Université de Nantes

Encadrant Scientifique : **Johan VANDENBORRE**, CR1, CNRS

سخن ماند از ما همی یادگار

تو با گنج ، دانش برابر مدار

حکیم ابوالقاسم فردوسی

ACKNOWLEDGEMENTS

First of all I would like to thank the jury members: Professor Philippe Moisy, Professor James Wishart, Professor Mehran Mostafavi, Professor Abdesselam Abdelouas, Professor Ferid Haddad and Dr. Pier-Lorenzo Solari for their precious time reading my thesis. It was an honor to present my work in front of respected people in our community.

I would like to extend thanks to the many people, in many laboratories, who so generously contributed to the work presented in this thesis.

Special mention goes to my enthusiastic supervisor, Professor Massoud Fattahi. My PhD has been an amazing experience and I thank Massoud wholeheartedly, not only for his tremendous academic support, but also for giving me so many wonderful opportunities. I am very grateful for his motivation, enthusiasm, and immense knowledge in technetium chemistry that, taken together, make him a great mentor.

I would like to express my special appreciate on and thanks to my co-supervisor Dr. Johan Vandenborre, you have been a tremendous mentor for me. I would like to thank you for encouraging my research and for allowing me to grow as a research scientist. Your advice on both research as well as on my career have been invaluable. I cannot forget the valuable conversations and suggestions of Johan. I have often looked towards his for valuable suggestion, and he always helped me whenever I needed support in my research.

I would like to thank Guillaume Blain, for his help for using different apparatuses, ARRONAX cyclotron and γ irradiator. I will miss the great photography we have done together. I really appreciate his attitude and I consider him more than a colleague, as a good friend.

To all SUBATECH staffs, it was my pleasure to meet you, we had our happy moments. I simply would like to say THANK YOU especially Radiochimie group. During my PhD I really had a great time with you. It is really difficult to leave good colleagues like you. I will never forget you. I take the opportunity to thanks Professor Bernd Grambow the director of SUBATECH and Professor Gilles Montavon the director of Radiochimie group.

My sincere gratitude is reserved for Professor Mehran Mostafavi for his invaluable insights and suggestions. He gave me the possibility of carrying out electron pico-second pulse radiolysis and also γ radiolysis in his lab in Orsay. I learnt lots of things from Mehran during my PhD and even basics of irradiation chemistry before.

I would like to thank the LCP staffs that helped me for doing my experiments especially Jun Ma, Uli Schmidhammer, Anna Balcerzyk, Jean-Philippe Larbre, Pierre Jeunesse, Alexandre Demarque and Mireille Benoit. I express my special thanks also to the head group of TEMIC at LCP, Professor Hynd Remita.

I would also like to take this opportunity to thank ARROANX staffs. It was a great discovery in my scientific life. Very special thanks to the Ferid Haddad, the ARRONAX director and radio protection service Laurent PERRIGAUD, Caroline ROUSTAN and Guillaume Mechin.

I am grateful to Dr. Pier-Lorenzo Solari at Mars beamline in SOLEIL synchrotron. During and after my experiments he helped me a lot. His help, advice, patience and permanent availability were beyond limits. Also I take this opportunity to thank other staffs at Mars beamline in SOLEIL. I would like to thank radio protection service at SOLEIL.

I would like to thank Dr. Frederic Poineau at University Nevada Las Vegas for his collaboration and the helpful, interesting discussion that we had about technetium chemistry.

I would like to thank Dr. Jérôme Roque at IPN Orsay for his collaboration on DFT simulation for fitting EXAFS spectra.

Le technétium (Tc) est un radioélément avec un temps de demi-vie de 211000 ans qui présente un intérêt considérable dans des contextes divers tels que la médecine nucléaire, le retraitement et le stockage du combustible nucléaire. La compréhension de la chimie de cet élément de transition est essentielle pour optimiser l'extraction des produits de fission au cours du retraitement des combustibles nucléaires usés. Une seconde raison de l'importance du Tc consiste en sa très grande versatilité vis-à-vis de la migration en fonction de son état redox. En effet, certaines espèces du Tc sont considérées comme très mobiles d'où l'importance de la connaissance de sa chimie. Le technétium peut être produit par deux procédés : en premier lieu, au cours de la fission de ^{235}U durant laquelle sont produits des produits de fission dont le Tc à hauteur de 6 % et, en second lieu, une méthode qui passe par l'irradiation de ^{98}Mo avec un faisceau de neutrons. En tant que source de rayonnement, le ^{99}Tc est utilisé comme source d'irradiation β de faible énergie. En outre, il est utilisé comme une source de rayonnement ionisant dans des détecteurs pour chromatographie en phase gazeuse. En 1968, une activité catalytique du ^{99}Tc pour l'hydrogénation du benzène a été rapportée. Le ^{99}Tc a montré une activité catalytique entre le platine et le rhénium. Le rôle d'oxydation des complexes de Tc(VII) pour les composés organiques a été rapporté. En outre, l'ion pertechnetate a été utilisé comme agent inhibiteur de corrosion. Malgré toutes ces applications du technétium dans le domaine du cycle électronucléaire, il a été surtout utilisé à des fins médicales. En 1961, le ^{99}Tc a été utilisé d'abord dans la science médicale pour imagerie de la thyroïde. En développant des derniers complexes de ^{99}Tc, il a été utilisé pour l'imagerie d'autres organes tels que le cerveau, le foie, les os, les reins et le cœur. Des complexes de ^{99}Tc avec des dérivés d'acides aminés sont utilisés pour l'imagerie du rein et hépatobiliaire. Des complexes de ^{99}Tc avec des ligands de phosphonate sont largement utilisés comme agent de diagnostic pour l'imagerie d'une maladie métastatique dans les os et l'infection par le myocarde. Les complexes de Tc(III) et Tc(I) sont utilisés pour l'imagerie du cerveau. Les complexes de Tc(V) sont largement utilisés comme un remplacement de ^{201}Tl pour l'imagerie myocardique.

Concernant la contamination de l'environnement, le technétium doit être stabilisé par modification de ses états d'oxydation et de complexation. Une voie possible pour la maîtrise des états d'oxydo-réduction du Tc passe par les phénomènes de radiolyse. Il y a peu de données concernant sur les complexes carbonates du technétium dans la littérature Comme le technétium est un radioélément et nécessite une réglementation spécifique les expériences ont été menées dasn un premier temps sur des éléments considérés comme ses analogues. Le

manganèse, le technétium et le rhénium sont dans le même groupe dans le tableau périodique et ils montrent des propriétés chimiques proches donc Mn et Re peuvent être choisis comme analogues du Tc. L'objet de cette étude est donc l'utilisation de la radiolyse α et γ pour initier et contrôler les mécanismes d'oxydation et de réduction du Tc, ainsi que Mn et Re, en milieu carbonate concentré. Ainsi, cette étude privilégie l'utilisation d'une part du cyclotron ARRONAX fournissant un faisceau d`α à haute énergie (E_α = 67 MeV, TEL = 22,7 keV.μm^{-1}) et d'autre part l'utilisation d'une irradiateur γ (E_γ = 0.667 MeV, TEL = 0.23 keV.μm^{-1}), disponible sur le même site, afin de couvrir une large gamme de TEL pour ces expériences d'oxydo/réduction sous faisceau.

Toutes les réactions chimiques qui sont initiées avec les radiations ionisantes (photons de haute énergie et de particules chargées) sont classées comme étant de la chimie sous rayonnement. L'énergie ionisante est absorbée par le solvant et crée des espèces excitées et chargées. L'interaction des photons de haute énergie (rayons γ et des rayons X) est différente de celle des particules chargées (par exemple $^4He^{2+}$). L'eau est le plus solvant utilisé dans la chimie et la radiolyse de l'eau est d'un intérêt dans de nombreuses études comme les réacteurs nucléaires et de cycle du combustible nucléaire. L'interaction du faisceau ionisant avec l'eau déclenche beaucoup d'événements que l'on peut diviser en quatre parties: 1) l'étape physique, 2) l'étape physico-chimique, 3) l'étape de la chimie hétérogène et 4) l'étape de la chimie homogène. La Figure 1 montre ces étapes de la radiolyse de l'eau.

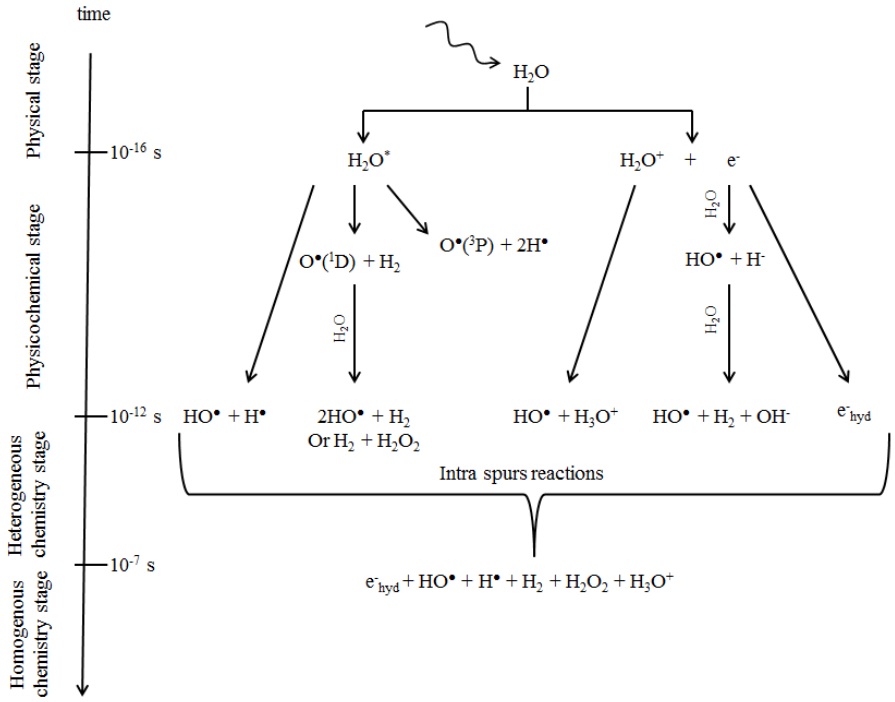

Figure 1 : Description des différentes étapes de la radiolyse de l'eau

Le nombre d'espèces disparues ou formées par la radiolyse est appelé rendement radiolytique. Il est calculé par l'équation (1). L'unité internationale de rendement radiolytique est le $mol.J^{-1}$:

$$G_t(X) = X_t / \rho D \qquad (1)$$

Où, X_t est la concentration des espèces concernées au moment t ($mol.l^{-1}$), ρ est la densité du milieu ($kg.l^{-1}$) et D est la dose absorbée par la solution ($J.kg^{-1}$).

Le TEL ou transfert d'énergie linéaire est définie comme la perte d'énergie (- dE) des particules dans le milieu en fonction la distance parcourue (dx). L'unité de TEL est le $keV.\mu m^{-1}$:

$$TEL = - dE / dx \qquad (2)$$

La valeur du TEL varie en fonction des différents types de rayonnements ionisants et il joue un rôle important pour le rendement radiolytique et les réactions chimiques induites. Pour une faible valeur de TEL, par exemple dans le cas d'un faisceau d'électrons ou γ avec environ 1 MeV d'énergie, le dépôt d'énergie créé les grappes sphériques. Les grappes formées ne sont pas proches les unes des autres et donc la densité des grappes est faible. La formation des espèces est dépendante de leur diffusion à partir des différentes grappes. Pour de forte valeur

de TEL, par exemple sous faisceau d'ions lourds avec des valeurs supérieures à 10-20 $keV.\mu m^{-1}$, les grappes sont formées proches les unes des autres et se chevauchent pour former une colonne continue d'espèces. Les espèces formées peuvent réagir et se recombiner à l'intérieur de cette colonne. Par conséquent le nombre de recombinaisons est plus élevé au cours d'expériences sous faisceaux avec des valeurs de TEL élevées. C'est la raison pour laquelle, il est généralement admis que les principales espèces sont sous forme radicalaires à faible TEL et moléculaire à fort TEL... Dans cette étude, l'effet de TEL est étudiée en étudiant les échantillons sous irradiation γ et α ($TEL_{\gamma} = 0,23\ keV.\mu m^{-1}$ et $TEL_{\alpha} = 22,7\ keV.\mu m^{-1}$).

Leradical anion de carbonate ($CO_3^{\bullet-}$) est formé par la réduction des ions carbonate ou bicarbonate. Systématiquement, il sera appelé « radical carbonate » dans ce travail. Sous irradiation, il est formé par l'effet indirect de la radiolyse de l'eau lors des réactions décrites ci-dessous:

$$HO^{\bullet} + CO_3^{2-} \rightarrow CO_3^{\bullet-} + HO^- \qquad k = 3.9 \times 10^8\ l.mol^{-1}.s^{-1} \qquad (3)$$

$$HO^{\bullet} + HCO_3^- \rightarrow CO_3^{\bullet-} + H_2O \qquad k = 8.5 \times 10^6\ l.mol^{-1}.s^{-1} \qquad (4)$$

La constante de vitesse de réaction dans le cas de ions carbonate est environ quarante fois plus élevée que pour l'ion bicarbonate. Le potentiel rédox $CO_3^{\bullet-}$ / CO_3^{2-} est 1,78 V à pH = 7,0. L'absorption maximale du radical carbonate est de 600 nm avec un coefficient d'absorption de $1970\ l.mol^{-1}.cm^{-1}$.

Afin d'obtenir le rendement radiolytique de la décomposition et de la formation d'espèces telless que Tc et Mn, la connaissance du rendement radiolytique de la formation de radicaux carbonate et de décroissance dans les solutions très concentrées de carbonate est obligatoire. En outre, pour de telles concentrations (> 2 $mol.L^{-1}$), les mécanismes décrits dans les solutions diluées (< 0.1 $mol.L^{-1}$) ne sont pas transposables. Des études récentes de radiolyse pulsée picoseconde de solutions aqueuses concentrées ont montré que les trois mécanismes d'oxydation de soluté peuvent se produire: i) l'effet direct de l'irradiation sur le soluté, dans ce cas, le soluté perd un électron qui peut être encore solvaté; ii) l'oxydation du soluté par le radical $H_2O^{\bullet+}$, produit seulement si le soluté est en contact avec ce radical; iii) l'oxydation du soluté par le radical $OH^{\bullet}$.

Le radical carbonate absorbe la lumière vers 600 nm et les données obtenues montrent que la solution de carbonate concentrée (> 2 $mol.L^{-1}$) décale l'absorption de l'électron solvaté à 600 nm également, par conséquent, pour avoir seulement une absorption du radical

carbonate, l'électron solvaté doit être capté. Trois solutions de carbonate avec des concentrations de 5, 3 et 2 mol.L^{-1} avec l'ion nitrate comme piégeur sont irradiées. Avec un spectre de l'électron mesuré pour chaque solution, il est possible de le soustraire au spectre obtenu afin d'obtenir le spectre du radical carbonate. La Figure 2 montre la cinétique après soustraction des spectres de l'électron pour les 3 solutions de carbonate. Les résultats indiquent que, dans la solution de carbonate avec une concentration de 5 mol.l^{-1}, au début la concentration du radical carbonate est plus élevée en raison de l'effet direct, mais celle-ci diminue et devient constante en raison de la production indirecte de radical carbonate par la présence du radical hydroxyle. Dans les solutions de carbonate avec des concentrations de 3 mol.l^{-1} et 2 mol.l^{-1}, au début il y a une petite quantité de radicaux carbonate en raison de l'effet direct, mais cette quantité augmente en raison de la production indirecte comme décrit ci-dessus.

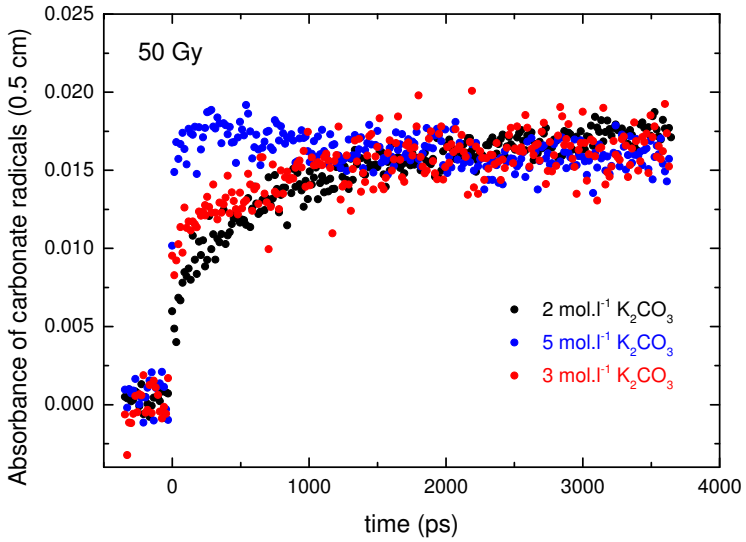

Figure 2 : Spectres d'absorption du radical carbonate en fonction du temps pour les 3 concentrations en carbonate (Collaboration LCP)

L'effet direct de la production des radicaux carbonate ne dure que 2000 ps et est donc largement plus rapide que les mécanismes d'oxydo/réduction de Mn, Re, Tc qui sont de l'ordre de la ms. Par conséquent, il peut être conclu que les radicaux carbonate qui viennent de l'effet direct de la radiolyse n'ont aucun effet sur la spéciation du Mn, Tc et Re dans une solution de carbonate concentré sous irradiation.

Dans l'étape suivante du travail, la spéciation du Mn dans les solutions de carbonate concentré (> 2 $mol.L^{-1}$) a été étudiée. Afin de déterminer les conditions expérimentales appropriées (concentrations de Mn et de carbonate, atmosphère, temps d'expérience), les mesures de réduction électrochimique sont effectuées. Après la calibration de la bande d'absorption et la caractérisation de l'espèce par électrochimie, les expériences dirradiations γ et α sont effectuées pour étudier l'oxydation du Mn(II) et la réduction du Mn(VII). Dans ces expériences il a été déterminé que la solution de carbonate doit être à sa concentration la plus élevée possible ((> 5 $mol.L^{-1}$) afin d'éviter la formation et la précipitation du MnO_2 solide. Le produit final de la réduction du Mn(VII) est Mn(IV) avec un spectre détectable de Mn(V) comme produit intermédiaire. Ces informations et les spectres UV-Vis sont utiles ont été déterminés pour comprendre la spéciation du manganèse sous irradiation dans le milieu carbonate.

Deux sources γ sont utilisées: l'une avec un faible débit de dose (^{137}Cs au laboratoire ARRONAX, Saint-Herblain, DD : 3 $Gy.min^{-1}$) et l'autre avec un débit de dose élevé (^{60}Co au LCP, Orsay, DD : 80 $Gy.min^{-1}$) afin d'étudier l'effet du débit de dose sur les mécanismes et la spéciation du Mn. 8 cellules pour les expériences de réduction (RedMn) : échantillon ([Mn (VII)] = 5×10^{-4} $mol.l^{-1}$, $[CO_3^{2-}]$ = 5 $mol.l^{-1}$) et 8 cellules pour les expériences d'oxydation (OxMn) ([Mn (II)] = 5×10^{-4} $mol.l^{-1}$, $[CO_3^{2-}]$ = 5 $mol.l^{-1}$) sous atmosphère Ar sont irradiés par une source γ. Afin d'obtenir des produits finaux et intermédiaires, les échantillons ont été irradiés selon des doses absorbées différentes. De plus des solutions de carbonate, sans Mn, ont été irradiées avec les même doses absorbées que pour les réactions d'oxydo/réduction. De plus, les résultats de ces expériences sans Mn sont considérés comme références (nommés «carbonate»). La concentration de dihydrogène de chaque échantillon est mesurée directement après l'irradiation par μ-GC. Le rendement radiolytique de l'hydrogène a été calculé pour les échantillons RedMn, OxMn et de carbonate. Le $G(H_2)$ pour la solution de carbonate avec une concentration de 5 $mol.l^{-1}$ est deux fois plus faible par rapport à l'eau pure ($G_{Carbonate}(H_2)$ = 1,4 ± 0,3 × 10^{-8} $mol.J^{-1}$ vs $G_{Water}(H_2)$ = 2,5 ± 0,3 × 10^{-8} $mol.J^{-1}$).. En outre, le $G(H_2)$ de l'échantillon OxMn est 2,2 ± 0,5 × 10^{-8} $mol.J^{-1}$ qui est environ deux fois plus élevé que la $G(H_2)$ pour échantillon de RedMn (1,3 ± 0,3 × 10^{-8}) qui est liée à la de consommation de l'électron aqueux et du radical $H^{\bullet}$ lors de la réduction du Mn(VII) tandis que l'$e^-_{(aq)}$ et $H^{\bullet}$ n'ont pas participé à la réaction d'oxydation du Mn(II).

Le spectre UV-Vis de chaque échantillon est enregistré pour chaque réaction (RedMn et OxMn) afin de suivre l'évolution de la spéciation en fonction de la dose. Les spectres UV-

Vis de réduction par la radiolyse montrent les mêmes bandes UV que pour l'expérience de l'électrochimie. Ces résultats montrent trois gammes de doses: (1) entre 0 et 1500 Gy (0 <temps d'irradiation <500 min), (2) entre 3300 et 5200 Gy (500 min <de temps d'irradiation <1733 min), (3) (temps 1733 min <irradiation de <2984 min) 7200 et 9000 Gy. De plus, entre ces trois gammes on peut déterminer deux points isobestiques (de $\lambda_{(1)-(2)}$ = 475 nm, $\lambda_{(2)-(3)}$ = 375 nm) qui sont induits par le changement d'état d'oxydation de Mn: (1) Mn(VII) → (2) Mn(V) → (3) Mn(IV). soluble LA Figure 3 montre les spectres de la réduction du Mn(VII) sous irradiation γ.

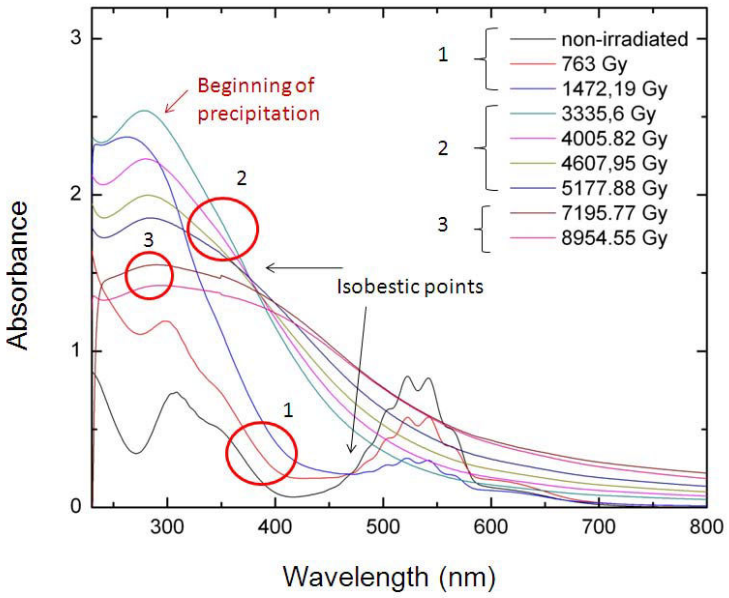

Figure 3 : Spectres UV-VIS enregistrés durant la réduction du Mn(VII) sous irradiation γ avec la source de ^{137}Cs.

Concernant les expériences de radiolyse α, le débit de dose a été déterminé avant les expériences d'irradiation. En utilisant la spectroscopie UV-Vis *in situ*, l'absorbance du Fe^{3+} en solution, provenant de l'irradiation de la solution de super Fricke, a été enregistré à 304 nm en fonction du temps. Le débit de dose a été calculé à partir des données obtenues à 3800 $Gy.min^{-1}$. La valeur du rendement radiolytique de l'hydrogène durant radiolyse α (Pour Mn (VII) = 2,7 ± 0,5 × 10^{-8} / Pour Mn (II) = 3,8 ± 0,8 × 10^{-8}) est environ deux fois plus élevée que celle obtenue lors de la radiolyse γ. Contrairement à la radiolyse γ, au cours de la radiolyse α un seul point isobestique a été observé dans les spectres de la réduction du Mn(VII). De plus,

nous pouvons conclure que, comme l'énergie déposée par le faisceau α est hétérogène, les espèces formées du Mn(IV) sont localisées dans une zone de faible volume et ils polymérisent rapidement. Ainsi, nous concluons que la solubilité du solide de Mn(IV) formé dépend de l'homogénéité de la formation de Mn(IV) dans la solution. Le produits finaux de la radiolyse α et γ ont été caractérisés et déterminés comme identiques. La Figure 4 montre le schéma récapitulatif des mécanismes d'oxydo/réduction de Mn sous irradiation α et γ.

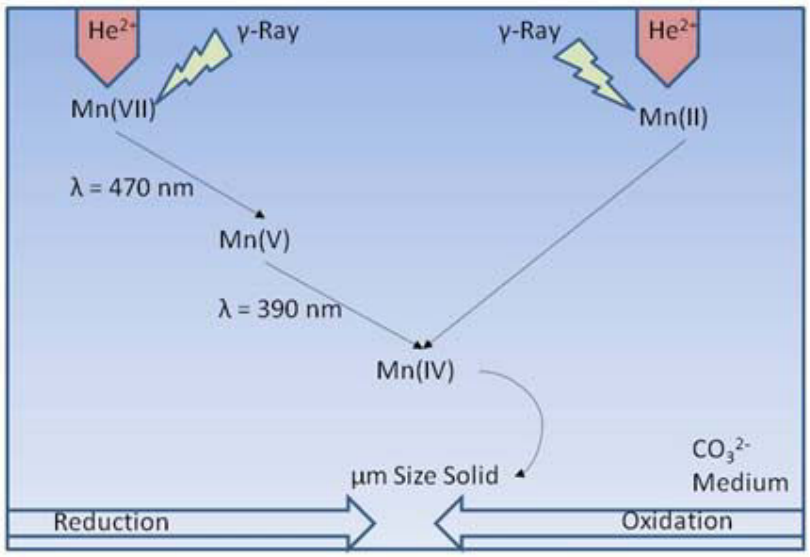

Figure 4 : Schéma du processus d'oxydo/réduction du Mn sous irradiation α et γ.

En complément des expériences sur le Mn, le rhénium a été étudié en tant qu'homologue du Tc. Le Re(III), sous la forme de $ReCl_3$, est irradié dans une solution de carbonate concentré (5 $mol.l^{-1}$) par sous faisceau γ. La solution rouge-brun est oxydée en solution transparente de Re(VII). Le Re (VII), sous forme d'espèces pertechnétate (ReO_4^-), est irradié également dans la même solution sous faisceau γ, sans qu'aucune réaction de réduction n'est pu être déterminée. Cette résistance à la réduction est due à la valeur élevée du potentiel redox de rhénium par rapport à celle du potentiel redox de l'$e^-_{(aq)}$ ou $H^\bullet$ en présences de $CO_3^{\bullet-}$ (E (ReO_4^- / ReO_2) = 5,10 V). L'ion formate est capable de piéger le radical hydroxyle de manière dix fois plus rapide que le carbonate. Ainsi, en ajoutant l'ion formate à la solution de carbonate, la concentration de $CO_3^{\bullet-}$ a diminué de manière significative ($CO_3^{\bullet-}$ restant est formé par l'effet direct). L'ion formiate à une concentration de 1 $mol.l^{-1}$ est donc ajouté à la solution de [ReO_4^-] = 5×10^{-4} $mol.l^{-1}$, [CO_3^{2-}] = 5 $mol.l^{-1}$ et [HCO_3^-] = 0,5 $mol.l^{-1}$ et irradiée sous faisceau γ. La solution transparente de Re(VII) est ainsi réduite en solution rouge de Re(IV) avec une bande d'absorption à 353 nm.

Une fois que toutes les conditions expérimentales ont été obtenues par les études préliminaires sur le radical carbonate, les espèces du Mn et la réduction du Re ; l'étude de la spéciation du Tc sous irradiation a été étudiée. En absence d'irradiation le complexe de Tc(IV) carbonate a été obtenu par réduction électrochimique. Pour la caractérisation de la structure de ce complexe, la spectroscopie EXAFS est utilisée. La méthodologie employée durant ce travail est : (1) La détermination des structures stables du complexe Tc-Carbonate par les simulations utilisant les calculs de chimie quantique avec le modèle de la Théorie de la Fonctionnelle de la Densité (DFT) en collaboration avec l'IPNO ; (2) L'utilisation des caractéristiques spatiales de ces structures afin de contraindre l'ajustement des spectres expérimentaux mesurés par EXAFS, par le synchrotron SOLEIL, sur les échantillons du complexe Tc-Carbonate.. Les spectres théoriques offrent différents types de diffusion et une combinaison de différentes diffusions doit être sélectionnée pour l'ajustement des spectres expérimentaux.. Les résultats de l'EXAFS indiquent la coordination 6 pour le technétium avec un état de d'oxydation +IV. La Figure 5 montre la structure de complexe du Tc(IV) - Carbonate.

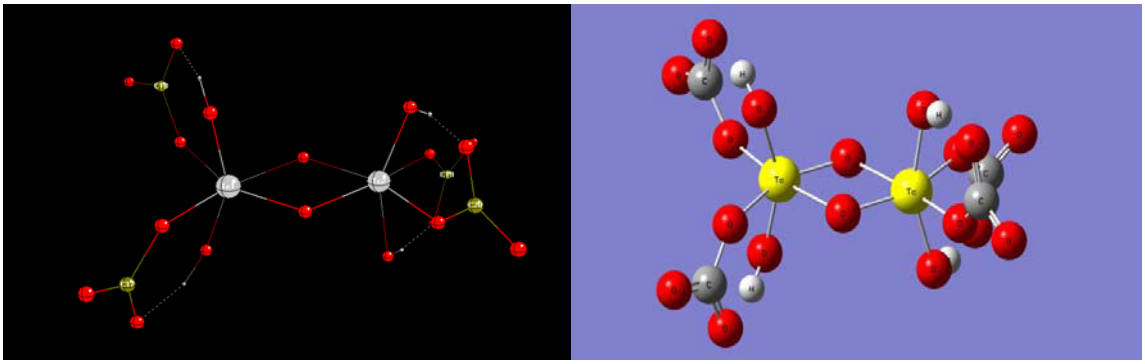

Figure 5 : Structure du complexe Tc(IV)-Carbonate déterminée à partir des mesures EXAFS et validée par les calculs de chimie quantique (DFT), Collaboration IPNO et SOLEIL.

L'espèce pertechnétate (TcO_4^-), avec une concentration de 5 x 10^{-4} mol.l^{-1} est ajoutée à la solution de carbonate concentrée (5 mol.l^{-1}) pour les études de spéciation sous irradiation. L'espèce Tc(VII) ne peut être réduit sous irradiation en raison de son potentiel redox en présence du radical carbonate. Comme il a été déjà observé pour le Re(VII), l'espèce Tc(VII) peut être réduit dans une solution de carbonate sous irradiation par l'addition de formiate. Ainsi, l'ion formiate est ajouté à la solution de carbonate afin de réduire Tc(VII). Dans une première étape, le formiate est ajouté à la concentration de 1 mol.l^{-1} dans la solution de carbonate concentrée (5 mol.l^{-1}) puis dans une seconde étape l'espèce Tc(VII) est réduite et

donne une solution rose attribuée à la formation du complexe Tc(IV). L'état d'oxydation +IV est identifiée par spectroscopie XANES.

La concentration de l'hydrogène gazeux est mesurée par µ-GC lors de l'expérience de la radiolyse du Tc(VII) en solution carbonate avec concentration de 0,7 mol.l^{-1}de formiate,. La forte densité de la solution (1,54 g.cm^{-3}) a été pris en compte pour le calcul de $G(H_2)$ (1,46 ± 0,3 × 10^{-8} mol.J^{-1}) et cette valeur est proche de la $G(H_2)$ pour la solution du carbonate sans Tc (1,4 ± 0,3 × 10^{-8} mol.J^{-1}). Compte tenu de ces données et de la $G(H_2)$ déterminé pour la réduction radiolytique du Mn(VII) dans une solution de carbonate (1,3 ± 0,3 × 10^{-8} mol.J^{-1}); nous pouvons conclure que le radical formate ($CO_2^{\bullet-}$) est impliqué dans le processus de réduction du Tc(VII). Ainsi, moins d'$e^-_{(aq)}$ est consommé lors de la réduction du Tc(VII) comparativement à la réduction du Mn(VII).

Le Tc(VII) avec une concentration de 5 × 10^{-4} mol.l^{-1} est irradié sous faisceau α dans les mêmes conditions expérimentales (concentration de carbonate de 5 mol.l^{-1} et 0,7 mol.l^{-1} de formiate) avec un débit de dose de 1000 Gy.min^{-1}. Les expériences de spectroscopie EXAFS est réalisée pour déterminer la structure du produit avec un centre de $Tc_2(\mu\text{-}O)_2$ obtenu lors de la radiolyse α. La formule du produit final identifiée est $Tc_2(\mu\text{-}O)_2(CO_3)_4(H_2O)_4$.

Les résultats marquant de ce travail de thèse concernant la spéciation du Tc sous irradiation en milieu carbonate concentré peuvent être récapitulés ainsi :

- Le complexe Tc(IV)-Carbonate présente une forme dimérique clarifiant ainsi les résultats contradictoires de la littérature..
- Cette étude montre que le complexe Tc(IV)-Carbonate est soluble pour une concentration de 5 × 10^{-4} mol.l^{-1}, tandis que dans la littérature sa solubilité a été proposée autour de 10^{-7} mol.l^{-1}.
- La structure exacte du complexe Tc(IV)-Carbonate a été identifiée dans cette étude telle que $(Tc_2(\mu\text{-}O)_2(CO_3)_4(H_2O)_4$ et $Tc_2(\mu\text{-}O)_2(CO_3)_4(OH)_4$.
- Le coefficient d'absorption du complexe Tc(IV)-Carbonate avec une absorption à 515 nm est de 200 l.mol^{-1}.cm^{-1}.

Table of Contents

Table of figures

Chapter III

Chapter IV

Chapter V

General Conclusion

General Introduction

After the Fermi discovery concerning the atoms splitting during the development of the nuclear science for military purpose at the end of the Second World War, the nuclear energy for peaceful purposes entered to people's life at December 21, 1951. In 50s lots of efforts have been done for commercial use of nuclear energy. Nuclear power grew up rapidly in 60s [1]. Nowadays, the global greenhouse-gas emission problems (69 % of greenhouse-gases comes from energy side) and also the need higher and higher of energy in the world cause more demand of nuclear energy [2]. Today, over 50 reactors are being built around the world and 100 more planned to come online in the next decade [3]. It implies there is more nuclear waste each day. The irradiated spent fuel is cooled off after unloading from nuclear reactor. Then, it is reprocessed for separation of recoverable materials. After the waste conditioned and sent to interim storage and, at the end, to deep disposal [4]. The radioelements that exist in the nuclear waste can migrate outside of disposal or storage place. Thus they should be stabilized in order to prevent their migration in terms of environmental pollution. One thing that must be taken in account is due to the different radio-elements inside nuclear waste, there are different types of irradiation (γ, α, β) thus the stabilization of radioelements should be done under these particles beam irradiation. Technetium (Tc) is one of the radioelements that must be taken into account in the nuclear waste management. Technetium has the lowest atomic number among the radioelements. ^{99}Tc is a β-emitter nuclide with a long half-life (2.11×10^5 years) [5]. This long half-life involves considerable amounts of nuclear fission products [6] which exist mainly as pertechnetate ion (TcO_4^-). Pertechnetate has high mobility and solubility, and in order to prevent the contamination of environment, it must be stabilized by changing the oxidation state and complexation reaction. As there is carbonate in natural waters and soil, thus the main aim of this study is to investigate the oxidation/reduction and also speciation of technetium in carbonate solution under irradiation. As technetium is a radioactive element and it needs special regulation for manipulation, the first experiments should be carried out on the non-radioactive elements. That is the reason why, in this study, manganese and rhenium (Re) have been chosen as the homologous of Tc. First they display close chemical properties to technetium and second the redox potential of technetium is between Mn and Re.

In this study different types of irradiation sources which involve He^{2+} with high energy (64 MeV), γ-ray with high dose rate (^{60}Co source), γ-ray with low dose rate (^{137}Cs Source) and pico-second electron pulse radiolysis were used. He^{2+} and γ particles have different linear energy transfer (LET) and also they enhance molecular and radical mechanisms respectively.

Therefore, using both of them for radiolysis brings any information about the mechanism of oxidation/reduction reactions. Using γ sources with high and low dose rate provide the information of dose rate effect on reactions and mechanism. Moreover, in order to understand the reactions mechanism, we should study on carbonate radicals that be produced by the carbonate species under irradiation. Therefore, the kinetics of formation and decay of carbonate radical have been investigated by electron pico-second pulse radiolysis. Finally, before studying the Mn, Re, Tc speciation under irradiation, electrochemistry was performed firstly in order to simulate the radiolysis phenomena. After the calibration of the absorption band and characterization of the species by electrochemistry, the γ and He^{2+} radiolysis are performed to initiate oxidation/reduction reactions. Figure 0.1 summarizes the schematic of different types of irradiation sources and their application in this study.

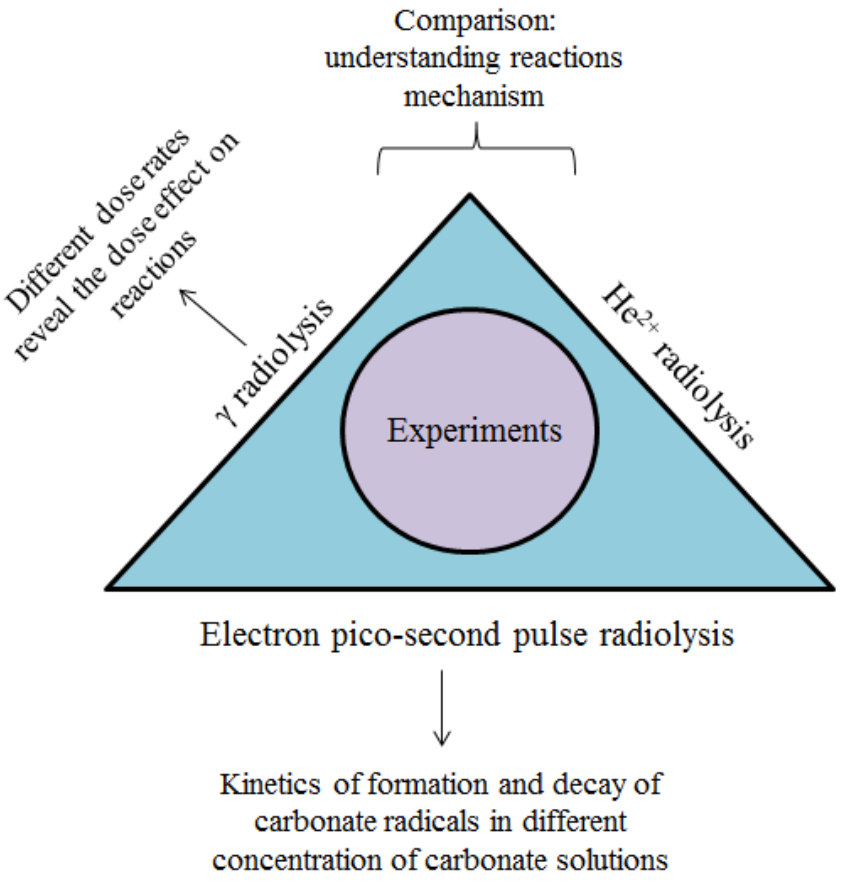

***Figure 0.1**: Schematic plan of irradiation experiments by different particles beam to perform speciation of Mn, Re and Tc under irradiation.*

All studies performed during this work can be summarized as follow:

- Chapter I presents the general chemical properties about technetium, manganese and carbonate under irradiation and its problematic and applications. Moreover, the radiolysis and measurement of radiolytic yield are discussed.
- Chapter II presents the materials and methods used during the experiments. In this part, all the analytical and experimental methods used in this study are described.
- Chapter III is devoted to the electron pico-second pulse radiolysis of carbonate solutions at different concentration of carbonate. The data in this part are useful to understand the mechanism of reactions and role of carbonate radicals for oxidation/reduction and speciation of Mn, Tc and Re.
- Chapter IV deals with the reduction of Mn(VII) and the oxidation of Mn(II) in concentrated carbonate solution under irradiation. Moreover, the chemical mechanisms and the dose rate effect are discussed. The oxidation states of final products and radiolytic yield of different products are determined.
- Chapter V, final objective of this work, is devoted to the oxidation/reduction reactions of Re and Tc in concentrated carbonate solution. The structure of final product of reduction of Tc(VII) in carbonate solution was characterized by using extended x-ray absorption fine structure spectroscopy (EXAFS) and the structure stability was checked by DFT simulation. Finally, the effect of carbonate concentration variation and also the reduction kinetic under irradiations are discussed in this part.

References

1. *The History of Nuclear Energy*, DOE/NE-0088, Editor, U.S. Department of Energy: Office of Nuclear Energy, Science and Technology Washington, D.C. 20585.
2. Hong, S., C.J.A. Bradshaw, and B.W. Brook, *South Korean energy scenarios show how nuclear power can reduce future energy and environmental costs.* Energy Policy, 2014. **74**: p. 569-578.
3. Eugene;, R., et al., *Nuclear Waste: Knowledge Waste?* Science, 2010. **329**(5993): p. 762-763.
4. Briggs, T., P.L. Kunsch, and B. Mareschal, *Nuclear waste management: An application of the multicriteria PROMETHEE methods.* European Journal of Operational Research, 1990. **44**(1): p. 1-10.
5. Bergquist, B.A., et al., *Technetium measurements by accelerator mass spectrometry at LLNL.* Nuclear Instruments and Methods in Physics Research B 2000. **172**: p. 328-332.
6. C.S.Dileep, P.J., P.S. Dhami, P.V. Achuthan, A. Dakshinamoorthy, B.S. Tomarb, S.K. Munshi, P.K. Dey, *Distribution of technetium in PUREX process streams.* De salination, 2008. **232**: p. 157-165.

Chapter I: State of the Art

A. Chemistry of technetium

A.1. Introduction

Technetium is the 43rd element in the seventh subgroup of periodic table which was discovered 14 years after rhenium (1937). Technetium has the lowest atomic number among the radioelements. Technetium was discovered during irradiation of a plate of natural molybdenum with deuteron beam in Berkeley cyclotron [1]. Technetium has 24 isotopes and their half-life varies from a couple of seconds to millions of years for ^{99}Tc. None of these isotopes are stable that is the reason why it is considered as radioelement. Technetium has electronic structure of [Kr]4d^{5}5s^2 and based on its d orbital, it shows 7 different oxidation states. ^{99}Tc is a β-emitter nuclide with a half-life of 2.11×10^5 years and $E_{\beta\text{-max.}}$ = 295.5 keV [2] that can be produced by 2 methods: First, during the fission of ^{235}U that involves 6 % of fission products [3], the second method is irradiation of ^{98}Mo with neutron beam [4]. Figure I.1 shows the natural radioactive formation and decay of technetium.

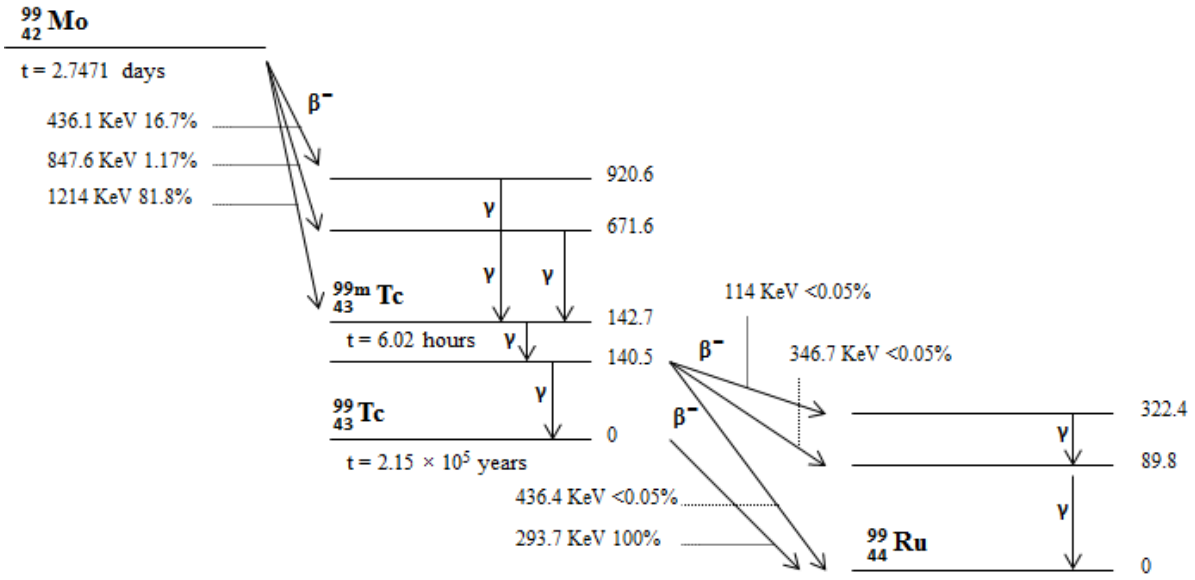

***Figure I.1**: Schematic of radioactive formation and decay of technetium [5].*

A.1.1. Technetium in the nuclear fuel cycle

The spent fuel from nuclear cycle contains different radioactive elements. Plutonium and uranium recovery by extraction (Purex) process is applied to reprocess those useful elements. In this method, the spent fuel is dissolved in HNO_3 at a concentration of 7.5 $mol.l^{-1}$. Despite small parts of technetium which is under metallic form and stays in highly active waste, the rest of produced technetium during the fission exists as pertechnetate ion (TcO_4^-). The TcO_4^- is extracted by tributyl phosphate (TBP) in n-dodecane [6-8]. The amount of residual ^{99}Tc in the cycle after extraction by TBP in n-dodecane is around 0.1 wt%. Almost all of ^{99}Tc remains in stream during the processing. The separated ^{99}Tc like other fission products is retained in the tank for solidification [9].

A.1.2. Technetium in stars

Astronomical spectroscopy is used for determination of chemical compounds, mass and temperature of stars. After discovery of technetium and characterization of its atomic emission spectrum, Moore has brought the evidence of the technetium attendance in the sun [10]. The existence of technetium in M, N and S stars has been verified (stars are categorized by their temperature and brightness). The discovery of technetium has induced a big impact on improving the cosmological theories (the mass transfer scenario). It is also a proof for the validation of heavy elements synthesis by slow neutron capturing [11, 12].

A.1.3. Technetium in natural environment

Except a few limited geographical zones, there is no study about the technetium concentration onto the earth planet. In the radius of 30 km around Chernobyl, the activity of technetium varies from 1.1 to 14.1 $Bq.kg^{-1}$ in dry soil which shows two-fold more activity than none-contaminated places [13]. In contrary to the soil, the concentration of ^{99}Tc is measured regularly in maritime zones due to nuclear tests in the past years. For example, an activity of 1850 $Bq.m^{-3}$ was reported by McCubin *et al.* at south of Ireland sea [14]. Then, a lack of data exists in the literature onto the Tc chemistry and must have a non-negligible impact onto the natural environment description around the radioactive accident areas.

A.1.3.1. Technetium in the ground soil

Generally, technetium is found as under TcO_4^- form which is the most mobile form of technetium due to its sorption on solid phase [15]. In the reducing conditions, technetium is reduced and then precipitates under sulphate or oxides forms [16]. Moreover, the sorption of technetium is correlated mainly with organic carbon contents, iron and aluminum oxides and soil clays [17]. Also it was determined in the literature that technetium can be reduced by iron-reducer and sulphate-reducer bacteria [18]. Then, the plants in a technetium contaminated soil could have metabolic malfunctioning for synthesis of amino acids. The transferring of technetium from the soil to the plants through their roots, would be proportional to its concentration in the soil [19]. Therefore, this transfer is obviously induced by the chemical properties (complexing or not) of the ligand present in the ground soil as carbonate for example.

A.1.3.2. Technetium in aquatic media

Technetium in the natural waters, seawater for example, was determined as its most stable form; TcO_4^- [20]. In sediments, pertechnetate ion is precipitated in acidic and/or reducing media. In seawater, the pertechnetate ion can be reduced but it will be re-oxidized rapidly. So, a high amount of technetium as TcO_4^- is released to the seas (sea of Ireland and Manche channel) by the recycling factories [21].

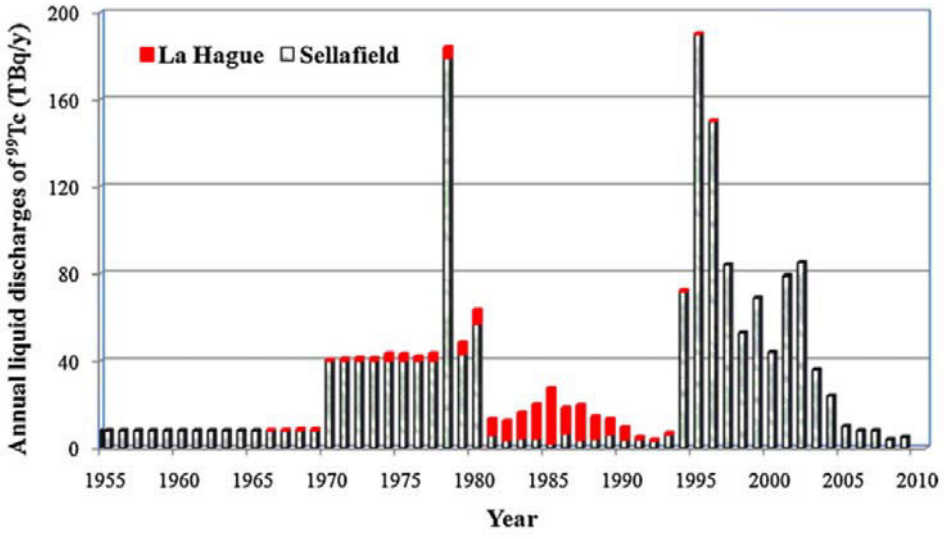

Figure I.2: *Liquid discharges of ^{99}Tc from two European reprocessing plants at Sellafield (UK) and Cap de La Hague (France) to the marine system [22].*

In maritime sediments, technetium can be reduced with bacteria and organic compounds to soluble and insoluble complexes of Tc(IV) with iron, aluminum, sulphate and organic matters [23]. Generally the concentration of technetium in the maritime creatures is low but higher concentration in some kinds of the polychaete like mollusk and particularly abalone were reported. Moreover very high concentration of technetium was reported for juvenile and adult lobster [24, 25]. Table I.1 displays the main sources of ^{99}Tc in maritime sediments in order to underline the high impact of the Tc radioactivity in the sea environment.

Table I.1: *Main sources of ^{99}Tc in maritime sediments from the environment [26, 27].*

Source	^{99}Tc released ($\times 10^{12}$ Bq)
Sellafield nuclear reprocessing plant	1720
La Hague nuclear reprocessing plant	154
Global weapons fallout (1940s–1970s)	140
Nuclear accident in Chernobyl	0.75
Estimated nuclear accident in Fukushima	>0.25
Estimated medical application (^{99}Mo–^{99m}Tc generator)	<0.02
Estimated nuclear power plants	<0.01

A.1.4. Applications of technetium-99

As a radiation source, ^{99}Tc is used as a source of weak β irradiation [28]. Also it is used as a radiation source to ionize detectors in gas chromatography [29]. In 1968 the catalytic activity of ^{99}Tc for hydrogenation of benzene was reported [30]. ^{99}Tc has shown a catalytic activity between platinum and rhenium. The oxidizing role of complexes of Tc(VII) for organic compounds was reported [31]. Moreover, pertechnetate species has been used as a corrosion inhibitor agent [32]. Despite all of those applications for technetium it has been mostly used for medical purposes. In 1961 ^{99}Tc was used firstly in medical science to image thyroid. Latter by developing complexes of ^{99}Tc, it has been used for imaging of other organs

such as brain, liver, bones, kidney and heart. Complexes of ^{99}Tc with derivatives of amino acids are used for renal and hepatobiliary imaging. Complexes of ^{99}Tc with phosphonate ligands are widely used as diagnostic agent for imaging of metastatic disease in bones and infarction infection. The complexes of Tc(III) and Tc(I) are used for brain imaging. The complexes of Tc(V) are largely used as a replace of ^{201}Tl for myocardial imaging [33].Then, for all these applications it seems interesting to study the behavior of the Tc, mainly its chemical properties, under γ/β irradiation.

A.2. Chemical properties of technetium

Technetium is situated in the 7th subgroup of periodic table with manganese and rhenium. They have the atomic radius of 183 pm, 161 pm and 188 pm respectively. As the atomic radius of technetium and rhenium are close each other, its chemical properties can be considered as close too. However, while manganese shows more different chemical properties in comparison to technetium by its higher oxidizing power. Table I.2 shows the potentials of the redox couples of manganese, technetium and rhenium. The redox potential, for the oxidation state of +VII, for technetium is lower than manganese but slightly higher than rhenium which indicates the stability of those couples is as follow:

perrhenate (ReO_4^-) > pertechnetate (TcO_4^-) > permanganate (MnO_4^-).

Table I.2: *Redox potentials of manganese, technetium and rhenium species in aqueous solutions [34, 35].*

Manganese	Eh(V)	Technetium	Eh(V)	Rhenium	Eh(V)
MnO_4^-/MnO_2	+1.679	TcO_4^-/TcO_2	+0.747	ReO_4^-/ReO_2	+0.510
MnO_4^-/Mn	+1.781	TcO_4^-/Tc	+0.477	ReO_4^-/Re	+0.361
MnO_2/Mn	+0.115	TcO_2/Tc	+0.281	ReO_2/Re	+0.251

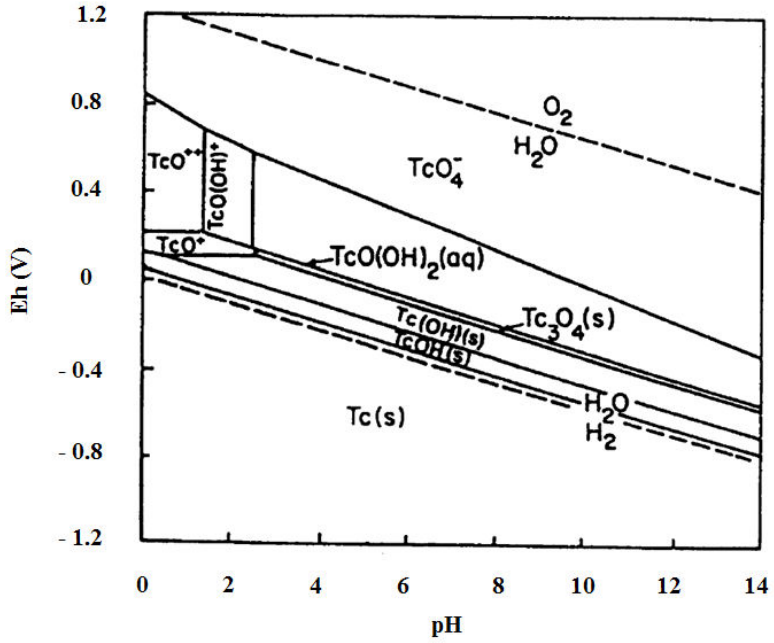

Figure I.3: *Eh vs. pH diagram for technetium species in aqueous solution at 298 K.*

The Pourbaix diagram in Figure I.3 indicates that technetium seems to be precipitated mostly in alkaline pH than acidic pH (pH higher than 8.0). The melting point of metallic technetium is 2140 ± 20°C which is 880 degrees higher than manganese melting point (1260°C) but 1000 degrees lower than rhenium (3140°C). Technetium is boiling at 4627°C. By the way our experiments have shown that TcO_4^- with a concentration of 5×10^{-4} mol.l^{-1} is soluble in carbonate solution with concentration of 5 mol.l^{-1} at pH = 10.8.

A.2.1. Speciation for the different oxidation states of technetium

A.2.1.1. Oxidation state (VII)

Pertechnetate ion (TcO_4^-) is the most abundant and well-known form of technetium at this oxidation state. As it is the most common oxidation state of technetium in aqueous media and reactors, its reactivity and mobility is very important [36]. Its stability is pH dependent and it is stable for pH higher than 4.0. Generally, in absence of complexing agent it is stable in sulfuric acid solution with concentration lower than 7 mol.l^{-1} [37]. Tc(VII) keeps its form as pertechnetate in diluted HNO_3, H_2SO_4 and $HClO_4$ media. The pertechnetic acid is formed in high concentrations of H_2SO_4 (< 7 mol.l^{-1}) and $HClO_4$ (< 8 mol.l^{-1}). However due to the low dissociation of HNO_3, even for high concentrations, the dominant form stays pertechnetate

[38]. Sodium pertechnetate is used for gastric cancer detection [39]. Despite that the alkaline salts of pertechnetate are more soluble, due to their hydrolysis in aqueous solutions, they have lower stability in comparison to the other salts. Equation 1-1 shows the dissociation reaction of the pertechnetate alkaline salts in aqueous solutions:

$$STcO_4 \leftrightarrow S^+ + TcO_4^- \quad \text{(I-1)}$$

The solubility of $NaTcO_4$, $KTcO_4$ and $CsTcO_4$ has inverse relation *vs.* their molecular weight and their solubility are 11.3 $mol.kg^{-1}$, 0.10 $mol.kg^{-1}$ and 0.014 $mol.kg^{-1}$ respectively at ambient conditions [40, 41]. Ubiquitous indigenous anaerobic bacteria in soils play a major role in immobilization of Tc(VII) by reduction of Tc(VII) to Tc(IV) [42]. Also the surface bacteria are capable to reduce technetium [43]. Pertechnetic acid oxidizes methanol to formic acid in sulfuric acid media [44]. The electro-reduction of Tc(VII) in chloride media resulting formation of a mixture of Tc(IV) and Tc(III) such as: Tc(VII) → Tc(IV) → Tc(III) [45].

A.2.1.2. Oxidation state (VI)

Technetium with oxidation state of +VI is formed in reducing media by the absorption of one electron by pertechnetate as described in the reaction:

$$TcO_4^- + e^- \rightarrow TcO_4^{2-} \quad \text{(I-2)}$$

Tc(VI) exists as TcO_4^{2-} or protonated forms which are H_2TcO_4 and $HTcO_4^-$. Tc(VI) is unstable and it decays rapidly thorough disproportionation reaction as below:

$$2\ Tc(VI) \rightarrow Tc(VII) + Tc(V) \quad \text{(I-3)}$$

Tc(VI) is stabilized in highly concentrated sulfuric media. The cationic peroxide complex of Tc(VI) is reported in sulfuric acid solution with a concentration of 16 $mol.l^{-1}$ in presence of H_2O_2 [46]. In alkaline pH, Tc(VII) is reduced to Tc(VI) by reacting with hydrazine [47].

A.2.1.3. Oxidation state (V)

Technetium with the oxidation state of (V) exists as cationic, anionic and polymeric forms in non-complexing aqueous media. This oxidation state is used more than other states in medical science. Due to the fast hydrolysis, Tc(V) is very unstable. Despite TcO^{3+} and TcO^{2+} have never been observed in non-complexing media, lots of complexes were reported for them [47]. Stability of complexes of Tc(V) is related to their ligands, for instance; the

halide complexes of Tc(V) are hydrolyzed and Tc(V) disproportionates to Tc(VII) and Tc(IV). Disproportionation reaction of Tc(V), depending on the pH of the solution, produces different forms of product but with the same oxidation states. The high concentrated hydrochloric acid stabilize chloride complexes of Tc(V) as $TcOCl_5^{2-}$ and $TcOCl_4^-$ [48, 49]. The complexes of Tc(V) with mono-dentate and bi-dentate of sulfate can be synthesized by He^{2+} irradiation of Tc(VII) in concentrated sulfuric acid (<13 $mol.l^{-1}$) [50]. So, the He^{2+} irradiation had been successfully used to change the Tc speciation into the solution.

A.2.1.4. Oxidation state (IV)

During the reduction of Tc(VII), the Tc(IV) is the most stable oxidation state among the others in absence of oxidant species. In function of the pH, a variety of soluble and non-soluble forms of Tc(IV) such as TcO_2^{2+}, $TcO_2.xH_2O$, TcO_2 and $TcO(OH)_3^-$ had been identified [47]. Moreover, the solubility of hydrated oxide depends on media, complexing reactions and its preparation pathway. In non-complexing media and high alkaline solutions, the increasing of solubility is due to the formation of $TcO(OH)_3^-$ [51]. The soluble forms of Tc(IV) are oxidized to Tc(VII) as pertechnetate in presence of oxygen. The chloride complexes of Tc(IV) exist as $TcCl_6^{2-}$and $TcCl_5^-$. X-ray absorption spectroscopy has made the evidence that Tc(IV) in chloric and sulfuric aqueous media have polymeric form [52]. $TcCl_6^{2-}$ is hydrolyzed in concentrated acidic solutions [53, 54]. Condensation of $TcCl_5(H_2O)^-$ implies $Tc_2OCl_{10}^{4-}$ as a dimer complex of Tc(IV) [55]. This complex is decomposed to $TcCl_5(H_2O)^-$ under light [56]. Oxo-polymeric species of Tc(IV) are formed by adding Tc(VII) to tri-fluoro methane sulfonic acid (HTFMS) with concentration between 4 and 8 $mol.l^{-1}$. He^{2+} irradiation of Tc(VII) in the same acid solution produces the same product but with higher kinetics [57]. In these media, the Tc(IV) complexes seem to be stable under irradiation. Alliot *et al.* have shown that Tc(IV) carbonate complexes are predicted to dominate in reducing conditions at P_{CO2} more than approximately 0.1 atm, which is one order of magnitude higher than the usual chemical conditions for deep geological formation studied for the storage of nuclear wastes [58]. They have suggested the monomeric form for carbonate complex of Tc(IV). Their hypothesis is examined in this study (Chapter V).

A.2.1.5. Other oxidation states

Tc(III) is obtained by electro-reduction of Tc(IV) in acidic and complexing media. The chloride complexes of Tc(III) are a bit stable. The carbonate complexes of Tc(III) are stable

and they do not disproportionate even at alkaline pH [59]. Tc(II) is stable at pH around 1.0 but it disproportionates at higher pH to Tc(III) and Tc(0). Technetium trichloride has been synthesized by reaction of $Tc_2(O_2CCH_3)_4Cl_2$ with HCl(g) at 300 °C [60]. Generally, the oxidation states lower than +IV are stabilized as complexes with cyanide and π acceptor ligands [61].

A.2.2. Technetium speciation in carbonate media

As hydrogen carbonate exists in nuclear waste storage, the carbonate complexes of Tc(IV) can be formed. The γ-ray seems to stabilize the Tc(VII) in absence of reducing agents in nuclear waste storage [62]. In presence of chemical reducers, such as Zn and hydrazine in carbonate media, the carbonate complexes of Tc(III) and Tc(IV) are formed. The formula for the complexes of technetium with oxidation states of +III and +IV are $Tc(CO_3)_q(OH)_{n+1}^{3-(n+1)-2q}$ and $Tc(CO_3)_q(OH)_n^{4-n-2q}$ respectively that indicate the carbonate complex of Tc(III) has one more hydroxyl group than carbonate complex of Tc(IV). Concerning the oxidation state of +IV, the insoluble TcO_2 is also formed. Tc(IV) in carbonate media can be formed by using electrochemistry as reduction tool [51, 59]. In reduction of Tc(VII) in carbonate media the UV-Vis absorption of Tc(VII), Tc(IV) and Tc(III) are determined at 280 nm , 512 nm and 630 nm respectively. Figure I.4 shows the spectra of technetium with oxidation states of+ VII, +IV and +III under reduction in carbonate media [59].

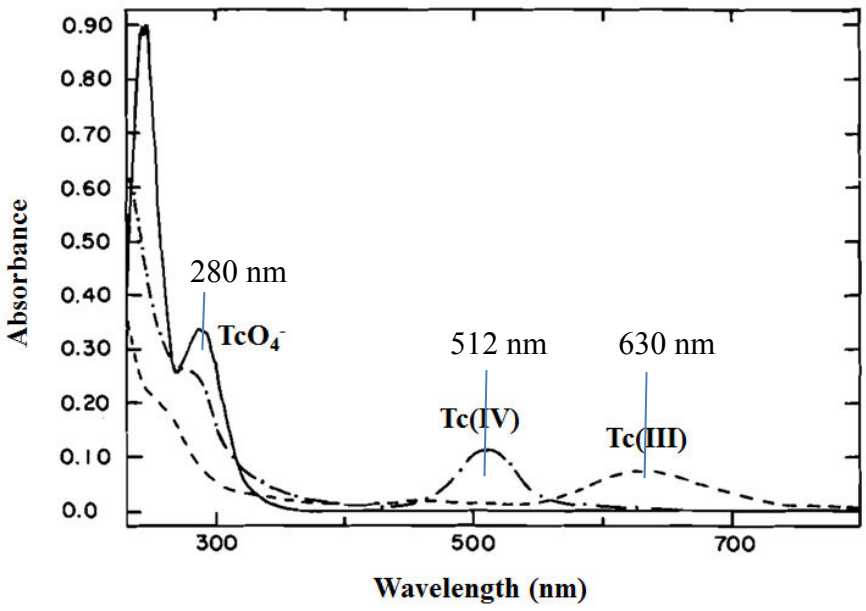

Figure I.4: *UV-Vis absorption spectra for Tc(VII), Tc(IV) and Tc(III) , at 1.2×10^{-4} mol.l^{-1} in 0.5 mol.l^{-1} HCO_3^- and pH = 8 [59].*

If the total concentration of carbonate is thirsty-fold more than total concentration of Tc(IV), the precipitation of $TcO_2.nH_2O$ is prevented. In CO_2-rich waters, the mixed hydroxo carbonato complexes may dominant the Tc(IV) forms [63]. The solubility of Tc(IV) in hydrocarbonate waters is pH-dependent and it increases at alkaline pH.

In order to summarize this part dedicated to the technetium speciation under irradiation, the existence of technetium with oxidation state of +VII in environment and fuel cycle brings important attention toward nuclear waste management and environmental disaster. Therefore, the technetium element must be stabilized by reducing its oxidation state and complexation reactions. In this aim, the carbonate solution can be used for stabilization and complexation of technetium. Moreover, it seems useful to study the behavior of this kind of complex under irradiation to predict its stability or not. Maybe this kind of work can open new window for medical and nuclear applications concerning the technetium speciation. As technetium is radioactive and needs special regulation for manipulation, it is better to work on its chemical homologous at first. As described in this chapter, manganese and rhenium can be consider as the homologous of technetium. In conclusion, the knowledge of the chemistry of manganese and rhenium and their behavior in carbonate solutions are mandatory to predict technetium behavior before oxidation/reduction of technetium in carbonate solutions under irradiation. Then the next part describes the chemistry of manganese.

B. Chemistry of Manganese

B.1. Introduction

Manganese is one of the most abundant elements in the earth crust and it plays an important role in chemical and biological systems [64, 65]. It is a main component of earth crust, around 0.1 %, and it is found in soil, rocks and waters. Manganese is an essential nutrient for micro-organism, plants and animals. Manganese oxides at different oxidation states are widely used for variety of applications such as water treatment, catalysts, energy, nano-photocatalysts and wave absorber in electromagnetic devices [66-70]. One of the important key to achieve these properties is the manganese oxidation state [71-74], then the study of the oxidation/reduction of manganese in different chemical conditions and media is necessary. Moreover, these studies seem to be helpful to understand the chemistry of

technetium. Table I.3 shows some of the manganese compounds with different oxidation states and their physical and chemical properties [75].

***Table I.3**: Several manganese compounds and their properties [75].*

Chemical formula	Oxidation state	Color	Physical state	Solubility
Mn	0	grey-white	solid	dissolves in diluted mineral acids
$MnCl_2$	II	pink	solid	very soluble in water and alcohols
$MnSO_4$	II	pale rose-red	solid	soluble in water and alcohols
Mn_3O_4	II,III	black	solid	insoluble in water. soluble in hydrochloric acid
MnO_2	IV	black	solid	insoluble in water. soluble in hydrochloric acid
$KMnO_4$	VII	purple	solid	soluble in water, acetone and sulfuric acid

B.2. Speciation for the different oxidation states of manganese

Manganese at high oxidation states, especially at oxidation state +VII shows some similar properties with the technetium and rhenium. That is the reason why, it can be considered as analogous of technetium.

B.2.1. Oxidation state (VII)

The compounds of manganese with oxidation state of +VII are very strong oxidizing agent and, except permanganate (MnO_4^-), they are not thermally stable. In temperatures higher than 0^oC the Mn_2O_7 is decomposed to MnO_2 and oxygen and can explode in presence of organic matter by forming Mn_2O_3 and oxygen. In order to obtain permanganic acid, a defined quantity of sulfuric acid is added to a saturated barium permanganate solution [76]. The dissolution process of potassium permanganate in concentrated sulfuric acid leads to a green solution of $MnO_3^+\backslash MnO_4SO_3H$. The MnO_4SO_3H species is a dominant product when the dissolution experiment occurs in a 100% sulfuric acid. The reaction of formation of MnO_3^+ and MnO_4SO_3H are described below [77]:

$$KMnO_4 + 3H_2SO_4 \rightarrow K^+ + H_3O^+ + MnO_3^+ + 3HSO_4^- \quad \text{(I-4)}$$

$$KMnO_4 + 3H_2SO_4 \rightarrow K^+ + H_3O^+ + MnO_4SO_3H + 2HSO_4^- \quad \text{(I-5)}$$

B.2.2. Oxidation state (VI)

Salts of manganese with an oxidation state of +VI are only stable in alkaline solutions and they disproportionate in neutral and acidic pH. Thermal decomposition of Mn(VII) produces Mn(VI). The mint-green liquid of $MnOCl_3$ is formed by the reduction of $KMnO_4$ in the solution of HSO_3Cl and $CHCl_3$. Due to the strong hydrolysis of manganese, no explosion is reported for it [78].

B.2.3. Oxidation state (V)

The blue Mn(V) is obtained by the reduction of $KMnO_4$ in NaOH or by the oxidation of MnO_2 or Mn(II) [79]. The permanganate heating produces pure anhydrous alkali Mn(V). In solution, the Mn(V) disproportionates to $Mn(VI)O_4^{2-}$ and $Mn(IV)O_2$. The Mn(V) oxo complexes are employed for various chemical reactions such as water oxidation and

purification, C-H bond activation and oxo transfer reactions. The complexes of Mn(V) involving various ligands of porphyrins, corroles, non-heme amide-based ligands and corrolazing are used for the conversion of alkenes to cyclic carbonate [80].

B.2.4. Oxidation state (IV)

Most of the Mn(IV) species, except MnO_2 which is insoluble, are hydrolyzed and can be reduced. Manganese dioxide is a black or dark gray solid. The dark brown active manganese dioxide is formed by the reaction between aqueous solution of permanganate and Mn(II) salt. The active manganese dioxide is used for selective oxidation of organic compounds. The addition of orthophosphoric acid with concentration of 3 $mol.l^{-1}$ to the fresh precipitated MnO_2 is employed for the detection of organic and inorganic compounds by chemiluminescence [81, 82]. Colloidal hydrous manganese with oxidation state of +IV shows high adsorption capacity for cations and it can be used, for example, for the separation of magnesium isotopes [83].

The yellow solution of Mn(IV) sulphate is formed by the decomposition of permanganate in oily sulfuric acid with oxygen liberation. Also Mn(IV) makes stable complexes with diphosphate ions in diphosphoric acid [84]. The only reactive halide of manganese (IV) is MnF_4. The complexes of hexa flouro-manganate (IV), hexa chloro-manganate (IV) and penta flouro-manganate (IV) are well-known. Nowadays, based on the effective electrical transport continuity and minimizing ions diffusion path, lots of efforts are done for synthesis of nano particles and nano rods of MnO_2 as the results of high surface area and short distance from the surface to the interior core of nanomaterials [85].

B.2.5. Oxidation state (III) and (II)

The chemistry of manganese (III) was more studied than other oxidation states of manganese. The ionic, neutral and cationic complexes of Mn(III) have been synthesized and they are fairly stable. Moreover, the Mn(III) complexes are important for biological system and, for example; they catalyze the disproportionation of superoxides [86]. The highly efficient epoxidation of alkenes and hydroxylation of alkanes catalyzed by tetra(4-N-pyridyl)porphyrinatomanganese(III) acetate, [Mn(TPyP)OAc], supported on silica coated magnetite nanoparticles, SiO_2–Fe_3O_4, are reported [87]. Mn(III)-BINOL-Salen complexes are used for asymmetric epoxidation of non-functionalized alkenes for its wide application in

chiral pharmaceutical chemistry [88]. Poly nuclear Mn(III) complexes such as $[MnIII_2(L–3H)_2(CH_3OH)_4]\_2CH_3OH$ and $[MnIII_2(L–3H)_2(Py)_4]\_2Py$ are synthesized. The polynuclear complexes are very important due to their large single ion anisotropy for molecular magnetism field and also their vital roles in metallo-biosites such as oxygen evolving complex of photosystem II [89].

Due to the rich photophysical and redox properties of manganese (II) complexes, they are used for analytical purposes and biological probes [90]. The mononuclear Mn(II) complexes with tptz (2,4,6-tris(2-pyridyl)-1,3,5-triazine) as a ligand, is an excellent catalysts for selective oxidation of various sulfides to the corresponding sulfoxides [91]. Mn(II) complexes are used as medical drugs also. In cancer chemotherapy, multidrug resistance remains as a big problem and manganese(II) N-(2-hydroxy acetophenone) shows considerable efficacy to overcome drug resistance cancer [92].

B.3. Manganese speciation under irradiation

Except $MnCO_3$ which is one of the natural mineral of manganese, the carbonate complexes of manganese have not been extensively studied. Knowledge about the carbonate complexes of manganese is critical in order to understand the natural phenomena where the manganese can be involved. This knowledge can be used indirectly for the chemistry of ^{99}Tc which can be stabilized by carbonate in both nuclear waste [62] and radiopharmaceutical [93] contexts. In previous attempts, the formation of manganese complexes at different oxidation states, reduction of Mn(VII) for example, in water with the presence of organic matter under γ-ray irradiation was investigated. In water the Mn(VII), as $KMnO_4$, is reduced to Mn(IV) by the formation of an insoluble amorphous MnO_2 colloids at pH = 10 in aerated solution. The colloid size and shape can be controlled by the irradiation intensity. Moreover, the formation of Mn(IV) through the oxidation reaction of Mn(II) by hydroxyl radical was studied. However, the size of formed Mn(IV) colloid by the oxidation reaction is larger than by the reduction reaction [94]. The soluble MnO_2 can be synthesized by the addition of small amounts of thioacetamide [95]. The reduction of permanganic acid ($HMnO_4$) by radiolysis induces Mn(IV) and Mn(III) by the formation of MnO_2 and MnOOH respectively. The ratio of Mn/O in reduction of $HMnO_4$ varies with the studied atmosphere [96]. The scavenging hydroxyl radical with alcohol produces MnO_2 with a particle size minimum at 6 nm [97]. Manganese nano rods can be synthesized by irradiation of aerated aqueous $KMnO_4$ solution with the addition of tertio butanol to scavenge the hydroxyl radical in N_2-purged solution in

order to produce nanospheres of manganese [98]. The same pattern during the reduction of $KMnO_4$ to MnO_2 has been observed by ultrasonic irradiation [99]. The reduction of Mn(VII) to Mn(IV) occurs by reactions between $KMnO_4$ with $H^{\bullet}$ and $e^-_{(aq)}$ but as permanganate is a strong oxidizing agent, in alkaline medium too, it can be reduced by the reactions with H_2O_2 and O_2^- [100].

In order to summarize this part dedicated to the manganese speciation under irradiation, the manganese element can be oxidized or reduced under irradiation and depending on medium, different species of manganese with different oxidation states are formed. Therefore, in order to control and understand the reactions mechanism, it can be need having knowledge about the radiolysis and its related phenomena which discussed in the next part.

C. Radiolysis in aqueous solutions

All the chemical reactions that are initiated with ionizing radiations (high energy photons and charged particles) are classified as radiation chemistry. Ionizing energy is absorbed by solvent and creates excited and charged species. The interaction of high energy photons (γ ray and X-ray) is different from charged particles (e.g. $^4He^{2+}$). High energy photons absorption occurs by the three following phenomena: photoelectric effect, Compton effect and pair production. The charged particles interact with matters in four types through coulombic forces: 1) inelastic collision with atomic electrons, 2) inelastic collision with atomic nucleus, 3) elastic collision with atomic electrons and 4) inelastic collision with atomic nucleus. Electron beam losses its energy inside the matter through inelastic coulombic collision.

C.1. Radiolysis of water

Water is the most used solvent in chemistry and the water radiolysis is of interest in many studies such as nuclear reactors and spent nuclear fuel [101, 102]. The incidence of ionizing beam with water initiates lots of events that they occurred in four parts: 1) physical stage, 2) physicochemical chemistry stage, 3) heterogeneous chemistry stage and 4) homogenous chemistry stage. In physical (10^{-16} s) stage the water is excited and followed by the formation of excited e^- and H_2O^+. The electron is excited by the other water molecule until it loses its extra energy. In physicochemical stage which occurs in the time window from 10^{-16}

s to 10^{-12} s, H_2O^+, H_2O^* and e^- are tended to be more stabilized. At the end of this stage, electron is solvated after losing its energy. H_2O^* is dissociated to $H^\bullet$ and $HO^\bullet$. Some parts of these radicals produced H_2 and H_2O_2. H_2O^+ is reacting with another water molecule and creates $HO^\bullet$ and H_3O^+. At the end of physicochemical stage the radiolytic species are: e^-_{hyd}, $H^\bullet$, $HO^\bullet$, H_3O^+, HO^-, H_2 and H_2O_2. The time window from 10^{-12} s to 10^{-7} s after incident of ionizing beams with water is devoted to the heterogeneous chemistry stage. At this stage in case of existence, the diluted solute is reacted with radicals and forms stable products. Moreover, at this stage the concentration of radiolytic species are decreased inside the spurs. In homogenous chemistry stage, that last 10 ns, the formed molecular and radical species are released from spurs to the solution with homogeneity [103]. Figure I.5 shows the schematic of water radiolysis vs. the timescale described above.

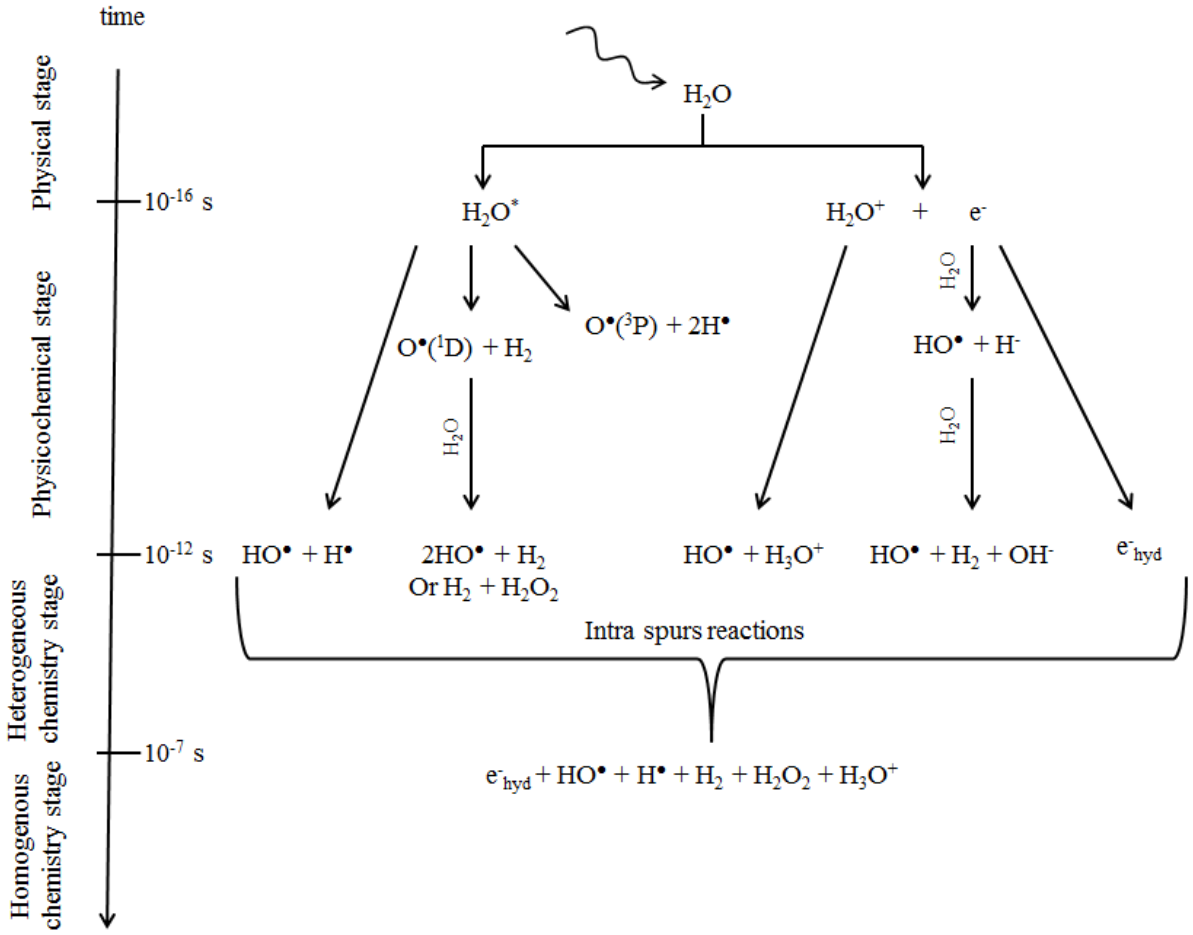

Figure I.5: *Schematic of radiolysis of water vs. the time scale [104].*

C.2. Radiolytic yield

The number of formed or disappeared species by radiolysis is called radiolytic yield. It is calculated by below formula. The international unit of radiolytic yield is $mol.J^{-1}$:

$$G_t(X) = X_t / \rho D \quad \text{(I-6)}$$

Where, Xt is the concentration of interested species at the time t ($mol.l^{-1}$), ρ is the density ($kg.l^{-1}$) and D is the absorbed dose by solution ($J.kg^{-1}$). Also the radiolytic yield can be introduced as one formed or disappeared species per 100 eV energy with:

$1 \text{ molecule } (100 \text{ eV})^{-1} = 1.038 \times 10^{-7} mol.J^{-1}$

There are three different types of radiolytic yield. The first type is initial radiolytic yield and is written with G°(X). The G°(X) is the yield of the species at the end of the physical chemistry stage (10^{-12} s). The second type is the primary radiolytic yield which is written with g(X). It is related to the molecular and radical species that escaped from spurs after 200 ns of irradiation. The last type is called global radiolytic yield with the symbol of G(X) that is related to the radiation yield after a couple of minutes of irradiation.

C.3. Effect of LET (Linear Energy Transfer)

LET or linear energy transfer is defined as the energy loss (-dE) of each particle inside the media during the traversed distance (dx) by particle. The unit for LET is $keV.\mu m^{-1}$:

$$LET = - dE / dx \quad \text{(I-7)}$$

The LET value varies with different kinds of ionizing radiations and it plays an important role for the radiolytic yield and induced chemical reactions. In low LET, for example electron beam or γ-ray radiolysis with about 1 MeV energy, the energy deposition creates the spherical spurs. The formed spurs are not close to each other therefore the spurs density is low. Reactions of the formed species are depending on their diffusion from different spurs. In high LET, for example heavy ion radiolysis with LET greater than 10-20 $keV.\mu m^{-1}$, the spurs are formed close to each other and they overlap to form a dens continuous column of species. The formed species can react and recombine each other inside this column. Hence, lower number of recombination are involved in low LET radiolysis than in high LET one. That is the reason why, it was commonly approved that the main formed species are mostly radicals during the low LET radiolysis. Nevertheless, in contrary to all other species, the $HO_2^{\bullet}$

yield increases with a higher LET. That is why, the LET effect can change the reaction mechanism or induced chemical reaction by radiolysis. In this study the LET effect is investigated by applying γ-ray and He^{2+} radiolysis (LET_{γ} = 0.23 keV.µm^{-1} and LET_{He2+} = 22.7 keV.µm^{-1}). It should be noticed that it is not possible to understand all the radiolysis processes by LET. Especially in high LET the processes are not like the radiolysis models [105].

As the technetium and the manganese are irradiated in carbonate solution, in order to understand their reactions mechanisms, the knowledge about the behavior of carbonate under irradiation is necessary.

C.4. Carbonate speciation in solution under irradiation

Carbonate anion radical ($CO_3^{\bullet -}$) is formed by one electron reduction of carbonate or bicarbonate ions [106]. Systematically, it will be called carbonate radical in this work. Under irradiation it is formed by the indirect effect of the water radiolysis by reactions described below:

$$HO^{\bullet} + CO_3^{2-} \rightarrow CO_3^{\bullet -} + HO^- \qquad k = 3.9 \times 10^8 \text{ l.mol}^{-1}.\text{s}^{-1} \qquad \text{(I-8)}$$

$$HO^{\bullet} + HCO_3^- \rightarrow CO_3^{\bullet -} + H_2O \qquad k = 8.5 \times 10^6 \text{ l.mol}^{-1}.\text{s}^{-1} \qquad \text{(I-9)}$$

The rate constant in case of carbonate is about forty-fold higher than for bicarbonate.

The reduction potential of the carbonate/carbonate radical anion pair is +1.78 V at pH = 7.0 [107]. The carbonate anion radical is an oxidizing agent in most of reactions by electron transfer, hydrogen subtraction and oxygen transfer (only in self-reaction) mechanisms. It also reacts with other radicals such as nitride (see Table I.4).

Unlike the fast reaction of hydroxyl radical, carbonate radical reacts selectively with organic compounds with a corresponding second order rate constant [108] by electron transfer or hydrogen transfer reactions [109]. The carbonate anion radical maximum absorption is 600 nm with absorption coefficient 1970 l.mol^{-1}.cm^{-1} [110, 111]. Table I.5 shows the extinction coefficient for mains wavelengths determined during radiolysis experiments. Moreover, pulse radiolysis experiments have shown that the carbonate radical is a strong acid with a pKa < 0 [112].

Table I.4: *Rate constant and mechanisms of carbonate radical anion reactions with several organic and inorganic compounds [106].*

Reactant	Reaction mechanism	Rate constant (M^{-1} . s^{-1}) (pH)
$^{\bullet}NO_2$	O^- transfer	1.0×10^9 (11)
$^{\bullet}NH_2$	O^- transfer	1.5×10^9 (7.8)
Ascorbate	Intermediate addition complex	1.1×10^9 (11)
Trp-H	Intermediate addition complex	7.0×10^8 (7.0)
Tyr-O-	Intermediate addition complex	1.4×10^8 (11.0)
Met	Intermediate addition complex	3.6×10^7 (7.0)
$CH_2NO_2^-$	Addition to carbon atom	1.5×10^7 (12.0)
Cys-SH	Hydrogen abstraction	4.6×10^7 (7.0)
Tyr-OH	Hydrogen abstraction	4.5×10^7 (7.0)
CH_3OH	Hydrogen abstraction	6.0×10^3 (alkaline)
$CH_3(CH_2)_3NH_2$	Hydrogen abstraction	4.0×10^5 (11.5)
$(C_2H_5)_3N$	Electron transfer	9.8×10^6 (13.0)
His	Electron transfer	5.6×10^6 (7.0)
GS^-	Electron transfer	7.1×10^8 (alkaline)
$CysS^-$	Electron transfer	1.8×10^8 (11.4)
8-oxo-dGuo	Electron transfer	7.9×10^8 (7.5)
$Fe(CN)_6^{4-}$	Electron transfer	3.6×10^8 (11.5)

Table I.5*: Extinction coefficients of carbonate anion radical [110, 113].*

Radical	Wavelength			
	400 nm	472 nm	600 nm	660 nm
$CO_3^{-\bullet}$	130	670	1970	1370

C.4.1. Radiolytic formation of the carbonate radical

The water radiolysis produces as radical species $e^-_{(aq)}$, $H^{\bullet}$ and $HO^{\bullet}$ [103]. But, the $CO_2^{\bullet-}$ (called in this work formate radical) is formed by the reaction of hydroxyl radical with carbonate and bicarbonate ions [114]. Different parameters such as atmosphere, temperature and additional salt can change the yield values of carbonate radical [111, 115]. Usually the carbonate solution studied is saturated with N_2O to increase the carbonate radical yield by

scavenging of the solvated electron in order to increase the $HO^{\bullet}$ and $CO_3^{\bullet-}$ concentrations [116]. The reactions are described below:

$$H_2O + \text{radiation} \rightarrow H^{\bullet} + (e^-)_{aq} + HO^{\bullet} + H_2O_2 \quad \text{(I-10)}$$

$$H^{\bullet} + HO^- \rightarrow (e^-)_{aq} + H_2O \quad \text{(I-11)}$$

$$(e^-)_{aq} + N_2O \rightarrow N_2 + HO^- + HO^{\bullet} \quad \text{(I-12)}$$

$$HO^{\bullet} + CO_3^{2-} \rightarrow CO_3^{\bullet-} + HO^- \quad \text{(I-13)}$$

$$HO^{\bullet} + HCO_3^- \rightarrow CO_3^{\bullet-} + H_2O \quad \text{(I-14)}$$

In this method all the produced radicals are converted to carbonate radical. So, we used it to calculate the total radiolysis yield. In upper reaction N_2O^- is formed as an intermediate, it should live either lower than 1 µs. Moreover, it is possible to generate carbonate anion radical by the radiolysis or photolysis of hydrogen peroxide to produce hydroxyl radical through below reaction [117]:

$$H_2O_2 \rightarrow 2\ HO^{\bullet} \quad \text{(I-15)}$$

N_2O saturated solution gives the opportunity to transform the quite amount of induced radical by the irradiation in carbonate anion radical in order to measure the total radiolysis yield (yield of all the produced radicals by water radiolysis) [118].

In carbonate system, analysis are based on the acid base equilibrium constant for the bicarbonate ion [119]:

$$HCO_3^- \leftrightarrow H^+ + CO_3^{2-} \qquad pKa = 9.6 \pm 0.3 \text{ in } pH < 7.5 \quad \text{(I-16)}$$

This equilibrium can be controlled by the pH control as displayed in Figure I.6.

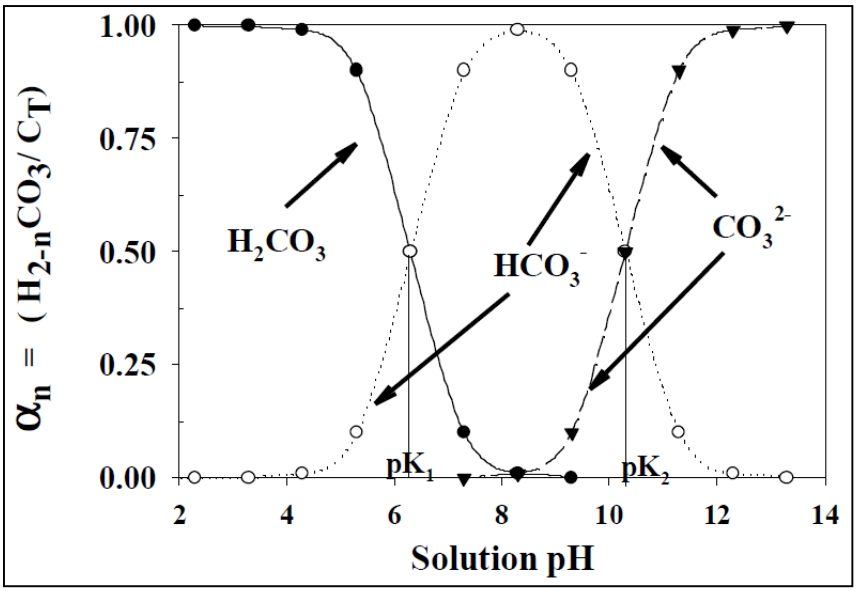

Figure I.6: *Distribution of carbonate species as a fraction of total dissolved carbonate vs. the pH solution [120].*

Moreover, this equilibrium is temperature dependent and increasing the temperature can produce bicarbonate and carbon dioxide from the carbonate ion as it is shown below:

$H_2CO_3 \leftrightarrow H^+ + HCO_3^-$ (I-17)

$H_2CO_3 \leftrightarrow CO_2 + H_2O$ (I-18)

Table I.6 presents the amount of carbonate converted to dissolved carbon dioxide in function of temperature. So, it can be noticed that, at 250°C, about 50 % of bicarbonate will be converted [113]. There are no obvious changes in carbonate radicals spectra shape by increasing temperature except a slightly broaden shoulder, but absorbance decrease due to the increasing bicarbonate concentration. Moreover, it is determined that the reactivity of hydroxyl radical is lower with bicarbonate than with carbonate [121].

Table I.6: *Percentage of bicarbonate remaining in solution after CO_2 conversion vs. temperature [121].*

	% of bicarbonate remaining			
T (°C)	0.001 M	0.002 M	0.02 M	0.1 M
0	98.6	98.6	98.6	98.6
25	97.1	97.1	97.1	97.1
50	96.5	96.6	96.6	96.6
75	95.3	95.7	95.9	95.9
100	93.3	94.2	94.8	94.8
125	90.1	91.8	93.2	93.3
150	85.5	88.1	90.8	90.8
175	79.1	82.9	86.9	87.0
200	70.5	75.4	80.7	80.9
225	59.3	65.0	70.7	70.9
250	45.5	50.9	55.7	55.8

Concerning hydrogen peroxide species, during the steady state γ-ray irradiation, the $G(H_2O_2)$ value, for an absorbed dose higher than 500 Gy, is higher in $NaHCO_3$ solution than with Na_2CO_3 solution [122].

During the pulse radiolysis experiments of alkaline carbonate solution, the production of $e^-_{(aq)}$, $H^\bullet$, $HO^\bullet$, H_2, OH^-, H_2O_2 and H_3O^+ must be considered. There is no reaction between H_2\$e^-_{(aq)}$ with carbonate ion although solvated electron reacts with bicarbonate ion and a well-known fast reaction with carbon dioxide [113]. H_2O_2 slowly decomposes itself in alkaline carbonate solution without any influence on carbonate ion. Moreover, it can be noticed that $^\bullet OH$ and H_3O^+ have a known effect by pH changes and O_2 and N_2O can be used as scavenger for the solvated electron. Therefore, the carbonate radical seems to be the radical species the most interesting to be studied for our work in order to understand the radiolysis of carbonate ion.

C.4.2. Decay of carbonate radical

The decay of carbonate radical at room temperature is relatively slow, with a rate constant of 1.4×10^7 $l.mol^{-1}s^{-1}$. Carbonate decay shows temperature dependence at low and high temperature [115]. Figure I.7 shows time-dependent profiles of carbonate radical for $NaCO_3$ and $NaHCO_3$ at 633 nm. As it is shown in Figure I.8, the rate constant decreases slightly for both $NaCO_3$ and $NaHCO_3$ with temperature increasing. Then, the rate constant

increases for a temperature above 150°C and the value at 400°C is about two orders of magnitude higher. It should be noted that at 400°C, the rate constant of decay becomes independent of solute concentration.

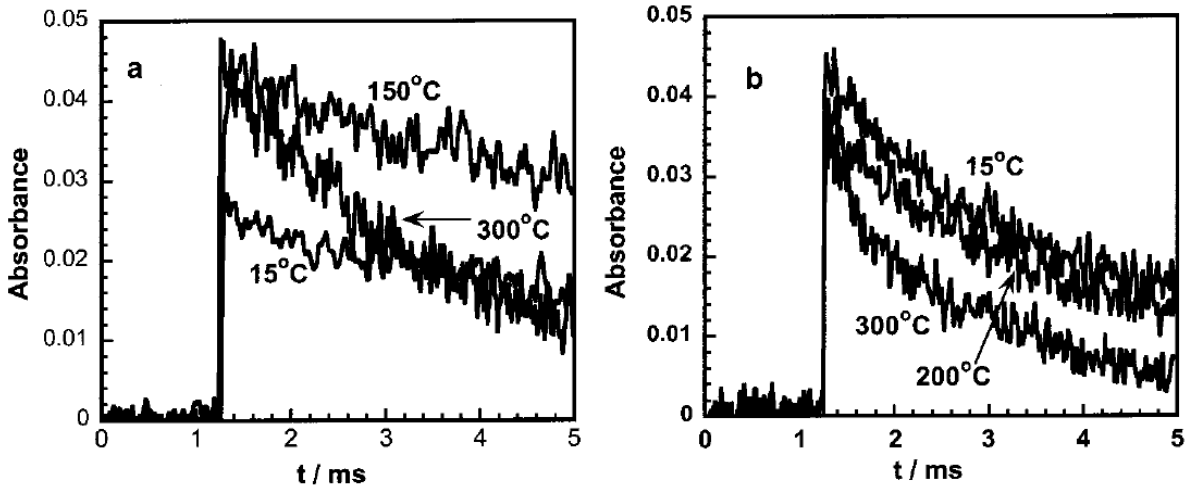

Figure I.7: *Time profiles of the carbonate radical in (a) [$NaHCO_3$] = 2×10^{-2} mol.l^{-1} and (b) [Na_2CO_3] = 5×10^{-3} mol.l^{-1} solutions at 250 atm. N_2O saturated, dose = 30 Gy per pulse [121].*

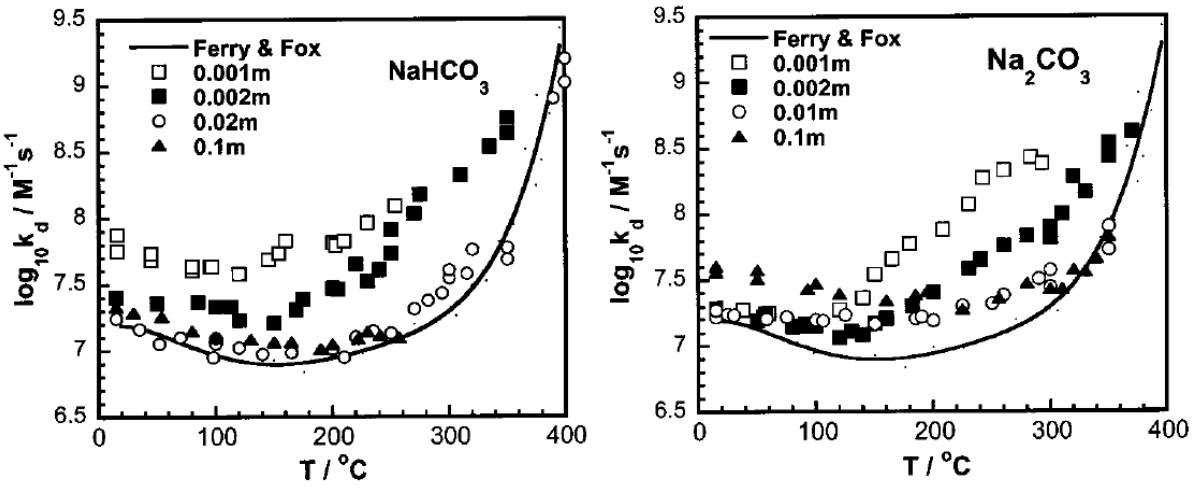

Figure I.8: *Temperature dependence of the second-order decay rate constant of the carbonate radical in $NaHCO_3$ and Na_2CO_3 solutions (up to 300 °C, P = 250 atm); higher than 300 °C, P= 350 atm) [121].*

The carbonate anion radical decay follows a second-order kinetic and its rate become faster in bicarbonate solution with concentration below 0.02 mol.l^{-1} at all temperatures [115]. Moreover, the carbonate anion radical reacts with itself and produces the dimer thorough the below reaction:

$CO_3^{\bullet-} + CO_3^{\bullet-} \leftrightarrow C_2O_6^{2-} \rightarrow$ products (I-19)

In some other works, other possibilities are suggested [110]:

$CO_3^{\bullet-} + CO_3^{\bullet-} \rightarrow CO_2 + CO_4^{2-}$ (I-20)

$CO_3^{\bullet-} + CO_3^{\bullet-} \rightarrow 2CO_2 + H_2O^- + HO^-$ (in presence of H_2O) (I-21)

At latest stages of carbonate anion radical decay, H_2O_2 production cause deviation from second-order decay kinetic [123]. Thus, the production of H_2O_2 brings the dominant reaction described below:

$CO_3^{\bullet-} + H_2O_2 \rightarrow HCO_3^- + O_2^{\bullet-} + H^+$ (I-22)

So, the produced superoxide will be participated also in carbonate anion decay [113]:

$CO_3^{\bullet-} + O_2^{\bullet-} \rightarrow CO_5^{2-}$ (I-23)

$CO_5^{2-} \rightarrow CO_3^{2-} + O_2$ (I-24)

The CO_5^{2-} species has been considered as stable for several seconds. Under the experimental conditions of most pulse radiolysis experiments, the decay of peroxymonocarbonate (HCO_4^-) into H_2O_2 and bicarbonate is essentially irreversible, but takes several thousand seconds. More decay reaction are suggested in previous investigations [110]:

$CO_3^{\bullet-} + HCO_4^- \rightarrow HCO_3^- + CO_4^{\bullet-}$ (I-25)

$CO_3^{\bullet-} + CO_4^{2-} \rightarrow CO_3^{2-} + CO_4^{\bullet-}$ (I-26)

$CO_3^{\bullet-} + CO_4^{\bullet-} \rightarrow C_2O_7^{2-}$ (I-27)

Table I.7 shows the growth and the decay reactions of carbonate radical. This table shows that the reaction rate of hydrogen radical with hydroxyl radical is twenty-fold faster than for the carbonate with hydroxyl radical. Then, the recombination of hydroxyl radical is twenty-fold faster than hydroxyl radical and carbonate reaction. Finally, the decay of carbonate, in absence of oxygen or other oxidant agents is done through recombination which resulting carbon dioxide and CO_4^{2-} that react rapidly with carbonate radical.

Table I.7: *Formation and decay reactions of carbonate radical [113].*

reaction	rate constant (M^{-1} s^{-1})
Carbonate Growth Kinetics	
$\cdot OH + CO_3^- \rightarrow \cdot CO_3^- + OH^-$	4.0×10^8
$\cdot OH + HCO_3^- \rightarrow \cdot CO_3^- + H_2O$	1.0×10^7
$\cdot H + OH^- \rightarrow (e^-)_{aq} + H_2O$	2.5×10^7
$(e^-)_{aq} + N_2O \rightarrow N_2 + OH^- + \cdot OH$	9.0×10^9
$\cdot OH + \cdot OH \rightarrow H_2O_2$	4.3×10^9
$\cdot OH + \cdot CO_3^- \rightarrow HOOCO_{2\cdot}$	$6.5 \pm 1.5 \times 10^9$
$\cdot H + \cdot OH \rightarrow H_2O$	9.7×10^9
$\cdot H + \cdot CO_3^- \rightarrow HCO_3^-$	2.5×10^9
Carbonate Decay Kinetics	
$\cdot CO_3^- + \cdot CO_3^- \rightarrow CO_2 + CO_4^{2-}$	$k_0 = 4.25 \pm 0.4 \times 10^6$
$\cdot CO_3^- + H_2O_2 \rightarrow \cdot HO_2 + HCO_3^-$	8×10^5
$\cdot CO_3^- + HO_2^- \rightarrow \cdot O_2^- + HCO_3^-$	
$\cdot CO_3^- + \cdot O_2^- \rightarrow CO_5^{2-}$	$k_0 = 2.0 \pm 0.2 \times 10^8$
$\cdot CO_3^- + HCO_4^- \rightarrow HCO_3^- + \cdot CO_4^-$	
$\cdot CO_3^- + CO_4^{2-} \rightarrow CO_3^{2-} + \cdot CO_4^-$	
$\cdot CO_3^- + \cdot CO_4^- \rightarrow C_2O_7^{2-}$	$k_0 = 1.0 \times 10^9$

In order to summarize this part dedicated to the radiolysis of carbonate, the carbonate radical is formed by indirect radiolysis of carbonate solution through reaction of carbonate or bicarbonate with hydroxyl radical. This carbonate radical is a powerful oxidant (1.78 V at pH = 7.0). Moreover, the radiolysis of carbonate solution induces a mixture of reducing and oxidizing agents. That is the reason why, metals, depending on their redox potential, can be reduced and/or oxidized in carbonate solution under irradiation.

D. Overview of this chapter

- ^{99}Tc is a β emitter nuclide with a half-life of 2.11×10^5 years and $E_{\beta\text{-max.}} = 295.5$ keV. The concentration of ^{99}Tc can be considered as an environmental matter and is measured regularly in maritime zones due to the nuclear tests in the past years.
- Technetium can be stabilized by reduction and change its oxidation state following by complexation in carbonate media for example.
- The radiolysis phenomena can be used as a tool for oxidation/reduction reactions and complexation of technetium. Using different sources of irradiation with different LET

values and energies bring the possibility to understand oxidation/reduction mechanisms.

- Carbonate solutions can be used for the synthesis of carbonate complexes of technetium with lower oxidation states toward oxidation state +VII.
- As technetium is a radioelement and it needs special regulation for running an experiment therefore the experiments should be carried out on its chemical homologous. In this study manganese and rhenium are considered as homologous of technetium due to their close chemical properties. Moreover, the redox potential of technetium is between manganese and rhenium
- In order to understand the mechanism inducing the speciation of manganese and also technetium in carbonate solutions under irradiation, it is necessary to study the radiolysis of highly concentrated carbonate media.
- From the literature, there is no data about pulse radiolysis experiments of concentrated carbonate solutions. Thus, in the aim of this study, we will perform pulse radiolysis of concentrated carbonate solution.
- After the understanding of the kinetics of formation and decay of carbonate radical, the speciation under irradiation of manganese and rhenium, as Tc homologous, should be carried out in concentrated carbonate solutions.
- At the end the speciation of the technetium under irradiation will be carried out in concentrated carbonate solutions and the structure of the complex formed is defined and characterized.

References

1. Kessler, K.G. and R.E. Trees, *The Nuclear Moments of Technetium-99.* Physical Review, 1953. **92**: p. 303-307.
2. Bergquist, B.A., et al., *Technetium measurements by accelerator mass spectrometry at LLNL.* Nuclear Instruments and Methods in Physics Research B 2000. **172**: p. 328-332.
3. C.S.Dileep, P.J., P.S. Dhami, P.V. Achuthan, A. Dakshinamoorthy, B.S. Tomarb, S.K. Munshi, P.K. Dey, *Distribution of technetium in PUREX process streams.* De salination, 2008. **232**: p. 157-165.
4. Targholizadeh, H., et al., *Cyclotron production of technetium radionuclides using a natural metallic molybdenum thick target and consequent preparation of [Tc]-BRIDA as a radio-labelled kit sample.* Nucleonika 2010. **55**: p. 113-118.
5. Millon, C., et al., *Table des radionucléides*. 2012, CEA.
6. Chmutova, M.K., et al., *Extraction of Actinides from HNO3 Solutions with Solutions of Dialkyl Methylphosphonates.* Radiochemistry, 2002. **44**(3): p. 261-265.
7. Mashkin, A.N., K.K. Korchenkin, and N.A. Svetlakova, *Technetium Distribution throughout Purex Process Cycles at RT-1 Plant.* Radiochemistry, 2002. **44**(1): p. 35-41.
8. Svantesson, et al., *Distribution rations and empirical equations for the extraction of elements in PUREX high level waste solution.* J. Inorg Nucl Chem., 1979. **41**: p. 383-389.
9. Gilliam, T.M. and R.D. Spence, *Solidification/stabilization of technetium in cement-based grouts* Journal of Hazardous Materials, 1990. **24**: p. 189-197.
10. Moore, C.E., *Technetium in the Sun.* Science 1951. **114**: p. 59-61.
11. Takahashi, K., G.J. Mathcms, and S.D. Bloom, *Shell-model calculation of Tc beta decay in astrophysical envirotitrients.* Physical Review C, 1986. **33**: p. 296-301.
12. F.Kappler, R.G., M.Busso, G.Piccio and C.M.Raiteri, *s-process nucleosynthesis: classical approach and asymptotic giant branch models for low mass stars* The Astorophysical Journal, 1990. **354**: p. 630-641.
13. Uchida S, et al., *Concentrations levels of technetium-99 in forest soils collected within the 30-km zone around the Chernobyl reactor.* Environ Pollut., 1999. **105**: p. 75-77.
14. Mc Cubbin D, et al., *Further studies of the distribution of technetium-99 and caesium-137 in UK and European coastal waters.* Cont Shelf Res, 2002. **22**: p. 1417-1445.
15. Echevarria G, et al., *Bioavailability of technetium-99 as affected by plant species and growth, application form, and soil incubation.* Journal of Environmental Quality, 1997. **26**: p. 947-956.
16. J. R. Lloyd, V.A.S., C. V. G. Van Praagh, and D. R. Lovley, *Direct and Fe(II)-Mediated Reduction of Technetium by Fe(III)-Reducing Bacteria.* Applied and Environmental Microbiology, 2000. **66**: p. 3743-3749.
17. Gu BS and Schulz RK, *Anion retention in soil: a reveiw. Application to reduce migration of buried technetium and iodine*. 1991, Office of Nuclear Regulatory Research, US Nuclear Regulatory Commission.
18. Lloyd JR, et al., *Direct and Fe(II)-mediated reduction of technetium by Fe(III)-reducing bacteria.* Appl Environ Microbiol, 2000. **66**: p. 3743-3749.
19. Van Loon L and Lembrechts JF, *Technetium in the environment* 1986, London, New-york: Elsevier Applied Science Publishers
20. Lieser KH and Bauscher C, *Technetium in the hydrosphere and in the geosphere.* Radiochimica Acta, 1987. **42**: p. 205-213.

21. Kershaw PJ, McCubbin D, and Leonard KS, *Continuing contamination of north Atlantic and Arctic waters by Sellafield radionuclides.* Science of the Total Environment, 1999. **237/238**: p. 119-132.
22. Shia, K., et al., *Determination of technetium-99 in environmental samples: A review.* Analytica Chimica Acta 2012. **709**: p. 1-20.
23. Wildung, R.E., et al., *Effect of Electron Donor and Solution Chemistry on Products of Dissimilatory Reduction of Technetium by Shewanella putrefaciens.* Applied and Environmental Microbiology, 2000. **66**: p. 2451-2460.
24. Beasley, T. M. Lorz, and H.V. Gonor, *Biokinetic Behavior of Technetium in the Red Abalone, Haliotis Rufescens: A Re-assessment.* The Radiation Safety Journal Health Physics, 1982. **43**: p. 501-507.
25. Swift, D.J., *The Accumulation of 95mTc from Sea Water by Juvenile Lobsters (Homarus gammarus L.).* J. Environ. Radioactivity, 1985. **2**: p. 229-243.
26. Aarkrog, A., et al., *Origin of technetium-99 and its use as a marine tracer.* Nature 1988. **335**: p. 338-340.
27. CEFAS, *Radioactivity in Food and the Environment*, in *RIFE-15*. 2009.
28. Matsuura, N. and H. Yumoto, *Deposition Potential of 99Tc from Alkaline Solution and its Application to Standard Pure B Source on thin Metallic Foil.* Radioisotopes, 1959. **8**: p. 28-33.
29. Shoemake, G.R., D.C. Fenimore, and A. Zlatkis, *Radiation Sources for lonization Detectors in Gas Chromatography.* Journal of Chromatographic Science, 1965. **3**(8): p. 285-286.
30. Kubicka, H., *The Specific Activity of Technetium, Rhenium, Ruthenium, Platinum, and Palladium in Catalytic Reactions of Benzene with Hydrogen.* Journal of Catalysis 1968. **12**: p. 223-237.
31. Anthony, J., Thomas, and A. Davison, *High oxidation state technetium and rhenium complexes of hydrotris(1-pyrazolyl)borate.* Inorganica Chimica Acra, 1991. **190**: p. 231-235.
32. Cartledge, G.H., *Twenty-Year Inhibition of Corrosion by the Pertechnetate Ion.* Corrosion, 1973. **29**: p. 361-362.
33. Abram, U. and R. Alberto, *Technetium and Rhenium - Coordination Chemistry and Nuclear Medical Applications.* J. Braz. Chem. Soc., 2006. **17**: p. 1486-1500.
34. Lide, D.R. and H.D.R. Frederiks, *CRC Handbook of Chemistry and Physics*, ed. 75. 1994/95: CRC Press. 11-59.
35. Meyer, R.E. and W.D. Arnold, *The Electrode Potential of the Tc(IV)-Tc(VII) Couple.* Radiochimica Acta 1991. **55**: p. 19-22.
36. Chotkowski, M. and A. Czerwinski, *Electrochemical and spectroelectrochemical studies of pertechnetate electroreduction in acidic media.* Electrochimica Acta 2015. **76**: p. 165-173.
37. Chotkowski, M. and A. Czerwinski, *Thin layer spectroelectrochemical studies of pertechnetate reduction on the gold electrodes in acidic media.* Electrochimica Acta 2014. **121**: p. 44-48.
38. Poineau, F., et al., *On the nature of heptavalent technetium in concentrated nitric and perchloric acid.* Inorganica Chimica Acta, 2013. **398**: p. 147-150.
39. Rao, P.N., et al., *Sodium pertechnetate in the detection of gastric cancer.* Radiography, 1999. **5**: p. 49-52.
40. Schwochau, K., *The Present Status of Technetium Chemistry.* Radiochimica Acta 1982. **32**: p. 139-152.
41. Boyd, G.E., *Osmotic and activity coefficients of aqueous pertechnetic acid and perrhenic acid solutions at 25.degree.C.* Inorganic Chemistry 1978. **7**: p. 229-238.

42. Abdelouas, A., et al., *Microbial reduction of 99Tc in organic matter-rich soils.* Science of The Total Environment, 2005. **336**(1-3): p. 255-268.
43. Abdelouas, A., et al., *Precipitation of technetium by subsurface sulfate-reducing bacteria.* Radiochimica Acta, 2002. **90**: p. 773-777.
44. Poineau, F., et al., *Reactivity of HTcO4 with methanol in sulfuric acid: Tc-sulfate complexes revealed by XAFS spectroscopy and first principles calculations.* Dalton Transactions, 2013. **42**(13): p. 4348-4352.
45. Poineau, F., et al., *Speciation of technetium and rhenium complexes by in situ XAS-electrochemistry.* Radiochimica Acta, 2006. **94**: p. 283-289.
46. Tumanova, D.N., et al., *Formation of technetium peroxides in anhydrous sulfuric acid.* J. Dokl. Phys. Chem, 2008. **420**: p. 114-117.
47. Rard, J.A., *Critical Review of the Chemistry and Thermodynamics of Technetium and Some of its Inorganic Compounds and Aqueous Species*, in *UCRL-53440*. 1983.
48. Cotton, F.A., et al., *Preparation and structural characterization of salts of oxotetrachlorotechnetate(V).* Inorganic Chemistry, 1979. **18**: p. 3024-3029.
49. Rudy W. Thomas , A.D., Harvey S. Trop , Edward Deutsch, *Technetium radiopharmaceutical development. 2. Preparation, characterization, and synthetic utility of the oxotetrahalotechnetate(V) species TcOX4- (X = chloro, bromo, iodo).* inorganic Chemistry, 1980. **19**: p. 2840-2842.
50. Denden, I., et al., *Behavior of Heptavalent Technetium in Sulfuric Acid under Î±-Irradiation: Structural Determination of Technetium Sulfate Complexes by X-ray Absorption Spectroscopy and First Principles Calculations.* The Journal of Physical Chemistry A, 2014. **118**(9): p. 1568-1575.
51. Eriksen, T.E., et al., *The Solubility of Tc02 · nH20 in Neutral to Alkaline Solutions under Constant pco2.* Radiochimica Acta 1992. **58**: p. 67-70.
52. Vichot, L., et al., *XAS study of technetium(IV) polymer formation in mixed sulphate/chloride media.* Radiochimica Acta, 2002. **90**: p. 575-579.
53. Kawashima, M., M. Koyama, and T. Fujinaga, *Aquation of Hexalogeno Technetium(IV).* J. Inorg. Nucl. Chem. , 1976. **38**: p. 819-822.
54. Ianovici, E., et al., *The Aquation of Hexachloro Technetate(IV).* Yournai of Radioanalyticai Chemistry, Vol. 64, No. 1-2 (1981) 315-326, 1981. **61**(1-2): p. 315-326.
55. Poineau, F., et al., *Condensation mechanisms of tetravalent technetium in chloride media.* Radiochimica Acta, 2006. **94**: p. 291-299.
56. Poineau, F., M. Fattahi, and B. Grambow, *Photochemical behaviour of $Tc_2OCl_{10}^{4-}$ and $Tc_nO_y^{4n-2y+}$ in chloride media.* Radiochimica Acta, 2006. **94**: p. 91-95.
57. Denden, I., R. Essehli, and M. Fattahi, *Spectrophotometric study of the behaviour of pertechnetate in trifluoromethanesulfonic acid: effect of alpha irradiation on the stability of Tc(VII).* Journal of Radioanalytical and Nuclear Chemistry, 2013. **296**(1): p. 149-155.
58. Alliot, I., et al., *Speciation of Technetium(IV) in Bicarbonate Media.* Environmental Science & Technology, 2009. **43**(24): p. 9174-9182.
59. Aquettaen, J. and D.W. Lawrence, *A spectro-electrochemical study of the technetium(IV)/technetium(III) couple in bicarbonate solutions.* Can. J. Chem, 1985. **63**: p. 2369-2373.
60. Poineau, F., et al., *Synthesis and Structure of Technetium Trichloride.* Journal of the American Chemical Society, 2010. **132**(45): p. 15864-15865.
61. Housecroft, C.E., *Technetium 1992.* Coordination Chemistry Reviews 1995. **142**: p. 21-41.

62. Ben Said, K., et al., *γ radiation effects on potassium pertechnetate in carbonate media.* Applied Radiation and Isotopes, 2001. **54**(1): p. 45-51.
63. Bruno, J., *The influence of dissolved carbon dioxide on trace metal speciation in seawater.* Marine Chemistry, 1990. **30**: p. 231-240.
64. Aisha, U., Qamruzzaman, and M.Z.A. Rafiquee, *Kinetics of Reduction of ColloidalMnO2 by Glyphosate in Aqueous and Micellar Media.* International Journal of Inorganic Chemistry, 2011. **2011**: p. 1-6.
65. Clares, M.P., et al., *Mn(II) complexes of scorpiand-like ligands. A model for the MnSOD active centre with high in vitro and in vivo activity.* Journal of Inorganic Biochemistry, 2015. **143**: p. 1-8.
66. Cai, J., et al., *Assembling fabrication and capacitance of manganese oxide nanosheets and functionalized carbon nanotubes hybrid material.* Colloids and Surfaces A: Physicochem. Eng. Aspects, 2013. **429**: p. 91-97.
67. Ting, T.-H., et al., *Optimisation of the electromagnetic matching of manganese dioxide/multi-wall carbon nanotube composites as dielectric microwave-absorbing materials.* Journal ofMagnetismandMagneticMaterials, 2013. **339**: p. 100-105.
68. Cai, J., et al., *Enhanced activity of Pt nanoparticle catalysts supported on manganese oxide-carbon nanotubes for ethanol oxidation.* i n t e rna t i onal journal o f hydrogen energy 2014. **39**: p. 798-807.
69. Saputra, E., et al., *Manganese oxides at different oxidation states for heterogeneousactivation of peroxymonosulfate for phenol degradation inaqueous solutions.* Applied Catalysis B: Environmental 2013. **142-143**: p. 729-735.
70. Li, J., et al., *Controlled synthesis of diverse manganese oxide-based catalysts for complete oxidation of toluene and carbon monoxide.* Chemical Engineering Journal 2014. **244**: p. 59-67.
71. Ramesh, K., et al., *Re-investigating the CO oxidation mechanism over unsupported MnO, Mn2O3 and MnO2 catalysts.* Catalysis Today 2008. **131**: p. 477-482.
72. Phuoc Hoang Ho , S.C.L., Jieun Kimb, Doohwan Lee , Hee ChulWoo, *Properties of a manganese oxide octahedralmolecular sieve (OMS-2) for adsorptive desulfurization of fuel gas for fuel cell applications.* Fuel Processing Technology 2015. **131**: p. 238-246.
73. Wu, G., et al., *Catalytic oxidation of benzyl alcohol over manganese oxide supported on MCM-41 zeolite.* Chemical Engineering Journal, 2015. **In Press**.
74. Chae, Y., J.K. Lee, and W. Choi, *Surface coating of spinel LiMn2O4 cathode electrode with lithium–nickel–manganese-oxide by RF sputtering method for lithium-ion batteries.* Journal of Electroanalytical Chemistry, 2014. **730**: p. 20-25.
75. Malcolm, H.M. and S. Dobson, *Manganese and its Compounds: Environmental Aspects*, in *LC/NLM Classification: QV 290*. 2005, the International Labour Organization, or the World Health Organization.
76. Strickland, J.D.H. and G. Spicer, *A note on the distillation of permangenic acid from sulfuric acid.* Analytica Chimica Acta, 1949. **3**: p. 543-546.
77. ROYER, D.J., *Evidence for the existence of the permanganyl ion in sulphuric acid solutions of potassium permanganate* J. Inorg. and Nucl. Chem., 1961. **17**: p. 159-167.
78. Briggs, T.S., *New and unusual compounds of manganese: MnO3Cl, MnO2Cl2 and MnOCl3 with remarks on Mn2O7.* Journal of Inorganic and Nuclear Chemistry, 1968. **30**: p. 2866-2869.
79. Levason, W. and C.A. McAuliffe, *Higher oxidation state chemistry of manganese.* Coonimatzon Chemrsny Revtews, 1972. **7**: p. 353-384.
80. Punnamchandar Ramidi, et al., *Synthesis and characterization of manganese(III) and high-valent manganese-oxo complexes and their roles in conversion of alkenes to cyclic carbonates.* Journal of CO2 Utilization, 2015. **9**: p. 48-57.

81. Jessica M. Terry, et al., *Chemiluminescence detection of aminoacids and related compounds using acidic potassium permanganate, manganese(IV) or tris (2,20-bipyridine) ruthenium(III).* Talanta, 2012. **99**: p. 1051-1056.
82. Zoe M. Smith, et al., *Ethanol as an alternative to formaldehyde for the enhancement of manganese(IV) chemiluminescence detection.* Talanta, 2014. **130**: p. 221-225.
83. Kim, D.W., et al., *Magnesium isotope separation by ion exchange using hydrous manganese(IV) oxide.* Talanta, 2002. **57**: p. 701-705.
84. Pastor, T.J. and F.T. Pastor, *The role of manganese(IV) compounds as oxidants — a review.* Talanta, 2000. **52**: p. 959-970.
85. Yousefi, T., et al., *Synthesis, characterization, and super capacitor studies of manganese(IV) oxide nanowires.* Materials ScienceinSemiconductorProcessing, 2013. **16**: p. 868-876.
86. Gabriela N. Ledesma , H.E., Elodie Anxolabéhère-Mallart , Christelle Hureau , Sandra R. Signorella, *A new mononuclear manganese(III) complex of an unsymmetrical hexadentate N3O3 ligand exhibiting superoxide dismutase and catalase-like activity: synthesis, characterization, properties and kinetics studies.* Journal of Inorganic Biochemistry, 2015. **146**: p. 69-76.
87. Saeedi, M.S., et al., *Magnetic nanoparticles supported manganese(III) tetrapyridylporphyrin catalyst via covalent interaction: A highly efficient and reusable catalyst for the oxidation of hydrocarbons.* Polyhedron, 2013. **49**: p. 158-166.
88. Chen, L., et al., *Manganese(III) complexes of novel chiral unsymmetrical BINOL-Salen ligands: Synthesis, characterization, and application in asymmetric epoxidation of olefins.* Applied Catalysis A: General, 2012. **415-416**: p. 40-46.
89. Penkova, L., et al., *Binuclear manganese(III) complexes of an unsymmetric pyrazolate-based compartmental ligand with hard donor set.* Inorganica Chimica Acta, 2010. **363**: p. 3036-3040.
90. Machura, B., et al., *Manganese(II) complexes of 2,3,5,6-tetra-(2-pyridyl)pyrazine – Syntheses, crystal structures, spectroscopic, magnetic and catalytic properties.* Polyhedron, 2013. **53**: p. 132-143.
91. Mohammad Mahdi Najafpour , M.H.s., Amir Nasser Shamkhali , Mojtaba Amini , Sayed Habib Kazemi , Sasan Zaynalpoor , Rahim Mohamadi , Mojtaba Bagherzadeh , Tadeusz Lis, *New mononuclear manganese(II) complexes with 2,4,6-tris(2-pyridyl)-1,3,5-triazine (tptz) – selective catalyst in UHP oxidation of sulfides.* Polyhedron, 2012. **34**: p. 202-209.
92. Ruma Dey Ghosh , K.B., Satyajit Das , Avishek Ganguly , Paramita Chakraborty , Avijit Sarkar , Mitali Chatterjee , Soumitra K. Choudhuri, *A novel manganese complex, Mn-(II) N-(2-hydroxy acetophenone) glycinate overcomes multidrug-resistance in cancer.* European Journal of Pharmaceutical Sciences, 2013. **49**: p. 737-747.
93. Hayes, T.R., et al., *Influence of Functionalized Pyridine Ligands on the Radio/Chemical Behavior of [MI(CO)3]+ (M = Re and 99mTc) 2 + 1 Complexes.* Inorganic Chemistry, 2015. **54**: p. 1528-1534.
94. Lume-Pereira, C., et al., *Chemistry of colloidal manganese dioxide.1.Mechanism of reduction by an organic radical (a radiation chemicalstudy).* J.Phys.Chem., 1985. **89**: p. 5772-5778.
95. Khan, S.A. and Z. Khan, *Formation of nanosize water-soluble colloidal MnO2: a kinetic study.* Journal of Experimental Nanoscience, 2011. **6**(2): p. 149-158.
96. Puspalata, R., et al., *Gamma radiation induced formation and characterization of the nano-oxides of manganese.* Radiation Physics and Chemistry, 2013. **85**: p. 152-160.

97. Liu, Y.P., et al., *γ-Ray radiation preparation and characterization of nanocrystalline manganese dioxide.* Mater.Res.Bull, 1997. **32**(8): p. 1055–1062.
98. Pooja Yadav , R.O., MatsJonsson, *Synthesis and characterization of MnO2 colloids.* Radiation Physics and Chemistry, 2009. **78**: p. 939-944.
99. Abulikemu Abulizi , G.H.Y., Kenji Okitsu a, Jun-Jie Zhu, *Synthesis of MnO_2 nanoparticles from sonochemical reduction of $MnO4^-$ in water under different pH conditions.* Ultrasonics Sonochemistry 2014. **21**: p. 1629-1634.
100. S. Baral , C.L.-P., E. Janata , A. Henglein, *Chemistry of colloidal manganese dioxide. 2. Reaction with superoxide anion (O_2^-) and hydrogen peroxide (pulse radiolysis and stop flow studies).* J. Phys. Chem., 1985. **89**(26): p. 5779-5783.
101. Jonsson, M., et al., *Radiation Induced Spent Nuclear Fuel Dissolution under Deep Repository Conditions.* Environ. Sci. Technol. , 2007. **41**: p. 7087-7093.
102. Burns, P.C., R.C. Ewing, and A. Navrotsky, *Nuclear Fuel in a Reactor Accident* Science, 2012. **335**: p. 1184-1188.
103. Stpotheim-Maurizot, M., et al., *Radiation chemistry from basics to applications in material and life sciences*. 2008: EDP Science.
104. Hatano, Y., Y. Katsumura, and A. Mozumder, *Charged Particle and Photon Interactions with Matter*. book. 2011, Boca Raton, USA: CRC Press.
105. Baldacchino, G., et al., *Effets de TEL dans la radiolyse de l'eau. Expériences de radiolyse pulsée avec les ions lourds.* J. Chim. Phys., 1999. **96**(1): p. 50-60.
106. Augusto, O., et al., *Nitrogen dioxide and carbonate radical anion: two emerging radicals in biology.* Free Radical Biology & Medicine, 2002. **32**(9): p. 841-859.
107. Alvarez, M.N., et al., *Reaction of the carbonate radical with the spin-trap 5,5-dimethyl-1-pyrroline-N-oxide in chemical and cellular systems: Pulse radiolysis, electron paramagnetic resonance, and kinetic-competition studies.* Free Radical Biology & Medicine 2007. **43**: p. 1523-1533.
108. Merouani, S., et al., *Influence of bicarbonate and carbonate ions on sonochemical degradation of Rhodamine B in aqueous phase.* Journal of Hazardous Materials, 2010. **175**: p. 593-599.
109. Mazellier, P., et al., *A comparison of fenuron degradation by hydroxyl and carbonate radicals in aqueous solution.* water research, 2007. **41**: p. 4585-4594.
110. Weeks, J.L. and J. Rabani, *The pulse radiolysis of deaerated aqueous carbonate solutions. I. transient optical spectrum and mechanism. II. pK for OH radicals.* The Journal of Physical Chemistry, 1966. **70**: p. 2100.
111. Lymar, S.V., H.A. Schwarz, and G. Czapski, *Medium e ects on reactions of the carbonate radical with thiocyanate, iodide, and ferrocyanide ions.* Radiation Physics and Chemistry, 2000. **59**: p. 387-392.
112. Lymar, S.V. and H.A. Schwarz, *acidity of the carbonate radical.* J. Phys. Chem. A, 1999. **103**: p. 3447-3450.
113. Haygarth, K.S., et al., *Carbonate Radical Formation in Radiolysis of Sodium Carbonate and Bicarbonate Solutions up to 250 °C and the Mechanism of its Second Order Decay.* J. Phys. Chem. A, 2010. **114**: p. 2142-2150.
114. Al-Assaf, S., et al., *Chain scission of hyaluronan by carbonate and dichloride radical anions: Potential reactive oxidative species in inflammation?* Free Radical Biology & Medicine 2006. **40**: p. 2018-2027.
115. Wu, G., et al., *temperature dependence of carbonate radical in NaHCO3 and Na2CO3 solutions: is the radicala single anion?* J. Phys. Chem. A, 2002. **106**: p. 2430-2437.
116. Hatano, Y., Y. Katsumura, and A. Mozumder, *Charged particle and photon interactions with matter, recent advances, applications and interfaces*. 2011: Taylor and Francis Group, LLC.

117. Wu, C. and K.G. Linden, *Photo transformation of selected organophosphorus pesticides: Roles of hydroxyl and carbonate radicals.* water research, 2010. **44**: p. 3585-3594.
118. Zegota, H., *The e ect of g-irradiation on citrus pectin in N_2O and N_2O/O_2 saturated aqueous solutions.* Food Hydrocolloids 1999. **13**: p. 51-58.
119. Buxton, G.V., N.D. Wood, and S. Dyster, *Ionisation constants of ˙OH and HO˙2 in aqueous solution up to 200 °C. A pulse radiolysis study.* J. Chem. Soc., Faraday 1988. **84**: p. 1113-1121.
120. Bohn, H.L., B.L. McNeal, and G.A. O'Connor, *Soil Chemistry*. 3rd Edition ed. 2001: Wiley
121. Guozhong Wu, et al., *Temperature Dependence of Carbonate Radical in NaHCO3 and Na2CO3 Solutions: Is the Radical a Single Anion?* J. Phys. Chem. A 2002. **106**: p. 2430-2437.
122. Cai, Z., et al., *radiolysis of bicarbonate and carbonate aqueous solutions: product analysis and simulation of radiolytic processes.* Radioactive waste managment and disposal, 2001. **136**: p. 2010231-240.
123. Behar, D., G. Czapski, and I. Duchovny, *Carbonate radical in flash photolysis and pulse radiolysis of aqueous carbonate solutions.* J. Phys. Chem., 1970. **10**: p. 2206-2210.

Chapter II: Material & Methods

This chapter is dedicated to the experimental techniques used during this work which deals with the study for oxidation/reduction of Mn, Tc and Re in highly concentrated carbonate media under irradiation and their speciation. In the first part of this chapter, the irradiation sources, used in this study, are presented. Among them: (i) the ARRONAX cyclotron facility is a new research accelerator for radiochemistry and oncology at Nantes (France) that provides He^{2+} particles with high energy (68 MeV) for samples irradiation, (ii) γ source of ^{137}Cs at ARRONAX site in Nantes, (iii) γ source of ^{60}Co in Laboratoire de Chimie Physique (LCP) in Orsay (France) and electron accelerator called ELYSE at LCP in Orsay that provides electron-pulse beam on different time windows from femto to milli seconds. The second part describes the irradiation cells for γ, He^{2+} and electron pulse radiolysis. The cells are different for each type of irradiation due to their geometry and the different LET range. Except electron pulse radiolysis the cells must be connected to μ-GC for gas measurement after irradiation. The third part is dedicated to the chemical systems under irradiation. The Fricke and super Fricke dosimetry are described. Also, the preparation of concentrated carbonate , Tc(VII), Re(VII) and Mn(VII) solutions are explained. The last part gives details about the different analytical methods and electrochemistry technique as oxidation/reduction tool. During this study several analytical methods have been used that are listed in follow: UV-Vis spectroscopy, μ-gas chromatography (μGC), x-ray diffraction spectroscopy (XRD), x-ray photo emission spectroscopy (XPS), x-ray absorption near edge structure spectroscopy (XANES), extended x-ray absorption fine structure spectroscopy (EXAFS) and scanning electron microscopy (SEM). The electron paired resonance (EPR), Infrared and RAMAN spectroscopies have been used also as small part of analysis in this study and they are described in appendix.

A. Irradiation beams particle

A.1. Source of ^{137}Cs (Arronax, Nantes)

Gamma-Service Medical, model GSM D1 with ^{137}Cs as radioactive source with LET = 0.23 $keV.\mu m^{-1}$ was used for γ-ray irradiation into the ARRONAX facility laboratory. The source activity was 200 TBq at December 2012 with dose uniformity less than 10 % over a 300 mm^2. Figure II.1 shows the source with sample holders and irradiation paths. It should be noticed that there are different levels inside irradiator and the absorption of γ rays by samples is not the same in different levels even different place in the same level.

Figure II.1: *a) γ source of ^{137}Cs at Arronax facilities, b) different irradiation levels and c) schematic of reaching γ rays from the source to different levels.*

This irradiator can heat the samples with maximum 80°C (not used in this study). The irradiation time can be set up from a couple of minutes to maximum one year. ^{137}Cs decays through two different paths. 5.4 % of it decays by β^- emission to stable ^{137}Ba and the rest (94.6 %) decays by β^- emission to ^{137}Ba-m which is not stable. ^{137}Ba-m decays to ^{137}Ba by γ emission with energy of 0.661 MeV.

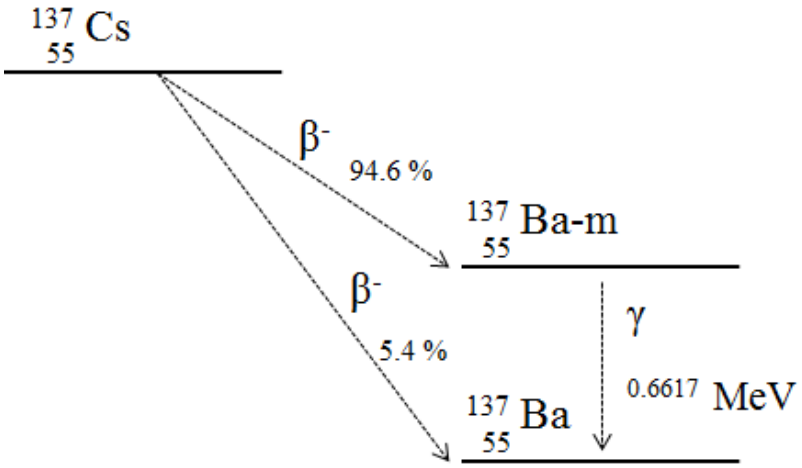

Figure II.2: *Radioactive decays of ^{137}Cs [1].*

A.2. Source of ^{60}Co (LCP, Orsay)

The γ source of ^{60}Co at laboratoire de chimie physique (LCP) is place in university Paris-sud XI in Orsay. The source is inside the cylindrical column that moves up and down by command for irradiation. It irradiates in all directions from column. The concrete walls and lead door together protect outside from γ rays.

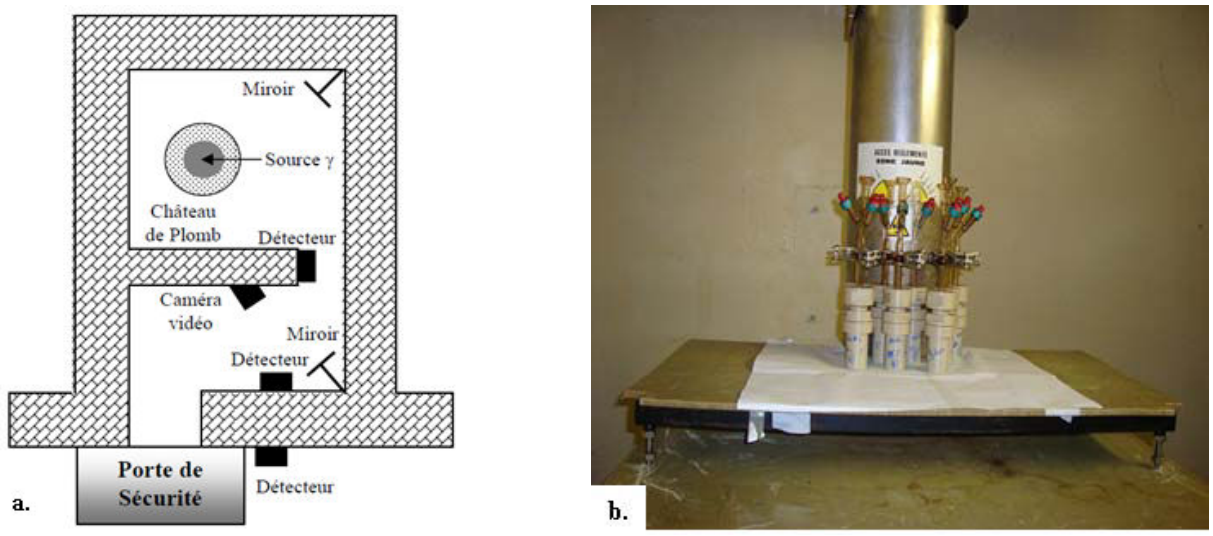

Figure II.3: *a) Schematic of ^{60}Co source at LCP, b) picture of irradiation cells used inside the source*

This set up provide the facility for irradiation of different samples at the same time with different dose rate. The initial activity of this source was 7000 Ci at 1995 but due to radioactive decay ($T_{1/2}$ = 5.27 years) it was renewed at 2011.

The ^{60}Co is an artificial radio-isotope and it obtains by neutron activation of ^{59}Co.

$$^{59}_{27}Co + {}^{1}_{0}n \longrightarrow {}^{60}_{27}Co \qquad \text{(II -1)}$$

The half-life of ^{60}Co is 5.27 years. Its emission products are β^- with energy of 0.31 MeV and two γ rays with energies of 1.14 and 1.33 MeV.

$$^{60}_{27}Co \longrightarrow {}^{60}_{28}Ni + e^- + \gamma \qquad \text{(II -2)}$$

The β^- is absorbed by the wall of the cylindrical column [1, 2].

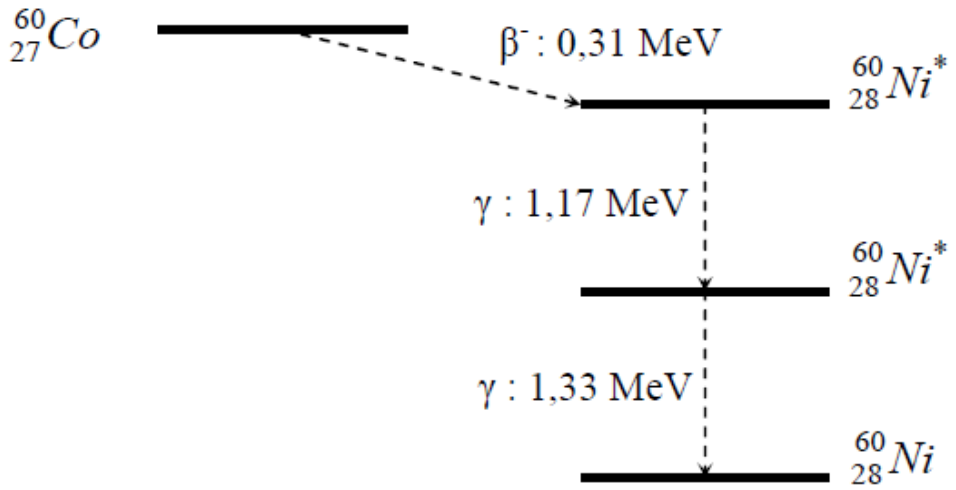

Figure II.4: *Radioactive decays of ^{60}Co [1].*

A.3. Cyclotron facility(ARRONAX, Nantes)

A cyclotron is a particle accelerator. It makes use of electric and magnetic fields in a clever way to accelerate a charge in a small space. A cyclotron consists of two D-shaped regions known as dees. In each dee there is a magnetic field perpendicular to the plane of the page. In the gap separating the dees there is a uniform electric field pointing from one dee to the other. When a charge is released from rest in the gap it is accelerated by the electric field and carried into one of the dees. The magnetic field in the dee causes the charge to follow a half-circle that carries it back to the gap. While the charge is in the dee the electric field in the gap is reversed, so the charge is once again accelerated across the gap. The cycle continues with the magnetic field in the dees continually bringing the charge back to the gap. Every time the charge crosses the gap it picks up speed. This causes the half-circles in the dees to increase in radius, and eventually the charge emerges from the cyclotron at high speed. Figure II.5 shows the schematic of one cyclotron core.

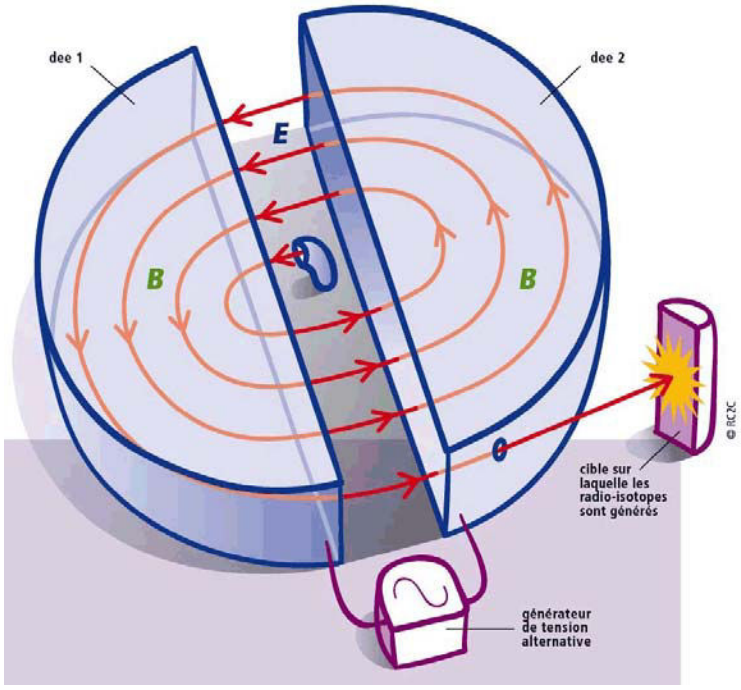

Figure II.5: *Schematic of cyclotron core during the production of charged particles [3].*

The ARRONAX cyclotron placed in Saint-Herblain close to Nantes. It is a prototype developed by IBA. This model called Cyclon® 70 (C 70) with the diameter of 4 meters and its magnetic field (maximum 1.6 Tesla) can deliver different particles with the maximum energies that are listed in Table II.1:

Table II.1: *Produced ionizing particles by ARRONAX cyclotron facility and their characteristics.*

Type of Ionizing particle	Maximum Energy (MeV)	Maximum Intensity (µA)
Negative Hydrogen H^-	70	750
Deuterium D^-	35	50
Helium He^{2+}	68.4	35

The Arronax cyclotron is composed by the core and six different vault that four of them (P1, P2, P3 and A2) are dedicated to production of radio-isotopes, one (A1) dedicated to neutron activation test and the last one (AX) is dedicated to the fundamental research (Figure II.6).

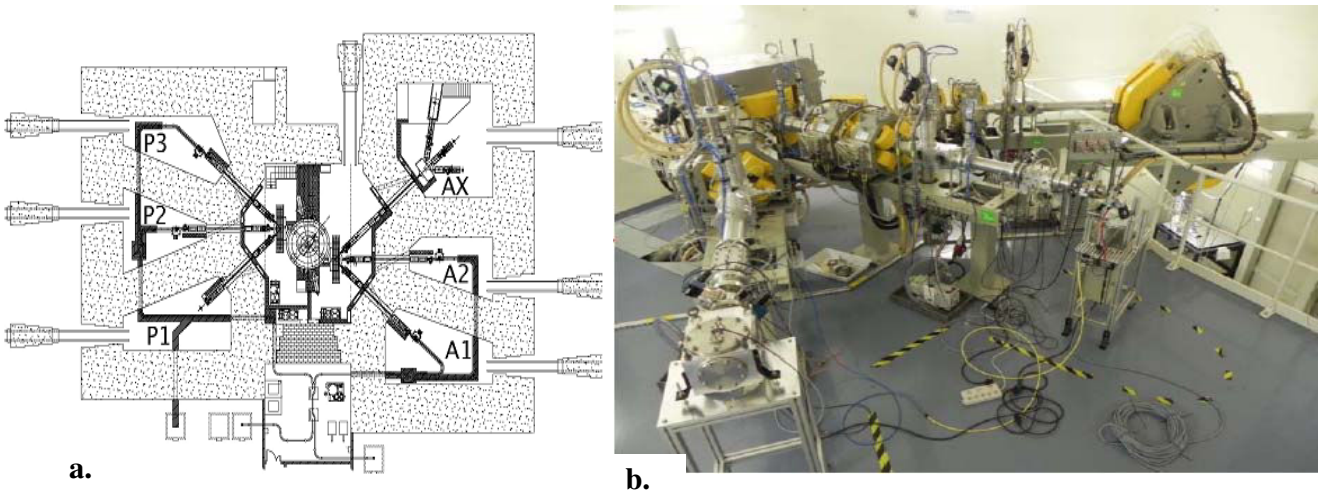

Figure II.6: *a) Map of ARRONAX cyclotron with its six vault, b) the AX4 vault for radiolysis experiments*

AX vault has three beamlines and the beamline AX4 which is the non-deviated one was used during this study. The energy deposition at this beamline is controled with a Faraday cage that has been developed by the ARRONAX staff. This system transforms the beam to electrical current. An aluminium plate (Al_2O_3) is used to pinpoint the beam by looking at the flurescence of the plate after particle collision. By that it is possible to adjust the beam direction in order to peneterate inside the samples.

A.4. Pico-second electron accelerator (LCP, Orsay)

Pico-second electron accelerator ELYSE is situated in basement of laboratoire chimie physique (LCP) in Orsay. This machine provides the pulse beam of some pico-seconds and repeat frequency higher or equal to 10 Hz for experiments in different domains such as; excited state of condensed phase, primary effects in radiolysis, surfaces, molecular biology and aggregates.

Laser pulse used to produce electrons from cesium telloride (CsTe) photocathode with good quantum efficiency (= 1%) which is well higher than metalic cathodes (0.0001 %). The diameter of the laser on photocathode is 5 mm. Electrons ejected from the photocathode are provided to electron accelerator. ELYSE use RF gun technology. Main characteristics of ELYSE are listed in Table II.2. Figure 2.7 shows the general view of ELYSE.

Table II.2: *Characteristics of ELYSE and the used laser for triggering.*

ELYSE characteristics	
Pulse duration	< 5 ps
Load per pulse	1 to 10 nC nC
Energy	4-9 MeV
Repetition frequency	50 Hz
Dispersion energy in rms	100 keV 1 % to 9 MeV
Diameter of the beam on the target	a few mm

titanium: sapphire laser	
Wavelength	790 nm giving tripled 264 nm
Mid-height width of the pulses	2 ps
Energy	70 micro joules

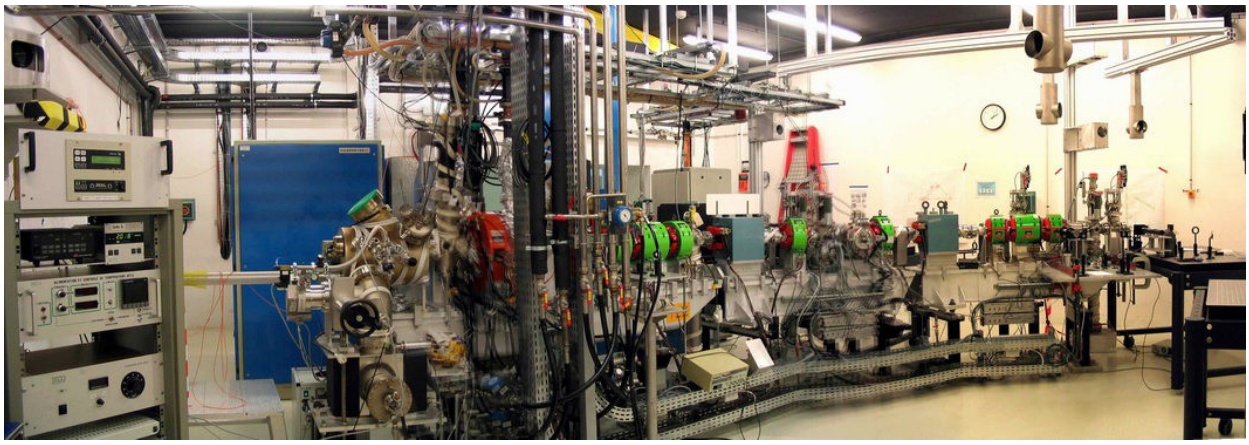

Figure II.7: *General view of pico-second electron accelerator (ELYSE, LCP)*

B. Irradiation cells description

In order to carry out different experiments, different types of cells with selected material and geometry that are specified for each type of irradiation have been developed in the radiochemistry group in SUBATECH laboratory in Nantes. Thess cells can be gasproof in order to have specific athmosphere during irradiation and measure the gases by μ-GC after irradiation to obtain the gas radiolytic yield.

B.1. γ-ray irradiation cells

The cells for γ-ray irradiation are shown in Figure II.8. They are cylindrical and composed of different parts: one container and two cover made by poly-rther-ether_keton (PEEK), a rotulex 19/9 tube and a glass metalic valve. Three O-rings can assure the tightness of cell for 120 hours. The total volume of each cell is 41 cm^3.

B.2. He^{2+} irradiation cells

The cell presents characteristics very similar to γ cells explained above. However, due to the heterogenity of solution irradiation by heavy ionizing particles, it has different geometry. Figure II.9 shows the cell for He^{2+} radiolysis experiment. Here the container changed from cylindrical to cubic shape.

The face that is in front of beam has a hole with a diameter of 20 mm and a borosilicate window (Marienfield®) with a thickness of 150 µm that allows particle beam enter to the cell by losing minimum amount of energy before reaching the solution. The total internal volume is 42 cm^3.

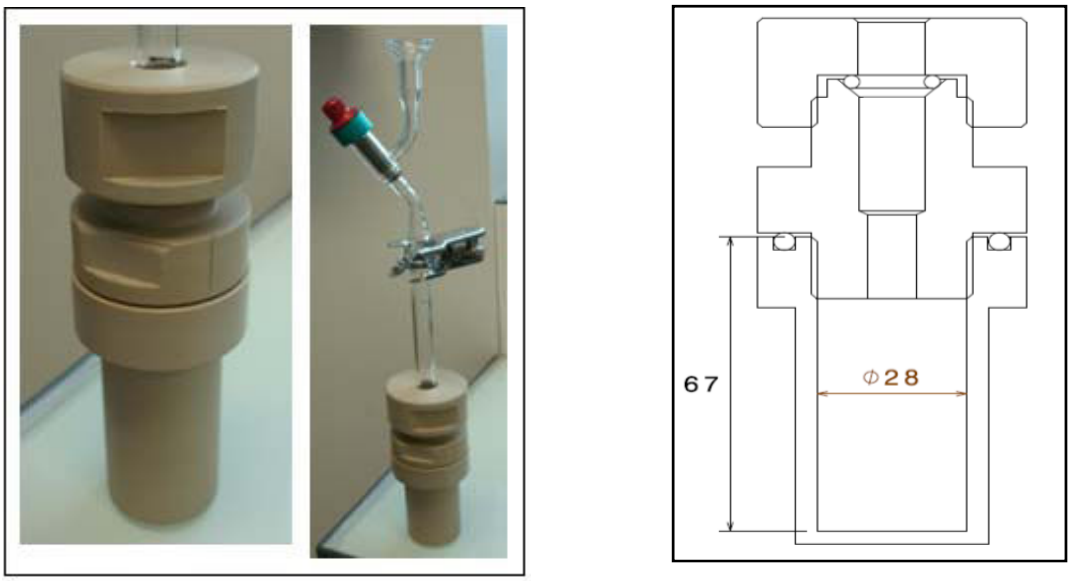

Figure II.8: *The irradiation cell for γ-ray irradiation*

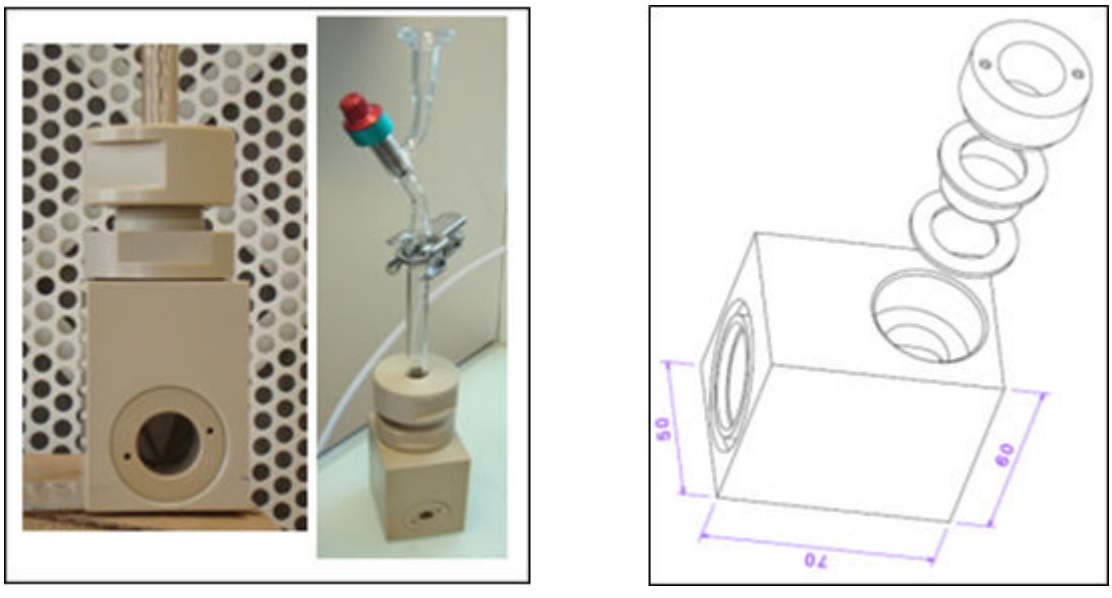

Figure II.9: *The irradiation cell for He^{2+} irradiation.*

B.3. Pico-second electron pulse irradiation cells

The irradiation cells, used in ELYSE, are made by quartz with the width of 0.5 mm. The sample has a continuous flow to the cell during irradiation. The sample pumps from liquid holder to the cell and returns back to the holder.

C. Chemical system under irradiation

C.1. Super Fricke and Fricke dosimetries

The He^{2+} ions beam was provided by the ARRONAX cyclotron facility with E = 64.5 MeV and linear transfer energy (LET) = 22.7 keV.µm^{-1}. For this high energetic hellion beam, the dose rate was determined *in situ* according to the Super Fricke dosimetry [4]. The super Fricke method is based on the oxidation of ferrous ions (Fe^{2+}) to ferric ones (Fe^{3+}) by H_2O_2 produced by water radiolysis. The variation of Fe^{3+} absorbance is then registered as a function of the irradiation time at 304 nm (ε = 2197 l mol^{-1} cm^{-1}). Super Fricke solutions are prepared by dissolving the desired quantity of ferrous sulphate (H_2SO_4, [Fe^{2+}] = 10 mmol l^{-1}) and sodium chloride NaCl (1 mmol l^{-1}) in aerated aqueous 0.4 mol l^{-1}sulfuric acid (H_2SO_4) solutions. All reagents are analytical grade or equivalent. NaCl is added to suppress organic impurities. All the samples were homogenized by stirring during irradiation.

As an example, Figure II.10 shows the absorbance of super Fricke solution at 304 nm under irradiation as a function of time. The diagram shows that the absorption of Fe^{3+} is 1.6 for ten seconds thus it is 9.6 for one minute. By Beer-Lambert formula:

$$[Fe^{3+}] = \frac{A}{\varepsilon \times l} = \frac{9.6}{2160 \times 1} = 4.44\,10^{-3}\ mol\ dm^{-3} \qquad \text{(II -3)}$$

Where A is the absorbance of Fe^{3+} for one minute irradiation. As the concentration of Fe^{3+} is calculated, the dose rate can be obtained by below formula:

$$Dose\ rate\ = \frac{[Fe^{3+}]}{\rho \times G(Fe^{3+})} = \frac{4.44\,10^{-3}}{1.024 \times 1.16\,10^{-6}} = 3740\ Gy\ \min^{-1} \qquad \text{(II -4)}$$

Where G(Fe^{3+}) is the radiolytic yield for Fricke solution and ρ is the density of solution.

Fricke dose rate was found around 3800 Gy.min^{-1} for most of irradiations using the ferric ion radiolytic yield from the literature [5] determined for the high energetic He^{2+} particle beam.

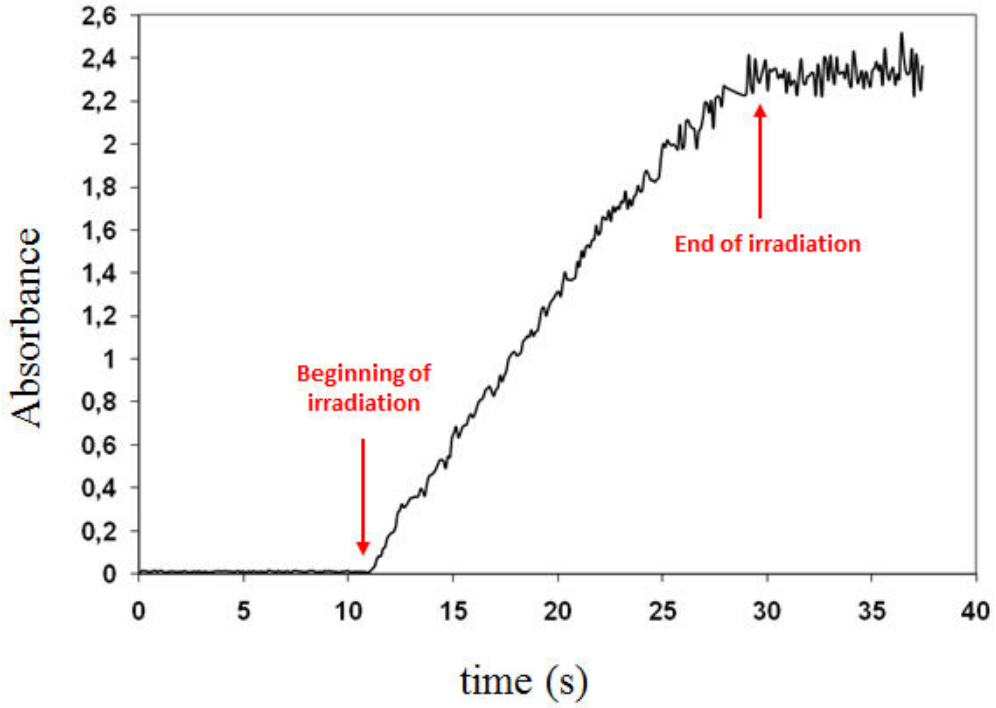

Figure II.10: *Measurements vs. irradiation time of absorption of Fe^{3+} at 304 nm under He^{2+} (64.7 MeV, I = 70 nA) irradiation in super Fricke solution.*

The Fricke dosimetry method was used for dose rate determination during the γ-ray irradiation experiments [4]. Fe^{3+} concentration was measured by recording the UV-Vis absorption of solution after irradiation at λ = 304 nm. The difference between Fricke and super Fricke solution is the concentration of Fe^{2+} which is ten-fold higher in super Fricke solution. Figure II.11 shows the spectra of Fricke solutions after γ-ray irradiation at different time. The Fricke solutions irradiated for 3, 5 and 7 minutes. By the absorbance values at 304 nm, the [Fe^{3+}] is calculated for each irradiation time by Beer-Lamber formula (absorption coefficient of Fe^{3+} = 2205 l.mol^{-1}.cm^{-1} [6]). Therefore, the dose for each irradiation time is calculated by formula (2-5):

$$D = \frac{[Fe^{3+}]}{\rho \times G(Fe^{3+})} \qquad \text{(II -5)}$$

The calculated doses are plotted as a function of time and the slope gives directly the dose rate in Gy.min^{-1} (Figure II.12).

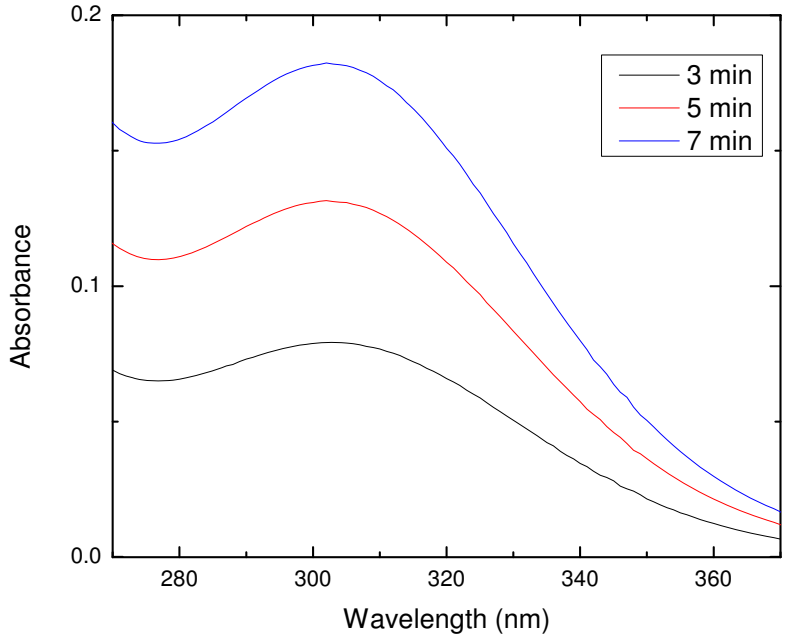

***Figure II.11**: Spectra of formed Fe^{3+} in Fricke solution after different times of γ-ray irradiation.*

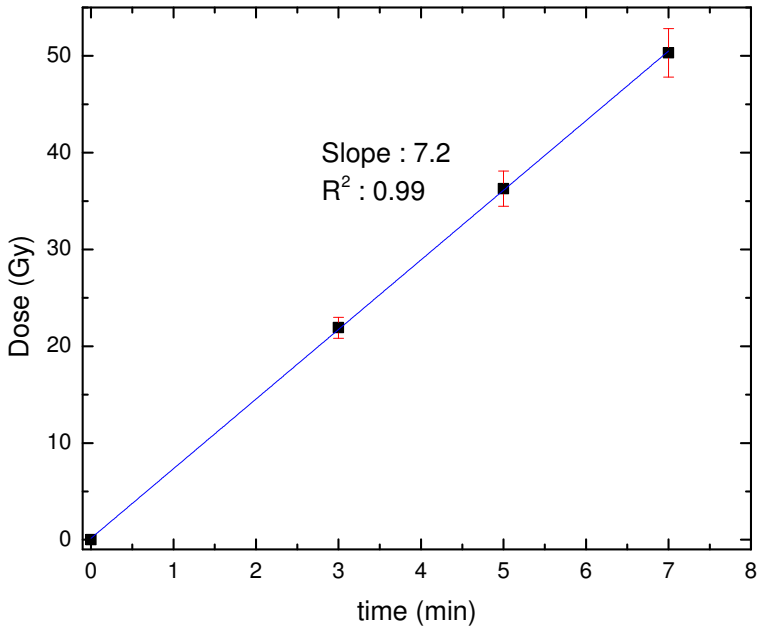

***Figure II.12**: Dose as a function of irradiation time.*

C.2. Solutions used in chemical systems

C.2.1. Ultra-pure water

The ultra-pure water, used in this study, is produced by Milipore simplicity 185 apparatus. This machine is equipped with a UV lab by emission UV light from 185 nm to 245 nm in order to obtain the water with lowest amount of organic carbon. The resistance of water is 18.2 MΩ at room temperature (25°C). Numerous techniques (ICP-MS, ionic chromatography, measurement of organic carbon by COT) used in our laboratory to check the purity of produced water.

C.2.2. Carbonate and M(VII) solutions (M = Tc, Mn, Re)

Carbonate solution is composed by K_2CO_3 and $KHCO_3$ with concentrations of 5 $mol.l^{-1}$ and 0.5 $mol.l^{-1}$ respectively. This concentration ratio buffers the solution at a pH value = 10.8. It has been observed that K_2CO_3 is dissolved easier than KHCO in water for these very high concentrations. First $KHCO_3$ should be dissolved in the water and after K_2CO_3 added for dissolution.

$KMnO_4$ and $KTcO_4$ can be dissolved easily with a concentration of 5×10^{-4} $mol.l^{-1}$ in carbonate solution; but ultra-sonic should be used for the dissolution of $KReO_4$ with the concentration of 5×10^{-4} $mol.l^{-1}$ in the carbonate solution presented above. The density of these solutions is 1.54 $g.cm^{-3}$.

D. Instrumental methods

D.1. UV-Vis spectroscopy

Many molecules absorb ultraviolet or visible light. The absorbance of a solution increases as attenuation of the beam increases. Absorbance is directly proportional to the path length, *b*, and the concentration, *c*, of the absorbing species. *Beer's Law* states that:

$$A = \varepsilon \times b \times c \qquad \text{(II -6)}$$

Where ε is a constant of proportionality, called the absorption coefficient *or the molar extinction coefficient*.

Different molecules absorb radiation of different wavelengths. An absorption spectrum will show a number of absorption bands corresponding to structural groups within the molecule. For example, the absorption that is observed in the UV region for the carbonyl group in acetone is of the same wavelength as the absorption from the carbonyl group in diethyl ketone.

In this study, CARY4000 (VARIAN) UV-Vis spectrophotometer and a HELLMA probe with an optical path of 10 mm are used to determine the dose rate, following kinetics and speciation analysis in electrochemistry and radiolysis. For the dose rate calculation, concentration of the ferric ions was monitored by *in situ* UV-Vis measurements at 304 nm ($\varepsilon = 2197\ l\ mol^{-1}\ cm^{-1}$). This probe used for kinetic study and observation of spectra evaluation during electrochemical reduction. Figure II.13 shows *in situ* UV-Vis spectroscopy apparatus with an electrochemical cell. The software (Cary winUV) of UV-Vis spectrophotometer is able to be programmed for a long time measurement. In this study it was programmed to measure one spectrum per ten minutes for duration of four days.

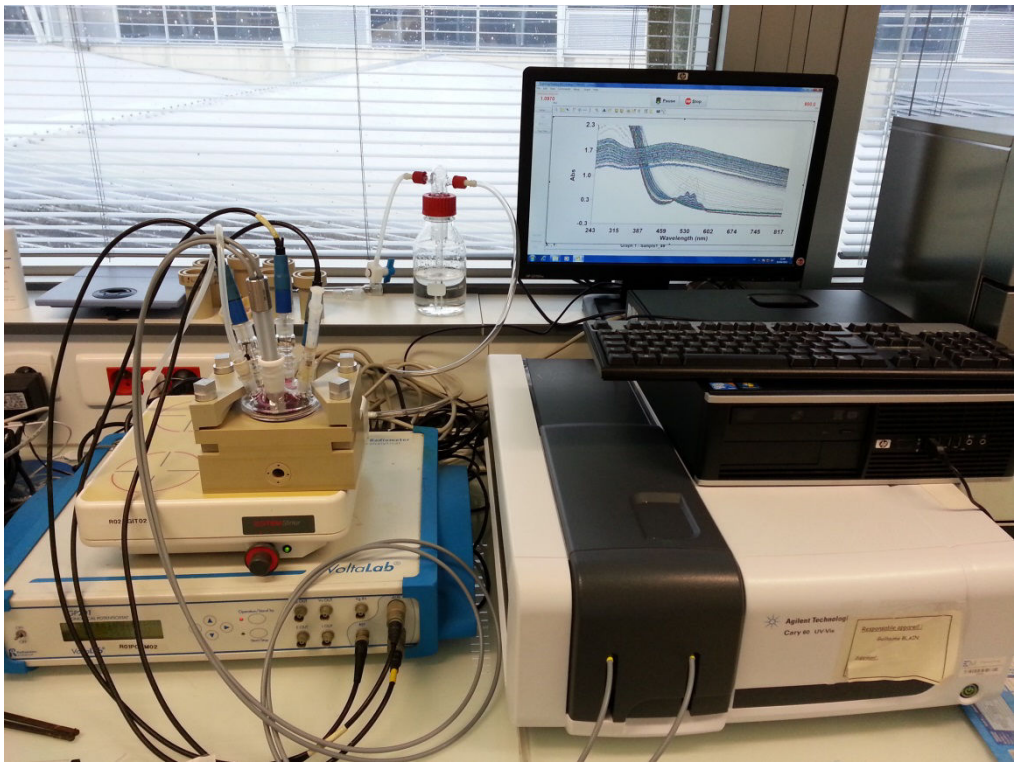

Figure II.13: *Coupling electrochemistry with in situ UV-Vis spectroscopy*

D.2. Electrochemistry tool

Electrochemistry experiments, in particular in galvanic mode with a current lower than -100 µA; experiments are carried out for the reduction of Mn(VII), in different concentrations, carbonate and different atmosphere to obtain the experimental conditions which will be used for all the experiments. Radiometer Voltalab 21 (PGP201) Potentiostat/Galvanostat is used in this study (see Figure II.13). UV-Vis spectra of sample are recorded *in situ* by using a glass probe designed by HELLMA, fiber optic (2 meters) and CARY 60/Agilent UV-Vis spectrophotometer. The spectrophotometer is programmed to measure spectrum each 10 minutes for duration of 4 days. This set up is used also for the reduction of Tc(VII) experiment in carbonate solution.

D.3. X-ray photoelectron spectroscopy (XPS)

X-ray photoelectron spectroscopy (XPS) is a surface characterization technique that can analyze a sample to a depth of 2 to 5 nanometers (nm). When an x-ray bombards a sample, some electrons become excited enough to escape the atom. XPS is conducted in ultrahigh vacuum (UHV) conditions, around 10^{-9} millibar [7]. Irradiating a sample with x-rays of sufficient energy results in electrons in specific bound states to be excited. In a typical XPS experiment, sufficient energy is input to break the photoelectron away from the nuclear attraction force of an element. Two key features are derived from XPS data. The first is that even photo-ejected electrons from core levels have slight shifts depending on the outer valence configuration of the material examined. The second is that the specific energy of an elemental core level transition occurs at a specific binding energy that can uniquely identify (and in favorable cases quantify) the element. In a typical XPS spectrum some of the photo-ejected electrons inelastically scatter through the sample to the surface, while others undergo prompt emission and suffer no energy loss in escaping the surface and into the surrounding vacuum. Once these photo-ejected electrons are in the vacuum, they are collected by an electron analyzer that measures their kinetic energy. An electron energy analyzer produces an energy spectrum of intensity (number of photo-ejected electrons versus time) versus binding energy (the energy the electrons had before they left the atom). Each prominent energy peak on the spectrum corresponds to a specific element. Besides identifying elements in the

specimen, the intensity of the peaks can also tell how much of each element is in the sample. Each peak area is proportional to the number of atoms present in each element.

XPS is used as a solid analysis tool for determination of oxidation state and qualifying of the final products. Powders are simply obtained by filtration with vacuum filter with micro meter porous size and rinsing six times with ultra-pure water to remove the unreacted carbonate. This technique is used only for final products of oxidation/reduction of manganese (solid products).

The Mn_{3s} and O_{1s} XPS spectra are collected by an XPS apparatus, installed at IMN laboratory, with a KRATOS AXIS ULTRA electron spectrometer working in fixed analyzer transmission (FAT) mode. The source of photons is an Al monochromatic X-ray source emitting an incident X-ray beam at 1486.7 eV with a FWHM (full-width half-maximum) of 0.25 eV. The sample, fixed on a metallic plate, is analyzed in a chamber under 5×10^{-7} Pa vacuum. The Mn_{3s} peaks are recorded at constant pass energy of 20 eV. The charge effects are corrected using the C_{1s} line of the carbon at 284.7 eV. The angle-resolved XPS spectra are fitted using a Gaussian–Lorentzian peak shape with a Shirley baseline as background. The binding energy precision is better than 0.2 eV. XPS spectra fitting were performed with CASAXPS software.

D.4. X-ray diffraction (XRD)

X-ray diffraction (XRD) is a rapid analytical technique primarily used for phase identification of a crystalline material and can provide information on unit cell dimensions. Max von Laue, in 1912, discovered that crystalline substances act as three-dimensional diffraction gratings for X-ray wavelengths similar to the spacing of planes in a crystal lattice. X-ray diffraction is now a common technique for the study of crystal structures and atomic spacing. X-ray diffraction is based on constructive interference of monochromatic X-rays and a crystalline sample. These X-rays are generated by a cathode ray tube, filtered to produce monochromatic radiation, collimated to concentrate, and directed toward the sample. The interaction of the incident rays with the sample produces constructive interference (and a diffracted ray) when conditions satisfy Bragg's Law ($n\lambda=2d$ sin θ). This law relates the wavelength of electromagnetic radiation to the diffraction angle and the lattice spacing in a crystalline sample. These diffracted X-rays are then detected, processed and counted. By scanning the sample through a range of 2θ angles, all possible diffraction directions of the

lattice should be attained due to the random orientation of the powdered material. Conversion of the diffraction peaks to d-spacings allows identification of the mineral because each mineral has a set of unique d-spacings. Typically, this is achieved by comparison of d-spacings with standard reference patterns.

The crystallographic phase content was monitored using X-ray diffraction (XRD, Kristalloflex 720 Model D5000, Siemens, using a copper electrode with λ_{K1} = 1.540 60 Å, and λ_{K2} = 1.544 43 Å). The Siemens D5000 instrument has a large diameter goniometer (600 mm), low divergence collimator, and Soller slits. Attachments include sample spinner stage, reflection/transmission holders, incident or diffracted beam monochromators, zero background holders, and odd sample shape holders. This instrument is useful for both powder and bulk materials. This diffractometer is the best utilized for high precision work. Data collection is performing under computer control using the "Diffract Plus" software.

D.5. X-ray absorption spectroscopy (XAS)

EXAFS (Extended X-ray Absorption Fine Structure) and XANES (X-Ray Absorption Near Edge structure) are regions of the spectrum obtained from XAS (X-ray Absorption Spectroscopy). EXAFS corresponds to the oscillating part of the spectrum to the right of the absorption edge (appearing as a sudden, sharp peak), starting at roughly 50 eV and extending to about 1000 eV above the edge. Through mathematical analysis of this region, one can obtain local structural information for the atom in question.

X-Ray spectroscopy involves a process in which an X-ray beam is applied to an atom and causes the ejection of an electron, usually a core electron. This leaves a vacancy in the core shell, and results in relaxation of an outer electron to fill that vacancy. This phenomenon is only observed when the energy of the X-ray exceeds the ionization energy of the electrons in that shell. We can relate this occurrence to the X-ray Absorption coefficient, which becomes the basis of EXAFS theory. The X-ray Absorption coefficient, or μ, describes the relationship between the intensity of an X-ray beam going into a sample and its intensity leaving the sample after traveling a distance x within the sample. The absorption coefficient is given by

$$\mu = -\frac{d \ln I}{dx} \qquad \text{(II -7)}$$

In this expression, dx is the traversed distance, and I is the intensity. In a typical EXAFS spectrum, various sharp peaks will be observed when energy (usually in eV) is plotted against

absorbance. These peaks (called edges), which vary by atom, correspond to the ionization of a core orbital, K-edges describing the excitation of the innermost 1s electron, and L-edges and M-edges referring to the same for higher energy orbitals.

After each edge, a series of downward oscillations will be observed. These oscillations correspond to wave interactions between the ejected photoelectron and electrons surrounding the absorbing atom. The neighboring atoms are called backscattering atoms, since the waves emitted from the absorbing atom change paths when they hit these neighboring atoms, returning to the original atom. Maxima in the oscillations result from constructive interference between these waves, and minima result from destructive interference. These oscillations are also characteristic of the surrounding atoms and their distances from the central atom, since varying distances will result in different backscattering paths, and as a result different wave interactions. The EXAFS fine structure begins at roughly 30 eV past each edge, where oscillations begin to decay. In addition, this wave interaction will depend on the mechanism of scattering, since the path taken by a wave sometimes involves collision with an intermediate atom, or even multiple atoms, before it reverts to the absorbing atom.

The effects of the absorbing atom and scattering atoms are shown in Figure II.14 the solid arcs are representative of outgoing waves from the absorbed atoms (a). The blue arcs are representative of the scattered waves caused by the outgoing photoelectron wave passing through the electron density around the scattering atom (s). The energies of interest are shown on the graph on Figure II.14. When $E = E_1$, the energy is lower (compared to E_2) giving longer wavelengths where the back scattering wave hits the absorbing atom. This gives rise to a transition moment, giving maximum amplitude, and a maximum modulation of μ. Correspondingly, when $E = E_2$, the energy is increased (compared to E_1) and gives rise to shorter wavelengths. The back scattering wave completely misses the absorbing atom, at this point in time the amplitude is at its minimum thusly making the μ modulation minimal as well. The very last picture represented in Figure II.14 effectively displays the phase shift that should occur (opposed to the diagram where E = E1) (the red arcs represent the original diagram and the blue arcs represent the phase shift).

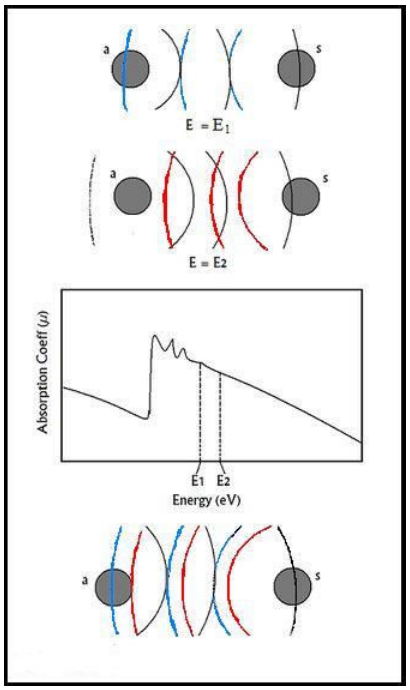

Figure II.14: *The effects of the absorbing atom and scattering atoms in EXAFS [8].*

The obtained EXAFS spectra must be fitted with theoretical EXAFS spectra from DFT (density functional theory) simulation of suggested structures In order to interpret obtained experimental data from sample to the sample structure. In this study DFT simulation was done in collaboration with IPN Orsay (By Jérôme Roque). The principle and information of carried out DFT are provided in appendix.

X-ray absorption spectroscopy (XAS) includes both extended X-Ray absorption fine structure (EXAFS) and X-ray Absorption near edge structure (XANES). Both of these techniques were done in MARS beamline at SOLEIL synchrotron. The MARS (Multi-Analyses on Radioactive Sample) beamline is the only SOLEIL beamline dedicated to the characterization of radioactive materials (^{99}Tc, ^{232}Th, ^{238}U, ^{239}Pu…) by X-ray diffraction, X-ray absorption spectroscopy in the energy range 3.5 to 35 keV. Optical elements have been installed to allow for experiments on complementary analysis equipment located in the same experimental hutch (Figure II.15): very high resolution and transmission X-ray diffraction, X-ray absorption spectroscopy (transmission, fluorescence and high resolution) and X-ray fluorescence spectroscopy These techniques can be used for a wide range of applications in various disciplines (solid state chemistry and physics, earth science, biology, etc.) on samples that have in common the presence of one or more unstable elements (radionuclides).

Radionuclide decay is the source of specific emissions from the samples at energies that may be in the same domain as the X-ray fluorescence energy. Table II.3 shows the technical data of the MARS beamline used in our study.

***Table II.3**: Technical characteristics of MARS beamline at SOLEIL synchrotron.*

Energy Range	Between 3.5 to 36 keV (focused beam)
Energy Resolution	$\Delta E/E < 3.\ 10^{-4}$
Source	Bending Magnet , maximum horizontal acceptance 3 mrad
Optics	Two long mirrors and one monochromator (DCM)
Sample Environment	Glove box (for second confinement change) Double-barrier confinements for ambient T and P measurements Cryostats Special environments in collaboration with users: Electrochemical cell Furnace High pressure cells (Diamond anvil-type) Special shielded containment
Beam size at sample	From 300x3000 μm^2 to 5x5 μm^2 (with additional K.B. optics) depending on the optical configuration (FWHM)
Flux on sample	About 1.10^{+12} Phot/s @ 10 keV (beam current 430 mA)
Detectors	2D detectors: imageplate (MAR345) Solid state detectors: multi-element Ge (ORTEC), silicon drift (Ketek)

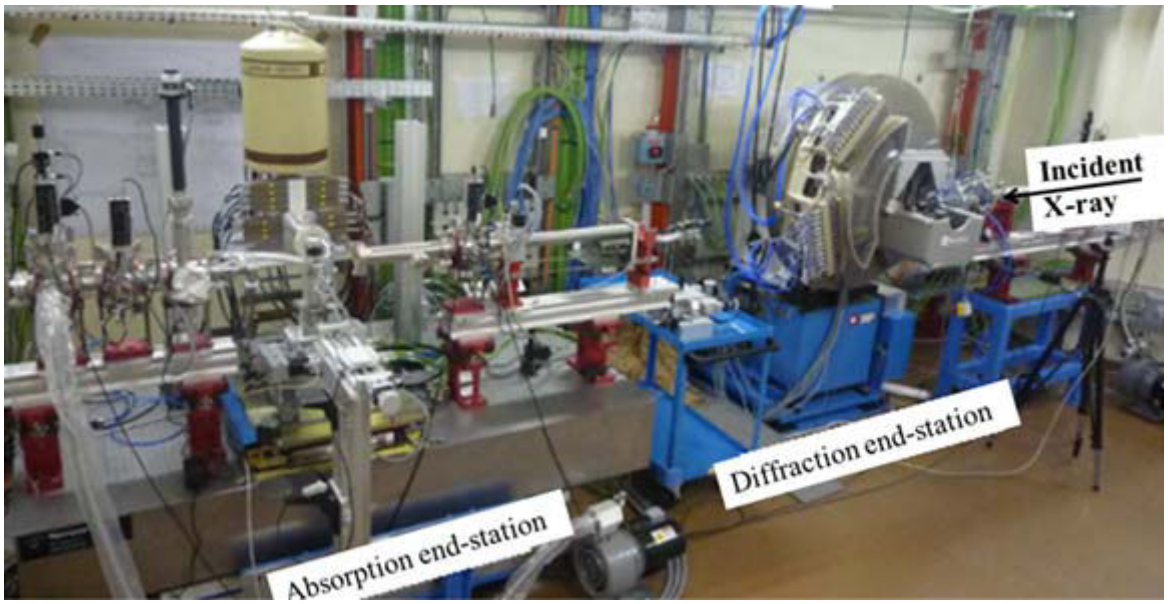

***Figure II.15**: MARS beam line used in this work at SOLEIL synchrotron.*

The sample holder for XAS consists of:

- Teflon recessed frame that can hold the measuring cell,
- Two Viton washer,
- Two Teflon windows with thickness of 200 µm,
- Two clamping stainless steel plates (316L) for sealing all parts.

Figure II.16 shows the sample holder for XAS at SOLEIL synchrotron.

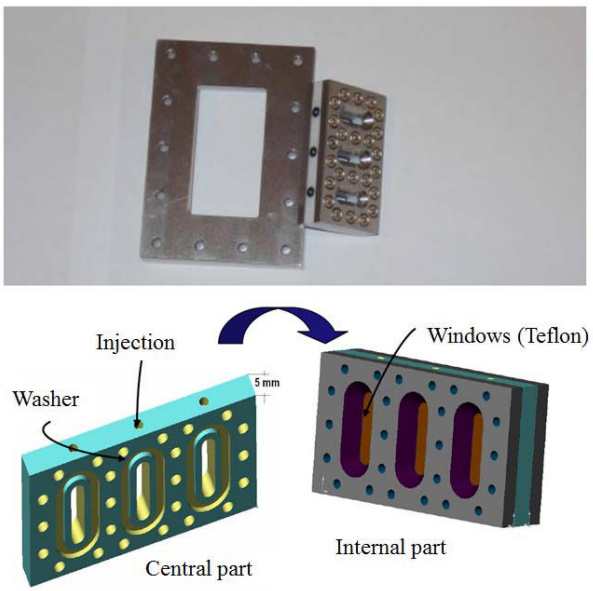

***Figure II.16:** Sample holder used for XAS at SOLEIL synchrotron.*

D.6. Scanning Electron Microscopy (SEM)

Scanning Electron Microscopy (SEM) is a powerful technique in the examination of materials. It is used widely in metallurgy, geology, biology and medicine, to name just a few. The user can obtain high magnification images, with a good depth of field, and can also analyze individual crystals or other features. A high-resolution SEM image can show detail down to 25 Angstroms, or better. A normal scanning electron microscope operates at a high vacuum. The basic principle is that a beam of electrons is generated by a suitable source, typically a tungsten filament or a field emission gun. The electron beam is accelerated through a high voltage (e.g.: 15 kV) and pass through a system of apertures and electromagnetic lenses to produce a thin beam of electrons., then the beam scans the surface of the specimen by means of scan coils (like the spot in a cathode-ray tube "old-style" television). Electrons are emitted from the specimen by the action of the scanning beam and collected by a suitably-positioned detector. The microscope operator is watching the image on a screen. The key to how the scanning electron microscope works (and this is the clever bit) is that the beam scanning the specimen surface is exactly synchronized with the spot in the screen that the operator is watching. The electron detector controls the brightness of the spot on the screen - as the detector "sees" more electrons from a particular feature, the screen brightness is increased. When there are fewer electrons, the spot on the screen gets darker.

The final products of reduction and oxidation were analyzed also by scanning electron microscopy (SEM) (JEOL JSM 5800 LV, 15 kV) at IMN laboratory. The SEM apparatus is coupled with an energy dispersive X-ray spectrometer (EDX), making quantitative chemical analysis possible on the carbon-metallized specimens. Also it was equipped with a thin beryllium window that allows detecting and accurately quantifying oxygen (about 1% relative error for flat sample). The final compositions were calculated assuming oxide stoichiometry and normalization to 100%. Cross section observation allowed the measurement of hydration layer thickness.

D.7. Micro-Gas chromatography (μ-GC)

A gas chromatograph (GC) is an analytical instrument that measures the content of various components in a sample. The analysis performed by a gas chromatograph is called gas chromatography. The principle of gas chromatography is described as follow. The sample

solution injected into the instrument enters a gas stream which transports the sample into a separation tube known as the "column." (Helium or nitrogen is used as the so-called carrier gas.) The various components are separated inside the column. The detector measures the quantity of the components that exit the column. To measure a sample with an unknown concentration, a standard sample with known concentration is injected into the instrument. The standard sample peak retention time (appearance time) and area are compared to the test sample to calculate the concentration.

Molecular hydrogen is measured with a gas chromatograph. Ultra-high purity argon is used as the carrier gas. The gas chromatograph is a 490-GC, which is a µ-GC model from VARIAN. Both injection and µ-GC systems are Argon-purged before each measurement. The gas sample of 10 µl is introduced at atmospheric pressure in an injection loop. Then, gas is compressed at 150 kPa in the column that is a Molecular Sieve 5 A (L~4 m, Ø~0.25 mm). The detection is performed using a thermal conductivity detector. Calibration of the detector is performed by injection of different gas mixtures of hydrogen in argon from 10 to 500 ppm hydrogen in the composition of the gas. Error in gas measurements is estimated to be less than 10 %. Figure II.17 shows the µ-GC that will be used in this study.

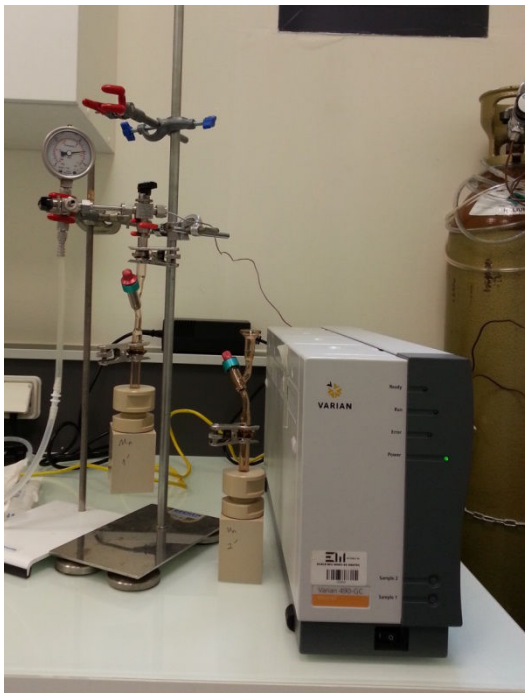

Figure II.17: *µ-GC model 490 Varian used in this study.*

E. Overview of the Experimental Section

In order to summarize this part, all the analytical techniques used in this work and their application for this study are listed in Table II.4.

Table II.4: *Analytical techniques and their application used in this study.*

Technique	Application
UV-Vis spectroscopy	Speciation of species Mn, Tc and Re
Electrochemistry	Reduction of Mn, Tc and Re species in concentrated carbonate media
XPS	1) Investigating oxidation state of synthesized Mn powder in both oxidation and reduction reactions 2) Structural characterization of those powder
XRD	Chrystalography determination of synthesized Mn powder in both oxidation and reduction reactions
XAS	1) XANES to find the oxidation state of obtained Tc complexes 2) EXAFS for structral definition of obtained Tc complexes
DFT	Structure stability check of the Tc complexes
SEM	Morphology determination of synthesized Mn in both oxidation and reduction reactions
μ-GC	Measurment of the produced gases during irradiation

References

1. D. Delacroix, J.P.G., P. Leblanc *Guide pratique radionucléides & radioprotection* 2006, CEA.
2. *Direction des technologies avancées* 1991, CEA, Département des applications et de la métrologie des rayonnements ionisants Radionucléides.
3. Lafargue, T., K. Pernin, and G. Zhu, *Rapport Projet OSE*, Subatech.
4. Fricke, H. and E.J. Hart, *Chemical Dosimetry, Radiation Dosimetry*. book, ed. A.F.H.e.R. W.C. 1966, New York, USA: Academic Press.
5. Costa, C., et al., *Chemical Dosimetry during Alpha Irradiation: A Specific System for UV-Vis in situ Measurement* American Journal of Analytical Chemistry, 2012. **3**: p. 6-11.
6. LaVerne, J.A. and R.H. Schuler, *Radiation chemical studies with heavy ions: oxidation of ferrous ion in the Fricke dosimeter.* The Journal of Physical Chemistry, 1987. **91**(22): p. 5770-5776.
7. De Combarieu, G., P. Barboux, and Y. Minet, *Iron corrosion in Callovo-Oxfordian argilite: From experiments to thermodynamic/kinetic modelling.* Physics and Chemistry of the Earth, Parts A/B/C, 2007. **32**(1-7): p. 346-358.
8. *Online data : X-ray Spectroscopy, EXAFS theory*, university california davis.

Chapter III: Radiolysis of highly concentrated carbonate solutions

This part of the study deals with the radiolytic degradation of carbonate (CO_3^{2-}) species and its kinetic rates determination. This study is one part of a larger one devoted to the technetium and manganese speciation under irradiation in highly concentrated carbonate medium.

Radiolysis of water produces radicals and molecules that they can initiate oxidation/reduction reaction [1]. One of the main products of radiolysis is hydroxyl radical which is scavenged by carbonate and bicarbonate in some nanoseconds which induces carbonate anion radical ($CO_3^{\bullet-}$) as a powerful oxidant [2]. In high concentrated carbonate solutions (concentration higher than 1 mol.l^{-1}), this radical can be produced through direct effect also [3]. So the carbonate solution under ionizing irradiation creates a mixture of oxidizing ($CO_3^{\bullet-}$) and reducing ($e^-_{(aq)}$ and $H^\bullet$) agents. Therefore, different species of one metal can be oxidized or reduced under the same condition depending on their redox potential. Despite production of oxidizing agent, carbonate plays the role of complex ligand in this medium. Carbonate anion radical ($CO_3^{\bullet-}$) is formed by one electron reduction of carbonate or bicarbonate [4]. Water radiolysis produces $e^-_{(aq)}$, $H^\bullet$ and $HO^\bullet$ [5]. Carbonate radical is formed by reaction of hydroxyl radical with carbonate and bicarbonate [6] .

$$HO^\bullet + CO_3^{2-} \rightarrow CO_3^{\bullet-} + HO^- \qquad k = 3.9 \times 10^8 \text{ l.mol}^{-1}.\text{s}^{-1} \qquad \text{(III-1)}$$

$$HO^\bullet + HCO_3^- \rightarrow CO_3^{\bullet-} + H_2O \qquad k = 8.5 \times 10^6 \text{ l.mol}^{-1}.\text{s}^{-1} \qquad \text{(III -2)}$$

The rate constant in case of carbonate is forty-fold higher than for bicarbonate. The reduction potential of the carbonate/carbonate radical anion pair is 1.78 V at pH = 7.0 [7]. Different parameters such as atmosphere, temperature and additional salt influence the yield of carbonate radical [8, 9]. In order to obtain the radiolytic yield of decay and formation of metals such as Tc and Mn, the knowledge of the radiolytic yield of carbonate radical formation and decay for highly concentrated carbonate solutions is mandatory. Moreover, in such high concentrated solutions, the mechanisms described in diluted solutions are not available. Recent studies on picosecond pulse radiolysis of concentrated inorganic aqueous solutions have shown that three mechanisms of oxidation of solute can occur: *i*) the direct effect of radiation on the solute, in that case the solute loses one electron which can be further solvated; *ii*) the oxidation of the solute by water radical hole $H_2O^{\bullet+}$, occurring only if the solute is in contact with this radical; *iii*) the oxidation of the solute by $OH^\bullet$ radical. In previous studies of concentrated sulfuric acid, it was possible to estimate the yield of radical formation in the picosecond range through oxidation by water hole through measuring directly the yield

of sulfate radical in sulfuric acid. For these systems, it was shown that the electron transfer reaction between the water hole and the solute could be more fast than a proton transfer reaction involving this hole as the number of water molecules in proximity decreases [10-16].

Thus, in this chapter to understand the reactions of oxidation/reduction of technetium and manganese in highly concentrated carbonate solution under irradiation; the picosecond pulse radiolysis of different highly concentrated carbonate solutions are studied and discussed. The pulse radiolysis in this chapter is done in collaboration with Mehran Mostafavi at LCP Orsay.

A. Calculation of dose

A.1. Dose calculation in water specific to the pulse radiolysis

The dose calculation in pulse radiolysis experiment is different than for the steady state one. Using the absorption of solvated electron in water is one of the ways for calculation of absorbed dose. Figure III.1 shows the obtained kinetics of solvated electron at 650 nm. By Beer-Lambert law the concentration of solvated electron can be calculated as:

$$c = \frac{A}{\varepsilon \times b} \qquad \text{(III -3)}$$

Where c is concentration, A is absorbance at 650 nm, ε at 650 nm is 18960 $l.mol^{-1}.cm^{-1}$ [17] and b = 0.5 cm. The maximum absorption for solvated electron (Figure III.1) is 0.2 at 10 ps. Thus, the concentration calculated of solvated electron is 2.2×10^{-5} $mol.l^{-1}$. With below formula, the dose of the pulse which last 10 ps is 52 Gy:

$$D = \frac{\mathrm{c}}{\mathrm{G} \times \rho} \qquad \text{(III -4)}$$

Where D is the dose (Gy), c the concentration ($mol.l^{-1}$), G the yield of the solvated electron at 10 ps (4.25×10^{-7} $mol.J^{-1}$) and ρ the density of water ($g.cm^{-3}$).

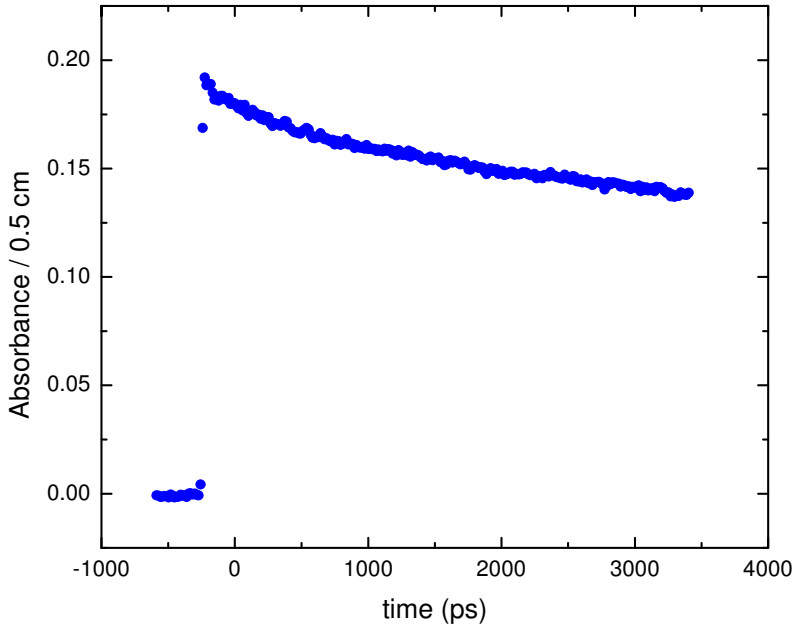

Figure III.1: *Kinetics of solvated electron decay after one pulse of electron at 650 nm.*

A.2. Dose calculation specific for the highly concentrated solution

The energy is not only absorbed by water in highly concentrated solutions but also by the high concentrated solute, here carbonate. In order to determine the amount of absorbed energy either by solvent, either by solute; the electron fraction of the component must be calculated. The dose in solution can be calculated by below formula [18]:

$$D_{sol}\ (J.l^{-1}) = F D_{water}\ (J.Kg^{-1}) \qquad \text{(III -5)}$$

With

$$F = d_{sol}\left[\frac{Z_{K2CO3}\text{-}p}{A_{K2CO3}} + \frac{Z_{water}(100\text{-}p)}{A_{water}}\right]\left(\left[\frac{Z_{water}100}{A_{water}}\right]\right)^{-1} \qquad \text{(III -6)}$$

Where ρ_{sol} is the density of solution, Z the number of electrons, A the mass number and p the weight fraction of the solute percent.

The density, calculated F and fractions of water and solute for 3 solutions of carbonate with different concentrations are presented in Table III.1.

Table III.1: *Concentrations of carbonate solutions and their relevant parameters*

C [mol.l^{-1}]	f_s	f_w	F (g.cm^3)	d_{sol} (g.cm^3)	[H_2O]/[CO_3^{2-}]
2	0.2	0.8	1.11	1.12	26.39
3	0.29	0.71	1.35	1.36	17.4
5	0.4	0.6	1.54	1.55	9.55

B. Pulse radiolysis of highly concentrated KOH

The carbonate solutions are prepared by the dissolution of K_2CO_3 in water. Both of K^+ and CO_3^{2-} can shift solvated electron spectrum [19]. Then, in the carbonate solution with a concentration of 5 mol.l^{-1}, the concentration of K^+ is 10 mol.l^{-1}. In order to determine the role of K^+ and CO_3^{2-} on shift of solvated electron spectrum, first picosecond pulse radiolysis of KOH solution with a concentration of 10 mol.l^{-1} is carried out. So, this solution has K^+ with a concentration of 10 mol.l^{-1} without presence of CO_3^{2-}. Figure III.2 shows the results where K^+ ion shifts the spectrum of solvated electron from 780 nm to 650 nm (Δ = 130 nm) which is non-negligible.

a

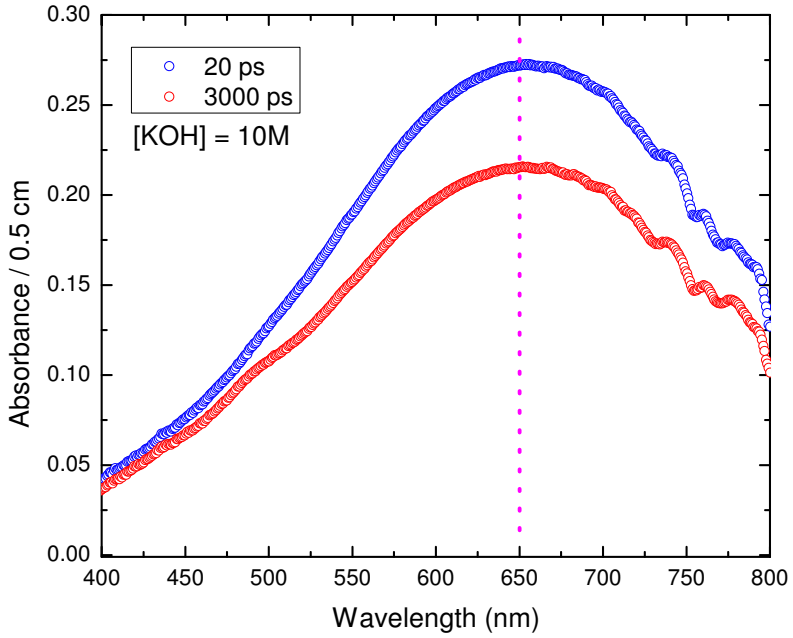

b

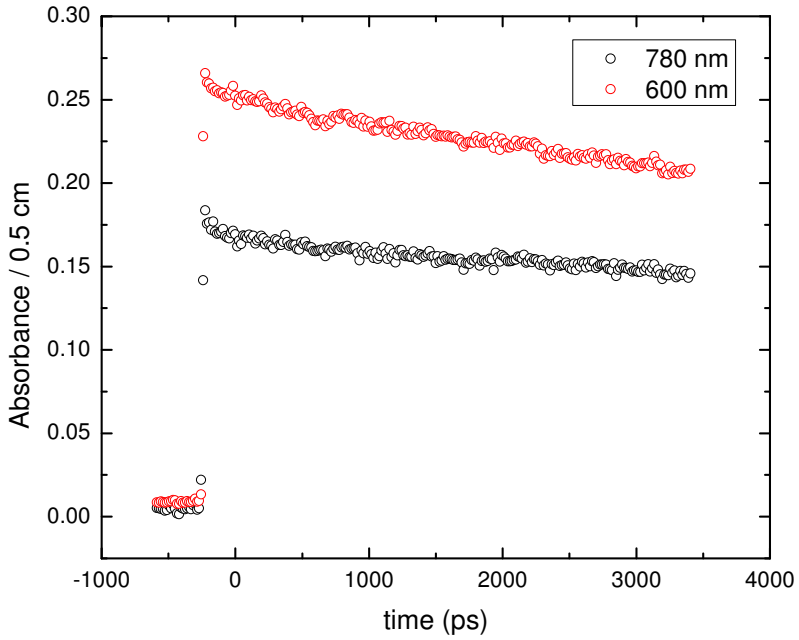

Figure III.2: *a) Spectra of solution of KOH with concentration of 10 mol.l^{-1} after 20 ps and 3000 ps of electron pulse, b) Kinetic decay of KOH with concentration of 10 mol.l^{-1} at 780 nm and 600 nm.*

C. Appropriate scavenger for solvated electron

The carbonate radical absorbs the light at 600 nm [20]. The obtained data show that the concentrated carbonate solution shifts the absorption of the solvated electron to 600 nm also, thus in order to have only absorption by carbonate radical, the solvated electron must be scavenged. Different types of scavengers have been tested but due to the high concentration of carbonate, either they could not be dissolved with a sufficient concentration in the solution (for example; Cd^{2+}); or they can induce the decomposition of carbonate (for example; H_2O_2). After testing almost all the scavengers only NO_2^- and NO_3^- could be used without any solubility or decomposition problem. NO_2^- has a higher solubility than NO_3^- in highly concentrated carbonate solutions. Our obtained data from the pulse radiolysis experiment has shown that NO_2^- with concentration of 1 $mol.l^{-1}$ scavenges solvated electron slower than NO_3^-. The nitrate cannot be dissolved more than 0.3 $mol.l^{-1}$ in our carbonate solution ($[CO_3^{2-}]$ = 5 $mol.l^{-1}$). Therefore, the NO_3^- is added with concentrations of 0.3 $mol.l^{-1}$, 0.7 $mol.l^{-1}$ and 0.7 $mol.l^{-1}$ to the carbonate solutions with concentrations of 5 $mol.l^{-1}$, 3 $mol.l^{-1}$ and 2 $mol.l^{-1}$ respectively.

D. Pulse radiolysis of carbonate solutions

Three solutions of carbonate with concentrations of 5, 3 and 2 $mol.l^{-1}$ with nitrate as scavenger are irradiated. Figure III.3 and III.4 show the kinetics of the carbonate decays at 780 nm and 600 nm respectively. At 600 nm, the absorption is due to electron and carbonate radical while at 780 nm there is only electron absorption. The kinetics at 780 nm shows a very fast decay of solvated electron (around 500 ps), especially in solutions containing nitrate with concentration of 0.7 $mol.l^{-1}$. The kinetics at 600 nm shows a very fast decay at the beginning which is related to the solvated electron and the carbonate radical residual absorption.

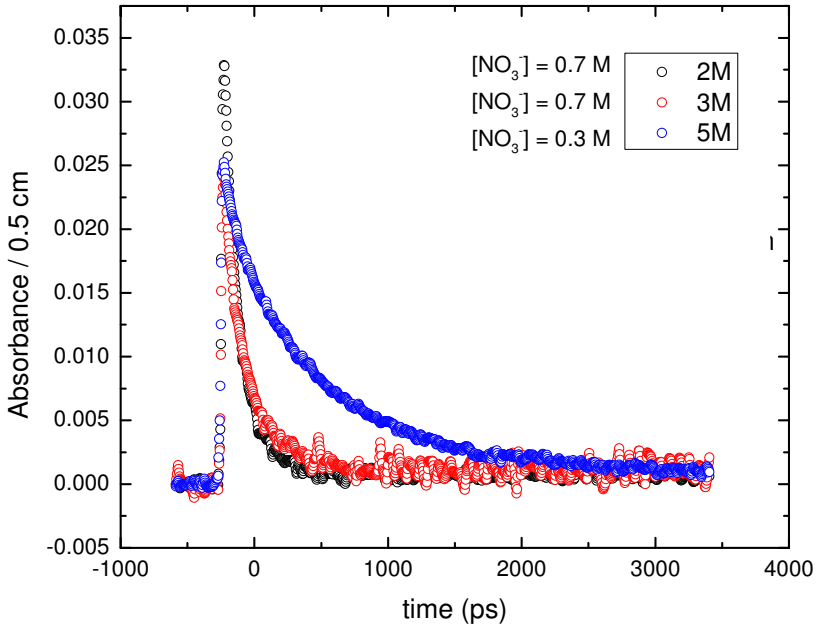

Figure III.3: *Kinetics of carbonate decay s at 780 nm with concentrations of 2, 3 and 5 mol.l*$^{-1}$ *after dose and F correction.*

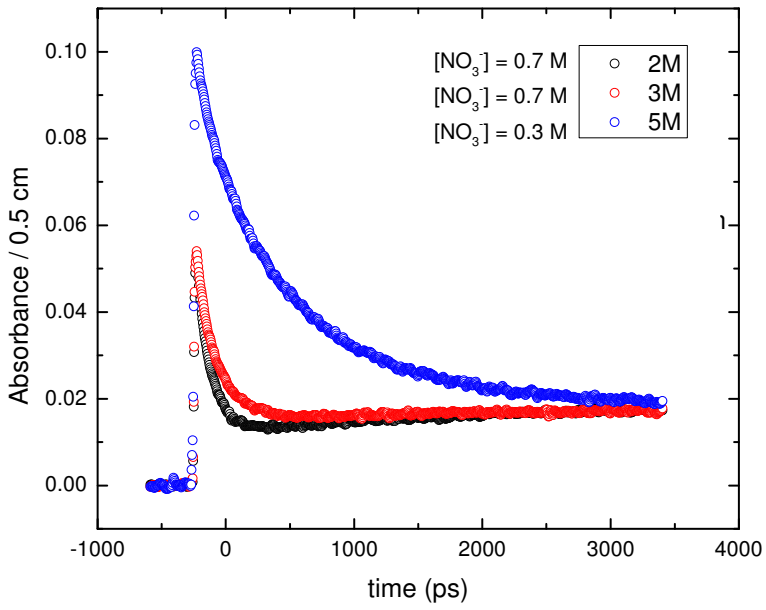

Figure III.4: *Kinetics of carbonate decay at 600 nm with concentrations of 2, 3 and 5 mol.l*$^{-1}$ *after dose and F correction.*

Figure III.5 presents the spectra for these three solutions at t = 20 ps. For each solution, fourteen measurements were done and their average after noise (offset) subtracted is considered as spectrum. As the dose was not the same for all solutions, so the dose correction was performed and followed by F normalization. The results, presented in Figure III.5, are calculated after F correction. The maximum absorption band is determined at 600 nm, 620 nm and 650 nm for carbonate solutions with concentrations of 5 mol.l^{-1}, 3 mol.l^{-1} and 2 mol.l^{-1} respectively. Before F correction the spectra of 3 mol.l^{-1} and 2 mol.l^{-1} have shown the same magnitude but after F correction, the 3 mol.l^{-1} shows lower magnitude.

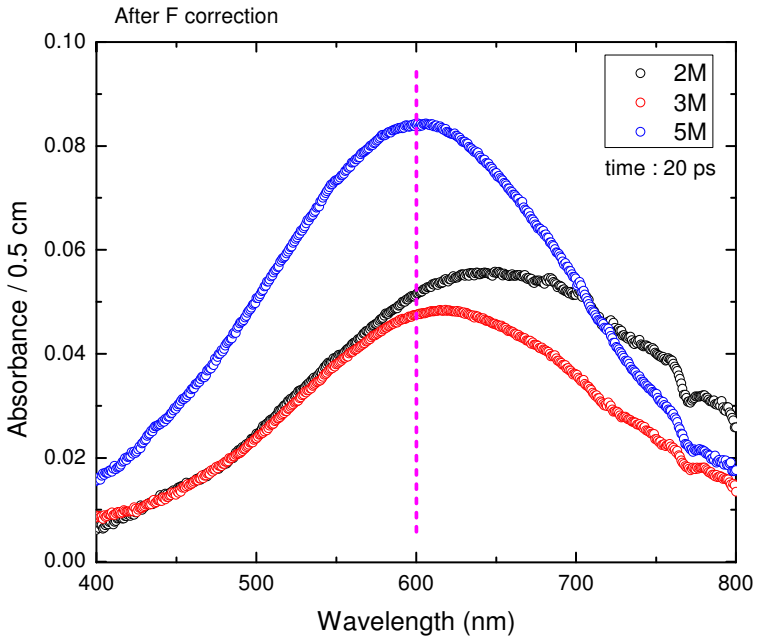

Figure III.5: *Spectra of the three carbonate solutions (c = 2, 3 and 5 mol.l^{-1}) at t = 20 ps after dose and F correction.*

With an electron spectrum monitored for each solution, it is possible to subtract it from the obtained spectra in order to get carbonate radical spectrum. Then, for each solution it is possible to calculate the electron concentration at interested time. So, this concentration is used to deduce the electron spectrum from the standard model (as detailed in appendix). It should be noticed that as there is different shift for each solution, so the shift for electron of each solution is different. We used the formula described below to determine this shift value:

$$S_{es} = \lambda_{sm} - S_{cs} \qquad \text{(III -7)}$$

Where S_{es} is the shift for electron spectrum, λ_{sm} the wavelength in standard model and S_{cs} the shift in carbonate solution.

For example, for a carbonate solution at 5 mol.l^{-1}, the shift is 120 nm. Figure III.6 shows the spectra of all 3 solutions at t = 20 ps after the electron spectrum subtraction. Then, the spectra in Figure III.6 can be considered as the spectra of the carbonate radical. Moreover, the obtained spectra are in good agreement with the reported spectra for the carbonate radical in previous studies [20].

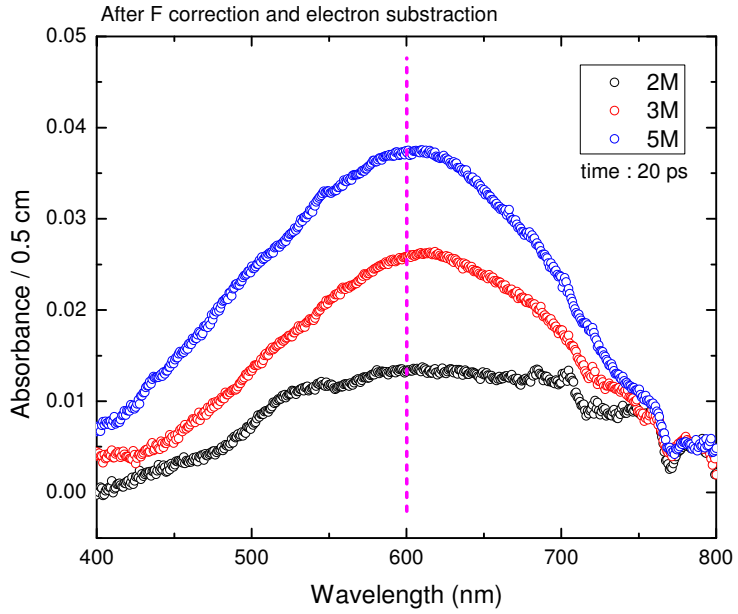

Figure III.6: *Spectra of carbonate radical obtained at t = 20 ps in the 3 carbonate solutions after F correction and subtraction of electron absorption.*

At 3000 ps after the pulse, the solvated electron is already quite scavenged by the nitrate ion. Thus, the spectra correspond only to the carbonate radical. Figure III.7 shows the spectra of the 3 carbonate solutions at 3000 ps.

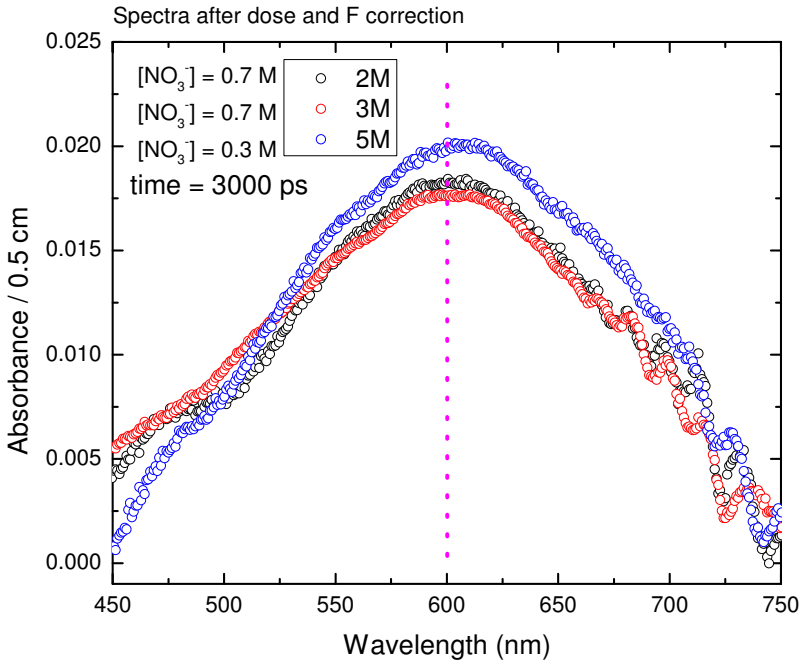

***Figure III.7**: Spectra of carbonate radical obtained at t = 3000 ps in the 3 carbonate solutions after F correction and subtraction of electron absorption.*

The spectra in Figure III.6 and Figure III.7 indicate that, at the beginning of the radiolysis process, the concentration of carbonate radical is higher in carbonate solutions with higher concentration. Then, it seems that higher is the initial concentration of carbonate ion, higher will be the concentration of carbonate radical. But after 3000 ps, the concentration of carbonate radical in the 3 solutions stays still similar. It implies that the direct effect should be taken into account for a timescale lower than 3000 ps.

Figure III.8 shows the kinetics after subtraction of electron for 3 carbonate solutions. The results indicate that, in carbonate solution with a concentration of 5 $mol.l^{-1}$, at the beginning the concentration of carbonate radical is higher due to the direct effect, but it decreased and becomes constant due to the indirect production of carbonate radical by hydroxyl radical. In carbonate solutions with concentrations of 3 $mol.l^{-1}$ and 2 $mol.l^{-1}$, at the beginning there is a small amount of carbonate radicals due to the direct effect but it increased due to the indirect production as described above.

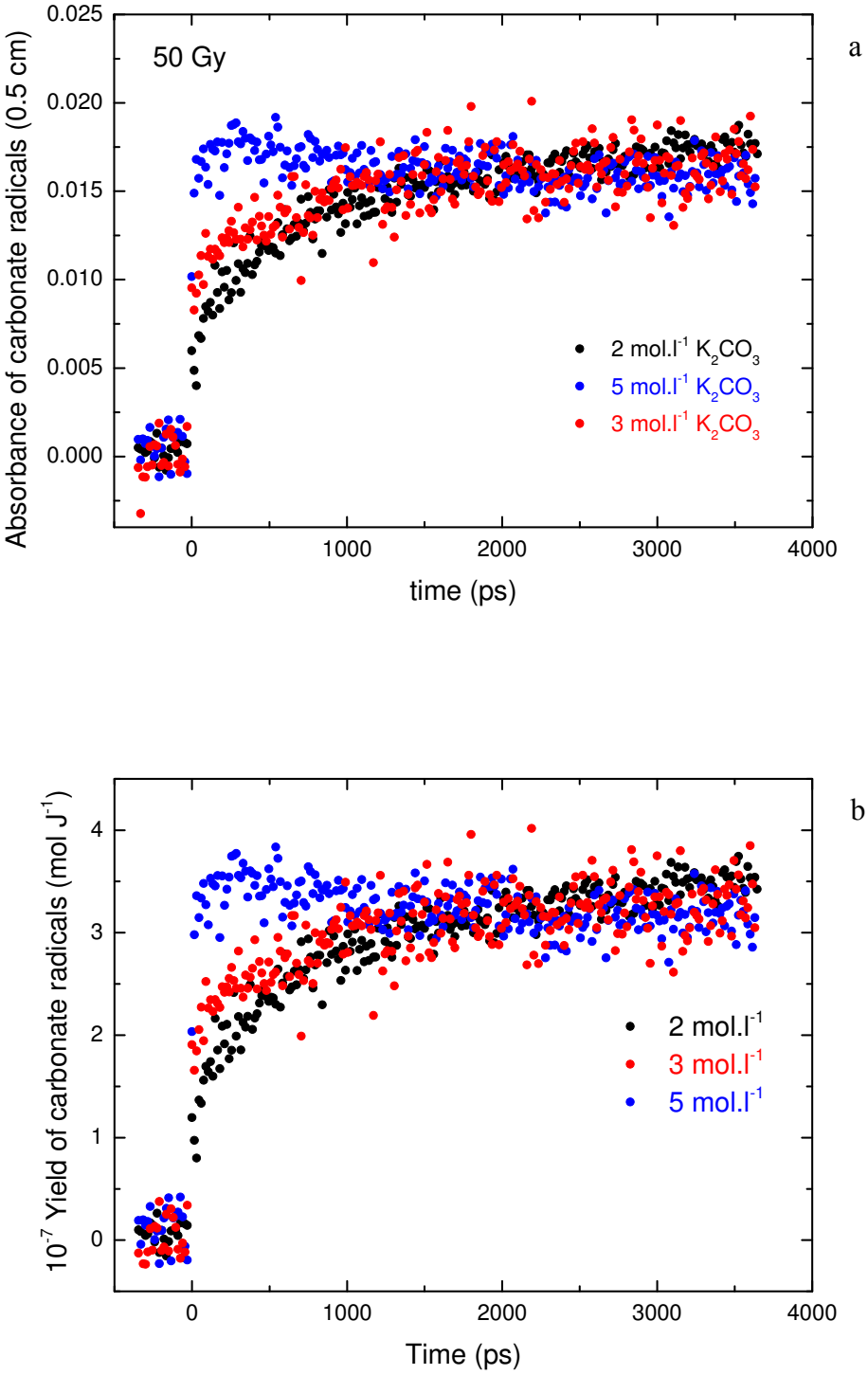

Figure III.8: *a) Absorbance of carbonate radical as a function of time, b) Radiolytic yield of carbonate radical as a function of time.*

E. Overview of the Pulse radiolysis experiment of carbonate solutions

As the conclusion of this part dedicated to the pulse radiolysis of carbonate, it was determined that:

- The shift of solvated electron due to carbonate is more important than K^+
- The only appropriate electron scavenger for highly concentrated carbonate solutions is the nitrate
- In carbonate solution with a concentration of 5 $mol.l^{-1}$, the production of carbonate radical is higher through direct effect than indirect effect while in lower concentrations of carbonate it is not the case.
- The direct effect of production of carbonate radical lasts only 2000 ps largely faster than the oxidation/reduction mechanisms of Mn, Re, Tc. Therefore it can be concluded that the carbonate radicals which come from the radiolytic direct effect has no effect on the speciation of Mn, Tc and Re in concentrated carbonate solution under irradiation.
- The radiolytic yield of carbonate radical for different carbonate concentration at different times after electron pulse are summarized in Table III.2.

***Table III.2**: Radiolytic yield of carbonate radical for different carbonate concentration at different times after electron pulse*

K_2CO_3 [$mol.l^{-1}$]	$G(CO_3^{\bullet-}) \times 10^{-7}$ $mol.J^{-1}$		
	50 ps	300 ps	3000 ps
2	1.3	1.9	3.6
3	1.9	2.4	3.6
5	3.0	3.7	3.4

References

1. Buxton, G.V., *The radiation chemistry of liquid water : Principles and applications, in Charged particle and photon interactions with Matter - Chemical, Physicochemical and Biological Consequences with Applications.* book, ed. A.M.a.Y.H. Dekker. 2004, New York, USA.
2. Lymar, S.V. and H.A. Schwarz, *acidity of the carbonate radical.* J. Phys. Chem. A, 1999. **103**: p. 3447-3450.
3. Mozurnder, A. and Y. Hatano, *Charged Particle and Photon Interactions with Matter ChemicaI, PhysicochemicaI, and BiologicaI Consequences with Applications*. 2004: New York : Marcel Dekker.
4. Augusto, O., et al., *Nitrogen dioxide and carbonate radical anion: two emerging radicals in biology.* Free Radical Biology & Medicine, 2002. **32**(9): p. 841-859.
5. Stpotheim-Maurizot, M., et al., *Radiation chemistry from basics to applications in material and life sciences*. 2008: EDP Science.
6. Al-Assaf, S., et al., *Chain scission of hyaluronan by carbonate and dichloride radical anions: Potential reactive oxidative species in inflammation?* Free Radical Biology & Medicine 2006. **40**: p. 2018-2027.
7. Alvarez, M.N., et al., *Reaction of the carbonate radical with the spin-trap 5,5-dimethyl-1-pyrroline-N-oxide in chemical and cellular systems: Pulse radiolysis, electron paramagnetic resonance, and kinetic-competition studies.* Free Radical Biology & Medicine 2007. **43**: p. 1523-1533.
8. Lymar, S.V., H.A. Schwarz, and G. Czapski, *Medium e ects on reactions of the carbonate radical with thiocyanate, iodide, and ferrocyanide ions.* Radiation Physics and Chemistry, 2000. **59**: p. 387-392.
9. Wu, G., et al., *temperature dependence of carbonate radical in NaHCO3 and Na2CO3 solutions: is the radicala single anion?* J. Phys. Chem. A, 2002. **106**: p. 2430-2437.
10. Balcerzyk, A., et al., *Direct and Indirect Radiolytic Effects in Highly Concentrated Aqueous Solutions of Bromide.* J. Phys. Chem. A, 2011. **115**: p. 4326-4333.
11. El Omar, A.K., et al., *Competition Reactions of H2O•+ Radical in Concentrated Cl- Aqueous Solutions: Picosecond Pulse Radiolysis Study.* J. Phys. Chem. A 2012. **116**: p. 11509-11518.
12. Balcerzyk, A., J. LaVerne, and M. Mostafavi, *Picosecond Pulse Radiolysis of Direct and Indirect Radiolytic Effects in Highly Concentrated Halide Aqueous Solutions.* J. Phys. Chem. A, 2011. **115**: p. 9151-9159.
13. Balcerzyk, A., et al., *Picosecond Pulse Radiolysis Study of Highly Concentrated Nitric Acid Solutions: Formation Mechanism of NO3• Radical.* J. Phys. Chem. A, 2012. **116**: p. 7302-7307.
14. El Omar, A.K., et al., *Spur Reactions Observed by Picosecond Pulse Radiolysis in Highly Concentrated Bromide Aqueous Solutions.* J. Phys. Chem. A, 2013. **117**: p. 2287-2293.
15. Ma, J.S., U.; Pernot, P.; Mostafavi, M, *Reactivity of the Strongest Oxidizing Species in Aqueous Solutions: The Short-Lived Radical Cation H2O•+.* J. Phys. Chem. Lett., 2014. **5**: p. 258-261.
16. Ma, J., U. Schmidhammer, and M. Mostafavi, *Picosecond Pulse Radiolysis of Highly Concentrated Sulfuric Acid Solutions: Evidence for the Oxidation Reactivity of Radical Cation H2O•+.* J. Phys. Chem. A, 2014. **118**: p. 4030-40307.
17. Muroya, Y., et al., *Ultra-fast pulse radiolysis: A review of the recent system progress and its application to study on initial yields and solvation processes of solvated*

electrons in various kinds of alcohols. Radiation Physics and Chemistry, 2008. **77**(10-12): p. 1176-1182.

18. Ma, J., U. Schmidhammer, and M. Mostafavi, *Picosecond Pulse Radiolysis of Highly Concentrated Phosphoric Acid Solutions: Mechanism of Phosphate Radical Formation.* J. Phys. Chem. B, 2015. **119**(24): p. 7180-7185.
19. Bonin, J., I. Lampre, and M. Mostafavi, *Absorption spectrum of the hydrated electron paired with nonreactive metal cations.* Radiation Physics and Chemistry, 2005. **74**(5): p. 288-296.
20. Guozhong Wu, et al., *Temperature Dependence of Carbonate Radical in NaHCO3 and Na2CO3 Solutions: Is the Radical a Single Anion?* J. Phys. Chem. A 2002. **106**: p. 2430-2437.

Chapter IV: Speciation of manganese in concentrated carbonate solution under irradiation

In this chapter, the oxidation/reduction reactions of manganese species with different oxidation states in highly concentrated carbonate solution (5 $mol.l^{-1}$) and their speciation are described. In order to determine the suitable experimental conditions (carbonate and Mn concentrations, atmosphere), electrochemistry measurements are performed. After calibration of the absorption band and characterization of the species by electrochemistry, the γ-ray and He^{2+} radiolysis experiments are performed to investigate the oxidation of Mn(II) and the reduction of Mn(VII). Thus this chapter is divided in three parts: (i)in a first part, the electrochemistry experiment results are discussed, (ii) in a second part the speciation of manganese under γ-ray radiolysis, with two different sources, to study dose rates effect, is investigated; (iii) in the last part, the speciation of manganese under He^{2+} radiolysis is performed in order to investigate the LET effect.

A. Mn speciation during electrochemistry experiments

The reduction process of Mn(VII) is performed by electrochemistry in galvanic mode for different concentrations of carbonate solutions. The results have shown that for the solutions with carbonate concentrations lower than 2 $mol.l^{-1}$, the final products of reduction precipitate onto the work electrode. For low carbonate concentration at alkaline pH manganese precipitates as MnO_2. In order to prevent the precipitation process as MnO_2 and to enhance the reaction between reduced manganese and carbonate, it is necessary to use carbonate solution with concentration of 5 $mol.l^{-1}$. The results have shown that the reduction in deaerated condition prevents the re-oxidation of reduced manganese with air. This result can be explained because the oxygen cannot compete with carbonate during the reduction reaction of manganese. All the experiments were carried out in carbonate 5 $mol.l^{-1}$ and deaerated condition (electrochemistry and radiolysis). During the reduction process, the purple color of Mn(VII) changes to red then follown by yellow-brown and finally transparent solution with brown precipitate (see Figure IV.1). *In situ* UV-Vis spectra of reduction are recorded automatically each 10 minutes for duration of 4 days (cf. Figure IV.2). For the time range of 2400 min, UV-Vis bands of Mn(VII) (585/541/521/505 nm) decrease with the time while the UV band at 270 nm increases. This trend reaches one isobestic point at $\lambda = 470$ nm with a Mn oxidation state change. The final step is a characteristic feature of a solid precipitation spectrum at the end of reduction time (2800 min).

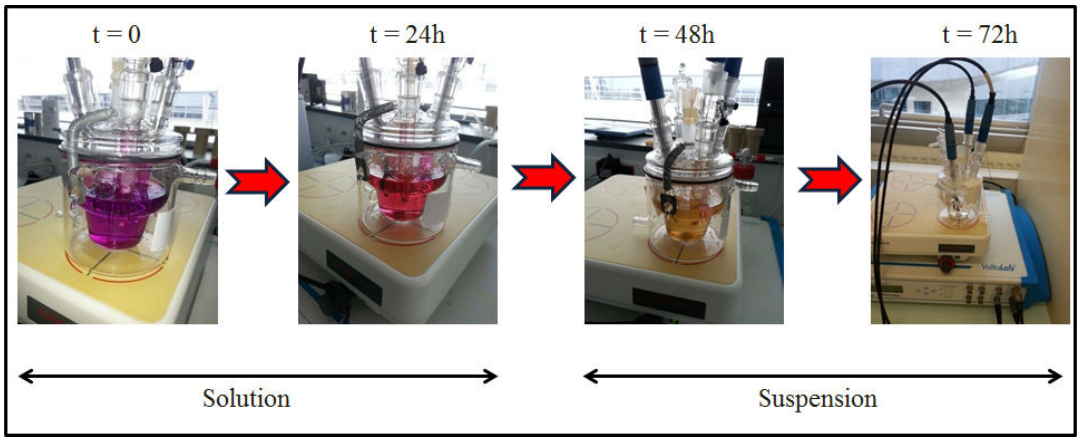

Figure IV.1: *Color change during the electrochemical reduction of Mn(VII) in carbonate 5 mol.l^{-1} for a time of 2800 min, Galvanic mode (I < -100 µA)*

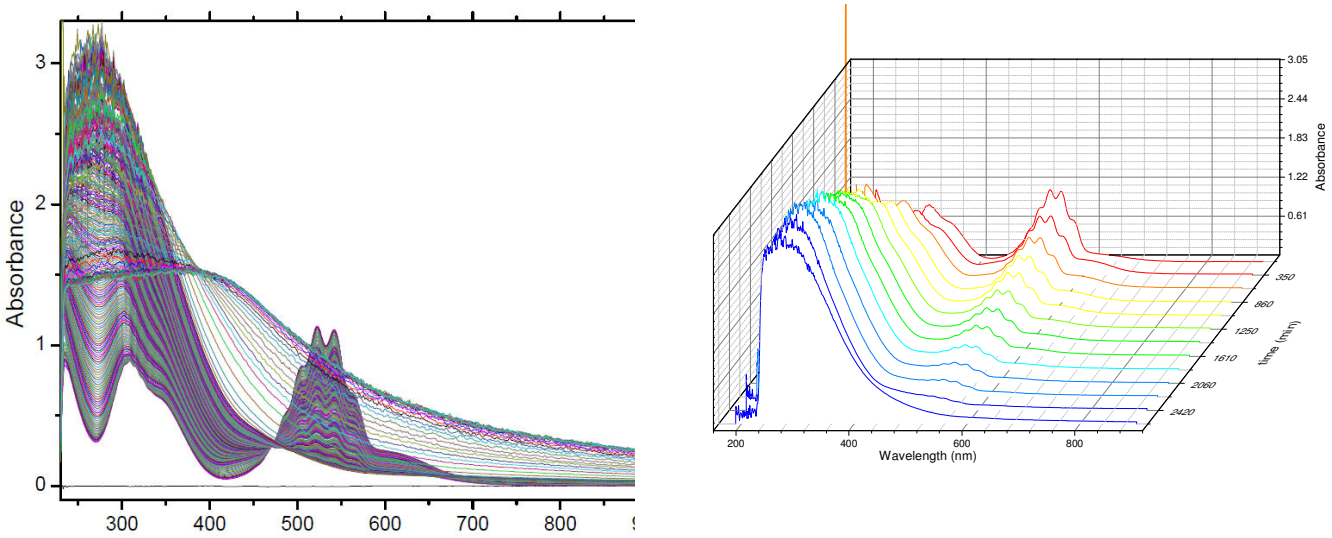

Figure IV.2: *In situ UV-Vis spectra for electrochemical reduction of $KMnO_4$) in carbonate 5 mol.l^{-1}, Galvanic mode (I < -100 µA), one spectrum monitored each 10 min for a total duration of 4 days.*

At our knowledge, no absorption coefficient for permanganate ($KMnO_4$) in carbonate solution with concentration of 5 mol.l^{-1} was reported in literature. Thus, 5 solutions with different concentrations of permanganate in carbonate solution are prepared. Moreover, the absorption coefficient is calculated for each concentration by Beer-Lambert law and their average is considered as absorption coefficient of permanganate. Figure IV.3 shows the diagram of the determined absorption coefficient of permanganate at 521 nm. The ε is defined

for the wavelengths at 521 nm and at 309 nm as 2282 $l.mol^{-1}.cm^{-1}$ and 1840 $l.mol^{-1}.cm^{-1}$ respectively.

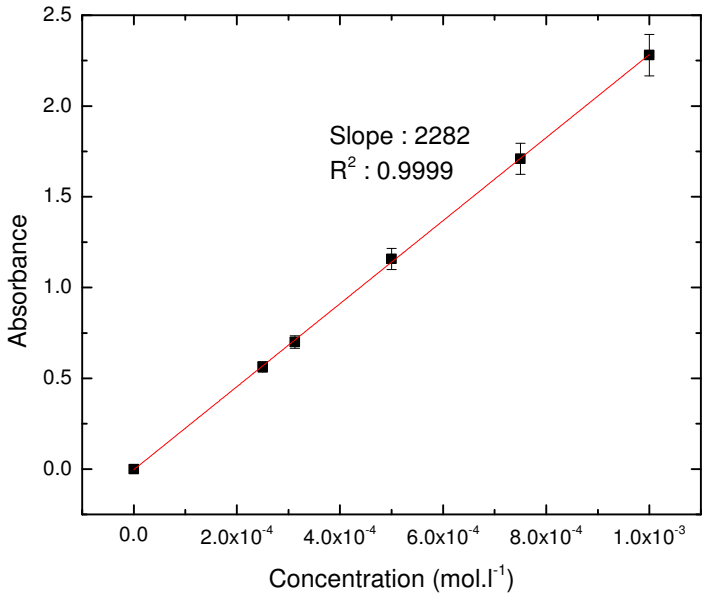

Figure IV.3: *Absorption of permanganate at 521 nm vs. concentration in solution of carbonate with concentration of 5 mol.l^{-1}*

As the final product of the electrochemical reduction is Mn(IV), thus the isobestic point is related to Mn(VII) and Mn(V). Therefore, the spectrum of Mn(V) is extracted from the UV spectra when almost all of Mn(VII) is reduced (Figure IV.4). It seems important to identify the spectra of intermediate species to understand the mechanism of electrochemical oxidation/reduction reactions. The Mn(V) spectrum obtained by the electrochemical way will be used as reference for the reduction process by radiolysis.

In summary, the carbonate solution should be at its higher possible concentration in order to prevent the formation of MnO_2 solid. The final product of reduction of Mn(VII) is Mn(IV) with a detectable spectrum of Mn(V) as an intermediate product. These information and UV spectra are useful to understand the speciation of manganese under irradiation in the carbonate media.

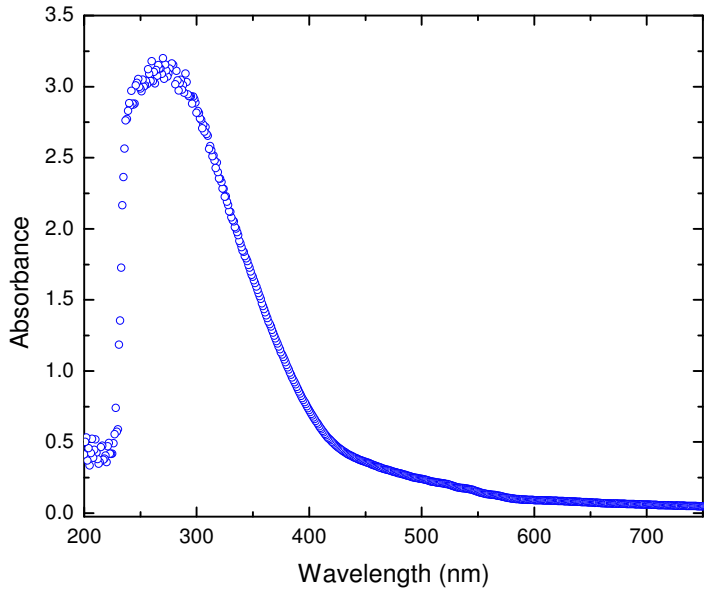

Figure IV.4: *Calculated spectrum of Mn(V) in reduction reaction by electrochemistry at [Mn(VII)] = 0 mol.l^{-1} ,*

B. Mn speciation during radiolysis experiments

Radiolysis of the solution containing carbonate ion produces reducing and oxidizing radicals and molecules. Metals can be reduced or oxidized due to their redox potentials by them. In carbonate media, $HO^{\bullet}$ is scavenged by CO_3^{2-} [1].

$$HO^{\bullet} + CO_3^{2-} \rightarrow CO_3^{\bullet-} + HO^- \qquad k = 3.9 \times 10^8\ M^{-1}.s^{-1} \qquad \text{(IV-1)}$$

Due to the high concentration of carbonate (5 mol.l^{-1}), $CO_3^{\bullet-}$ is produced by the direct effect too. Thus in this system, $e^-_{(aq)}$ and $H^{\bullet}$ are considered as reductive species in contrary to the $CO_3^{\bullet-}$ that is a strong oxidant (E = 1.5 V) [2]. The difference between redox potentials of Mn(VII) and Mn(II) allows the reduction/oxidation of Mn(VII)/Mn(II) respectively by the radiolysis of the carbonate solution. The XPS technique, which is discussed in the solid characterization part (B.3), shows that the final products of both reduction and oxidation are one Mn(IV) oxide phase. In this study, the final product of the reduction of Mn(VII) by radiolysis is called RedMn and the final product of the oxidation of Mn(VII) by radiolysis of Mn(II) is called OxMn.

B.1. Mn speciation during γ-ray experiments

Two γ sources are used: one with a low dose rate (^{137}Cs at ARRONAX) and one with a high dose rate (^{60}Co at LCP) in order to investigate the dose rate effect on reactions mechanism and speciation. 8 cells for RedMn sample ([Mn(VII)] = 5×10^{-4} mol.l^{-1} in 5 mol.l^{-1} carbonate) and 8 cells for OxMn sample (([Mn(II)] = 5×10^{-4} mol.l^{-1} in 5 mol.l^{-1} carbonate) under Ar atmosphere are irradiated with a γ source. The dose rate was determined exactly for each position and it was around 3 ± 0.5 Gy.min^{-1}. In order to get final and intermediate products, the samples have been irradiated for different dose. Also carbonate solutions, without Mn, have been irradiated with the same absorbed dose than for the oxidation/reduction reactions. Moreover, the results of these experiments without Mn are considered as references (named "Carbonate"). The hydrogen concentration of each sample is measured directly after irradiation by μ-GC. The radiolytic yield of hydrogen was calculated for RedMn, OxMn and Carbonate samples.

The $G(H_2)$ for the carbonate solution with concentration of 5 mol.l^{-1} is two-fold lower in comparison to the pure water [3] ($G_{Carbonate}(H_2) = 1.4 \pm 0.3 \times 10^{-8}$ mol.J^{-1} *vs.* $G_{Water}(H_2) = 2.5 \pm 0.3 \times 10^{-8}$ mol.J^{-1}). No data was found in literature about the hydrogen yield of irradiated concentrated carbonate solutions. Moreover the $G(H_2)$ for OxMn sample is $2.2 \pm 0.5 \times 10^{-8}$ mol.J^{-1} that is around two-fold the $G(H_2)$ for RedMn sample ($1.3 \pm 0.3 \times 10^{-8}$) which is related to the consumption of $e^-_{(aq)}$ and $H^\bullet$ during the reduction of Mn(VII) while $e^-_{(aq)}$ and $H^\bullet$ have not participated during the oxidation reaction.

UV-Vis spectrum of each sample is recorded for each reaction (RedMn and OxMn) in order to follow the speciation evolution as function of the dose for the Mn(VII) reduction and the Mn(II) oxidation processes. The UV-Vis spectra of reduction radiolysis (Figure IV.5), with the same UV bands progressing than for the electrochemistry experiment, have shown three dose ranges: (1) between 0 and 1500 Gy (0 < irradiation time < 500 min), (2) between 3300 and 5200 Gy (500 min < irradiation time < 1733 min), (3) 7200 and 9000 Gy (1733 min < irradiation time < 2984 min). Moreover, between these three ranges we can determine two isobestic points ($\lambda_{(1)-(2)}$ = 475 nm, $\lambda_{(2)-(3)}$ = 375 nm) which are induced by the change in oxidation state of the Mn: (1) Mn(VII) → (2) Mn(V) → (3) soluble Mn(IV).

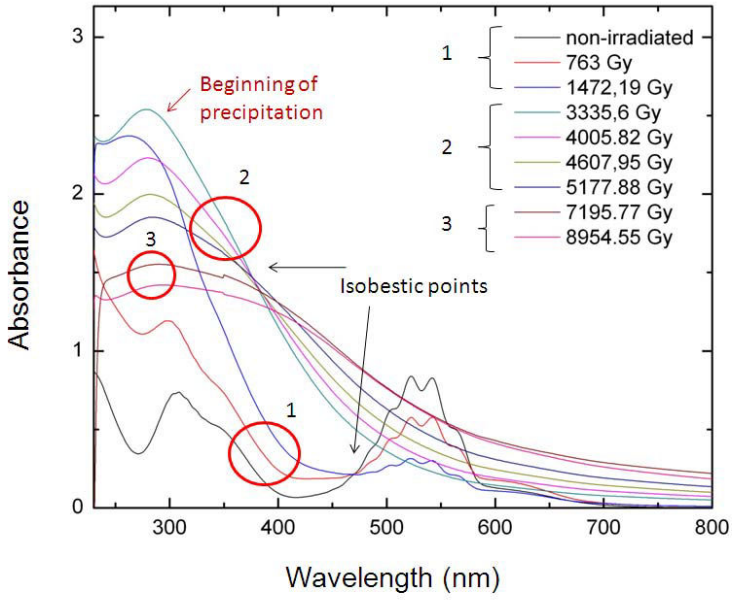

Figure IV.5: *UV-Vis spectra measured during the reduction of [$KMnO_4$] = 5 × 10^{-4} mol.l^{-1} by a) γ-ray radiolysis in carbonate 5 mol.l^{-1} media with two isobestic points (λ_1 = 475 nm, λ_2 = 370 nm) with dose rate = 3 Gy.min^{-1}.*

The spectra of γ radiolysis displays one additional isobestic point in comparison to the electrochemistry experiment, so it can be concluded that in γ radiolysis with a low dose rate, the polymerization rate of Mn(IV) is much lower than for electrochemistry. It is well-known that the γ radiolysis has reduced the solution homogenously, and then the formed Mn(IV) have more distance to each other, in comparison to the more localized formed Mn(IV) by the electrochemistry process. That is the reason why, the second isobestic point between Mn(V) and Mn(IV) appears in UV-Vis spectra of γ radiolysis. Therefore, in γ radiolysis, Mn(V) has been reduced to the soluble Mn(IV) and it is follown by the precipitation while this step is faster than in electrochemistry. The spectra of the oxidation reaction are shown (Figure IV.6). It can be noticed that, before the irradiation run, the Mn(II) is quickly oxidized to Mn(III) in comparison with the spectra from the literature [4]. After the irradiation run, the Mn(III) is oxidized into soluble Mn(IV) which absorbed the light at 430 nm. Further irradiation process induces the oxidation of all Mn(III) to soluble Mn(IV) and, at the end of the process, Mn(IV) is precipitated by polymerization reaction. The characteristic features spectra of solid precipitation were observed for both oxidation and reduction radiolysis. Moreover, it had been checked, by ICP-MS, that more than 90 % of the Mn is precipitated at the final step of the

reduction/oxidation processes. No UV-Vis spectrum is observed for Carbonate sample, and then no impact from carbonate solution can be detected during the Mn species evolution.

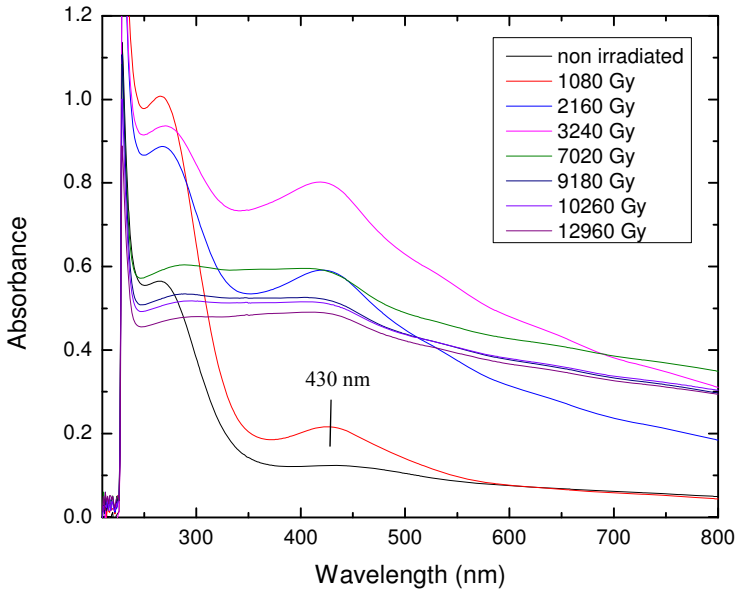

Figure IV.6: *UV-Vis spectra of the oxidation of Mn(II) to Mn(IV) by γ-ray radiolysis, [Mn] = 5 x 10^{-4} mol.l^{-1}, [K_2CO_3] = 5 mol.l^{-1} + [$KHCO_3$] = 0.5 mol.l^{-1}, dose rate = 3 Gy.min^{-1}*

In order to determine the radiolytic yield of final product, the formation yield of Mn(V) must be studied. The knowledge of the concentration of Mn(V), to calculate its yield, is mandatory. Hence, no absorption coefficient for Mn(V) in solution of carbonate at 5 mol.l^{-1} was reported in literature. That is the reason why, another experiment is carried out in order to calculate the absorption coefficient of Mn(V). In this experiment, a set of Mn(VII) solutions with the same experimental conditions (initial concentrations, chemical media, atmosphere) is irradiated with high dose rate γ source (83 Gy.min^{-1}) in order to prevent hydrolysis of Mn(IV). Figure IV.7a shows the spectra of this set. The maximum absorption for Mn(V) is at 270 nm which has been shifted due to the absorption of Mn(VII) in the same region. Moreover, this shift seems to be increased by the radiolysis reaction. Mn(VII) absorbs the light at the wavelengths 309 nm and 521 nm with the absorption coefficient of 1840 l.mol^{-1}.cm^{-1} and 2282 l.mol^{-1}.cm^{-1} respectively in carbonate solution with a concentration of 5 mol.l^{-1}. At each spectrum in Figure IV.7a, the absorbance at 309 nm is equal to (Eq.4-1) where l = 1 cm:

$$A = (l \times \varepsilon_{309} \times c)_{Mn(VII)} + (l \times \varepsilon_{309} \times c)_{Mn(V)} \quad \text{(IV -1)}$$

Each concentration of Mn(V) is calculated by the difference between initial concentration of Mn(VII) and concentration of Mn(VII) at each absorbed dose. The concentration of Mn(VII) is deduced from its absorption at 521 nm. From the previous described formula, the absorption coefficient of Mn(V) in the carbonate solution with concentration of 5 $mol.l^{-1}$ is defined for each spectrum. Therefore, the average of obtained ε is considered as the absorption coefficient of Mn(V). Then, the calculated absorption coefficient of Mn(V) is equal to 6900 $l.mol^{-1}.cm^{-1}$. This absorption coefficient is calculated by electrochemistry spectra also and they are in good agreement. The comparison of the spectra of reduction reaction by electrochemistry and low dose rate γ radiolysis, when most of Mn(VII) is reduced, indicates that the maximum absorption of Mn(V) at 270 nm is shifted in radiolysis and the soluble Mn(IV) absorbs the light in the same region of Mn(V) (Figure IV.7b).The radiolytic yield of Mn(V) formation under γ irradiation ($G\gamma(Mn(V) = 1.00 \times 10^{-7}$ $mol.J^{-1}$) is equal to the radiolytic yield of Mn(VII) decay. Figure IV.8 displays radiolytic yield of Mn(V) formation vs. radiolytic yield of Mn(VII) decay. This diagram shows that, when most of the Mn(VII) is reduced, the concentration of Mn(V) is lower than concentration of Mn(VII) before irradiation. Moreover, with calculation, when there is no Mn(VII) in the solution, approximately 90 % of the total manganese exists as Mn(V). The equality of Mn(VII) decay radiolytic yield with Mn(V) formation radiolytic yield indicates that the reduction of Mn(VII) to Mn(V) is very fast and; thus the Mn(VI) must be disappeared by disproportionation. Therefore, the reduction mechanism of manganese from the oxidation state of +VII to +IV can be induced by the radiolysis and the disproportionation phenomena. The global reduction mechanism is listed below (Eq. IV -2):

$$Mn(VII) \xrightarrow{\text{Radiolysis}} Mn(VI)$$

$$Mn(VI) + Mn(VI) \xrightarrow{\text{Disproportionation}} Mn(VII) + Mn(V)$$

$$Mn(V) \xrightarrow{\text{Radiolysis}} Mn(IV)_{\text{soluble}}$$

$$Mn(IV)_{\text{soluble}} \xrightarrow{\text{Hydrolysis}} Mn(IV)_{\text{insoluble}} \qquad \text{(IV -2)}$$

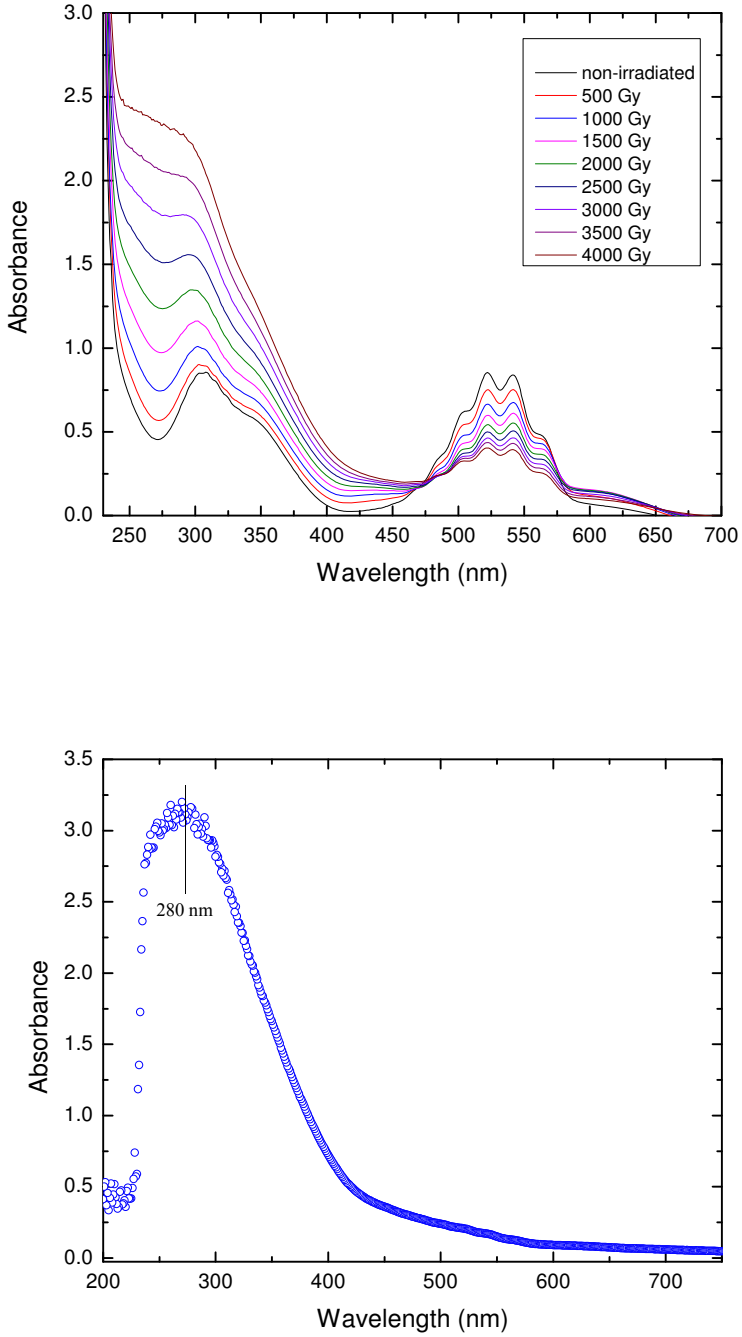

Figure IV.7: *a) UV-VIS Spectra of γ radiolytic reduction of Mn(VII) to Mn(V) under γ irradiation with high dose rate = 83 Gy.min^{-1} for Mn(V) ε = 6900 l.mol^{-1}.cm^{-1}, λ = 309 nm , b) Spectrum of Mn(V) in reduction reaction by electrochemistry at [Mn(VII)] = 0 mol.l^{-1}, Galvanic mode (I < -100 µA). [Mn] = 5 x 10^{-4} mol.l^{-1}, [K_2CO_3] = 5 mol.l^{-1} + [$KHCO_3$] = 0.5 mol.l^{-1}*

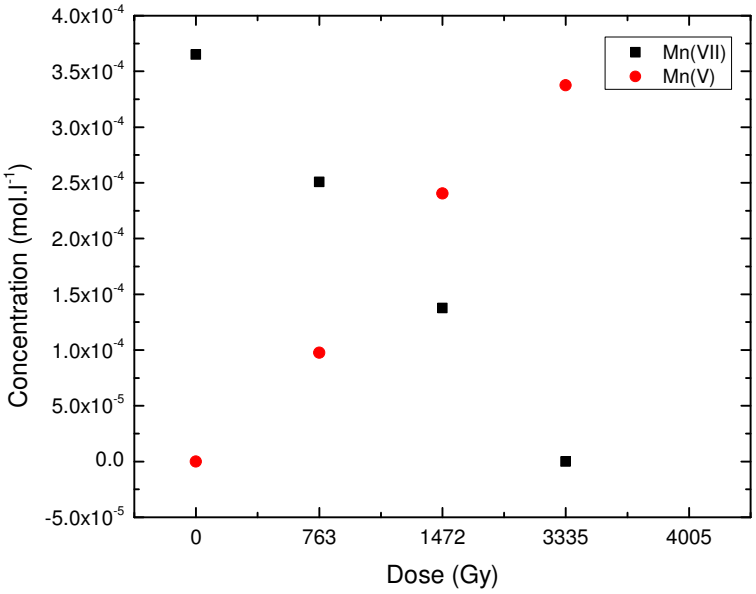

Figure IV.8: *Concentrations of Mn(VII) and Mn(V) as a function of absorbed dose. Dose rate = 83 Gy.min^{-1}.*

B.2. Mn speciation during He^{2+} radiolysis experiments

During He^{2+} radiolysis, the dose rate was determined before irradiation experiments. By using *in situ* UV-Vis spectroscopy, the absorbance of Fe^{3+} in super Fricke solution was recorded at 304 nm *vs.* time during the irradiation run [5]. The dose rate was calculated from the data obtained at 3800 Gy.min^{-1}. The same set of samples for the oxidation of Mn(II), the reduction of Mn(VII) and the carbonate solution alone, are irradiated in the same experimental conditions but with irradiation time much lower (between 1 and 20 min). Hydrogen radiolytic yield in He^{2+} radiolysis (For Mn(VII) = 2.7 ± 0.5 × 10^{-8}/ For Mn(II) = 3.8 ± 0.8 × 10^{-8}) is around two-fold more than γ radiolysis (For Mn(VII) = 1.3 ± 0.3 × 10^{-8} / For Mn(II) = 2.2 ± 0.5 × 10^{-8}) for all samples as described in Figure IV.9 specific to the Mn(VII) sample. During He^{2+} radiolysis, more inter radical reaction occurs between $e^-_{(aq)}$ and $H^\bullet$ than for γ radiolysis which induces more production of H_2 molecules. The obtained results have shown that the radicals are consumed more than molecules through reduction reaction. Thus, the reduction reaction occurs with a radical mechanism.

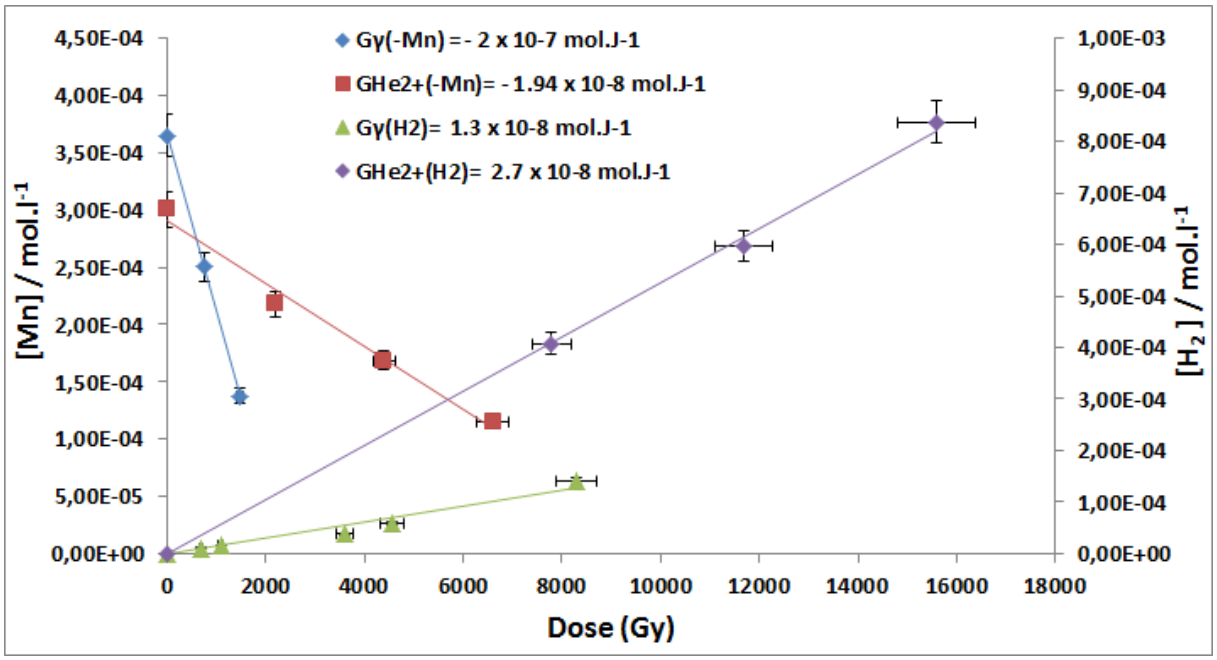

Figure IV.9: *For RedMn sample, Radiolytic yields of produced H_2 and consumed Mn(VII) vs. dose under γ-ray and He^{2+} irradiation in carbonate 5 mol.l^{-1}. γ-Ray Dose Rate = 3 Gy.min^{-1}, He^{2+} particle Dose Rate = 3800 Gy.min^{-1}*

In contrary to γ radiolysis, during the He^{2+}radiolysis only one isobestic point has been observed in the reduction radiolysis spectra (Figure IV.10). Then, we can conclude that, as the He^{2+} radiolysis energy deposition is heterogonous, the formed Mn(IV) species are localized in a low volume area and they rapidly polymerize each other. So we can conclude that the solubility of formed Mn(IV) is dependent to the homogeneity of formation of Mn(IV) in the solution. This result implies that, for a heterogeneous irradiation, the hydrolysis process is accelerated. In order to quantify this difference of kinetic, we have follown the evolution of the 521 nm UV band of Mn(VII) to determine the radiolytic yield of consumption of Mn(VII). The comparison of Gγ(-Mn(VII)) = 1.07×10^{-7} mol.J^{-1} and G_{He2+}(-Mn(VII))= 1.94×10^{-8} mol.J^{-1} has shown (Figure IV.9) that the reduction of manganese is around five-fold faster under γ irradiation even its dose rate is 1000-fold lower than under He^{2+} beam (D.Rγ = 3 Gy.min^{-1}, D.R_{He2+} = 3.8 kGy.min^{-1}).

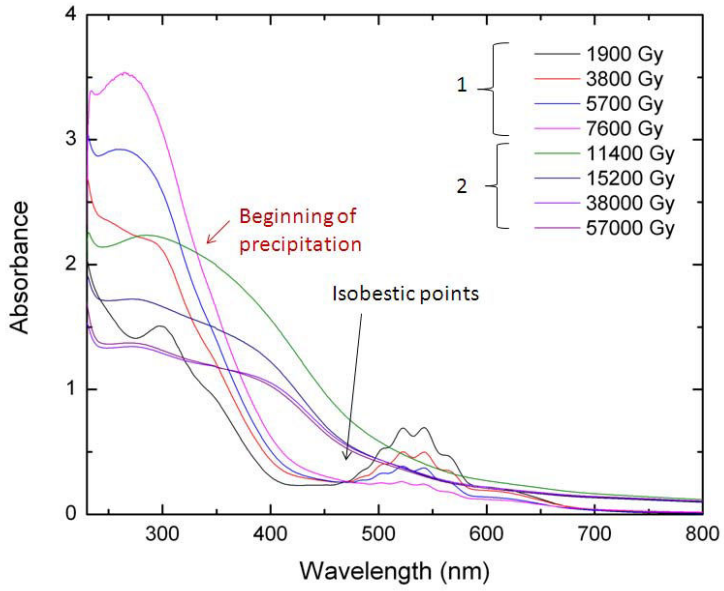

Figure IV.10: *UV spectra during the reduction of Mn(VII) by He^{2+} radiolysis in carbonate 5 $mol.l^{-1}$ media with one isobestic points (λ_1 = 475 nm), dose rate = 3800 $Gy.min^{-1}$.*

For the determination of the Mn(VI) radiolytic yield and kinetic constants, pulse radiolysis with the time window from nano to micro second should be carried out. The final product of the oxidation reaction is Mn(IV) also. In order to determine the radiolytic yield of the oxidation reaction of Mn(II) to Mn(IV), the knowledge of the radiolytic yield of carbonate radical is necessary. However, as there is no data about the radiolytic yield of carbonate radical in this solution, to understand the mechanism and kinetics, we must carry out the radiolysis of highly concentrated carbonate solutions (see Chapter III). Also, the oxidation of Mn(II) in carbonate media under He^{2+} is studied. The final product has precipitated with an oxidation state of +IV. Nevertheless, in contrary to the γ radiolysis, the He^{2+} irradiation energy deposition is heterogeneous and thus the polymerization of Mn(IV) is much more faster than for the oxidation experiment under γ irradiation. That is the reason why, no spectrum of the soluble Mn(IV) can be observed. Figure IV.11 presents the UV spectra monitored during the radiolytic oxidation of Mn(II) to Mn(IV) under He^{2+} irradiation.

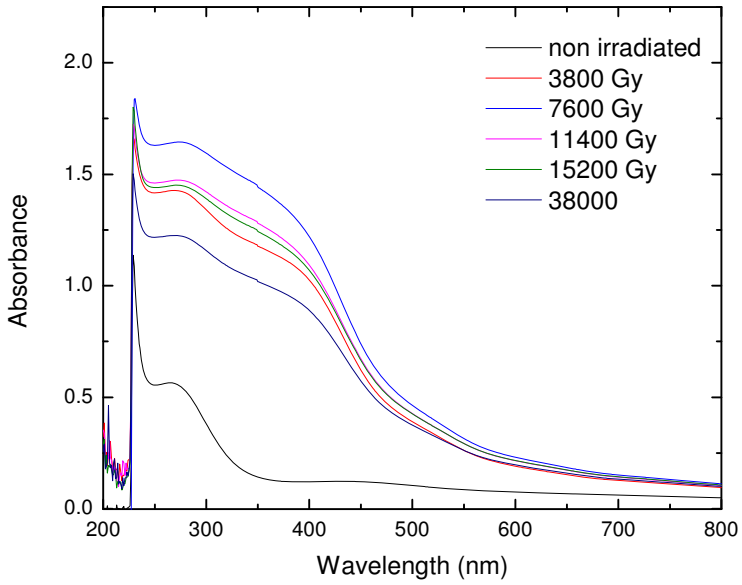

Figure IV.11: *UV-Vis spectra of radiolytic oxidation of Mn(II) to Mn(IV), He^{2+} dose rate = 3800 Gy.min^{-1}.*

B.3. Solid Characterization

When the solid precipitation have occurred during the oxidation and the reduction radiolysis experiments under both γ-ray and He^{2+} irradiations, precipitated solids are filtered in order to characterize them. As the carbonate solution with concentration of 5 mol.l^{-1} has high viscosity and there is lots of non-reacted carbonate, so all the filtered precipitate are washed six times with ultra-pure water to prevent non-reacted carbonate layers on precipitates. All the processes were done inside glove box under pure Ar atmosphere to avoid reoxidation of the solids. SEM is used for the determination of the solids morphology and size. The scanning electron micrographs are shown in Figure IV.12. The morphology of the two samples seems comparable with a particle size about 1 µm. Both the oxidation and reduction products seem to be amorphous which has been checked by XRD (Figure IV.13).

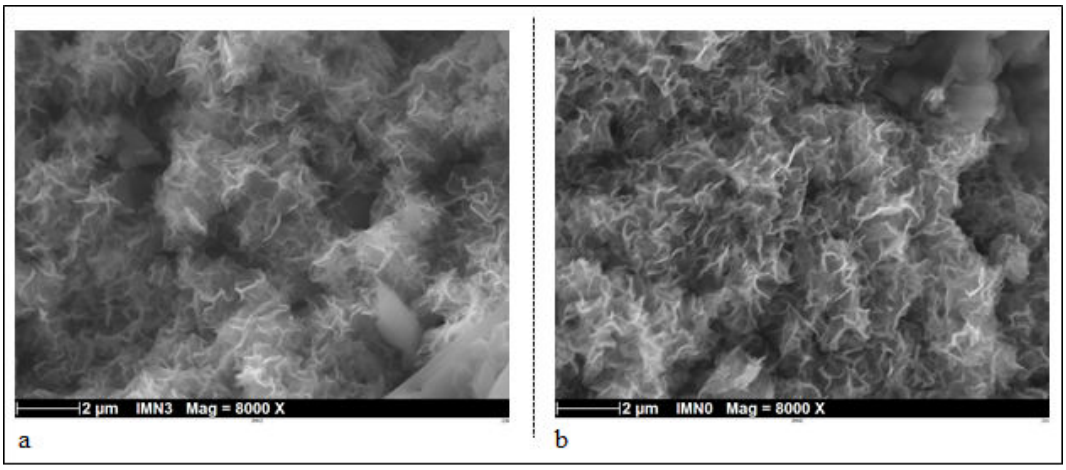

Figure IV.12: *Pictures of scanning electron microscope (SEM) , a) Final product of sample RedMn in carbonate 5 mol.l^{-1} media, b) Final product of sample OxMn in carbonate 5 mol.l^{-1} media.*

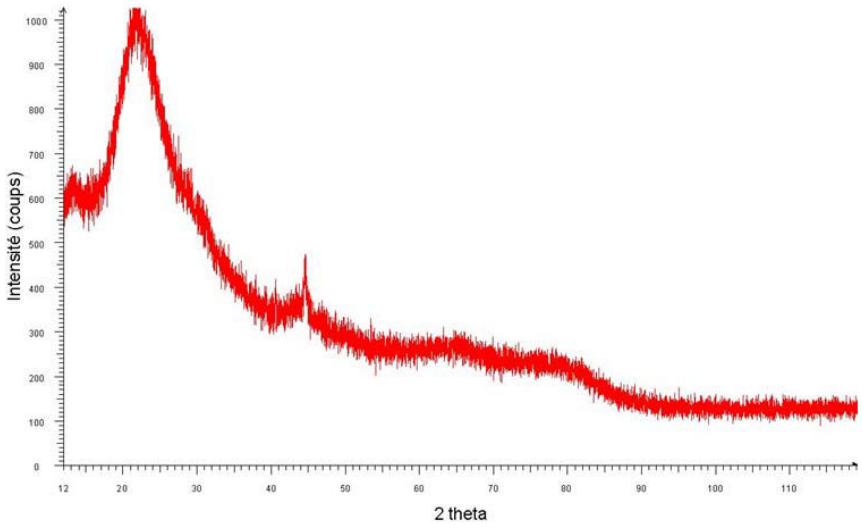

Figure IV.13: *XRD diagram of the solid obtained by radiolytic reduction of Mn(VII) under γ-ray irradiation.*

The Mn_{3s} and O_{1s} XPS spectra for the RedMn and OxMn samples are presented in Figure IV.14 with a binding energy and fitting parameters in Table IV.1. These XPS spectra have been ever used in the literature [6] in order to determine the oxidation state of Mn into solids. The results have shown that the Mn_{3s} XPS spectra present an energy splitting ΔB.E = 4.8 eV for Mn^{4+} oxide and ΔB.E = 5.9 eV for Mn^{3+} oxide due to the exchange between electrons in the 3s-3d level of Mn [7]. Figure IV.14 presents Mn_{3s} spectra for RedMn and OxMn samples. Two peaks are appeared at 84.0 eV and 88.7 eV for both samples with a

difference equal to 4.7 ± 0.2 eV which indicate the oxidation state of final products of both experiments as +IV. XPS measurements allow to characterize the final products for the oxygen chemical environment. Figure IV.14 shows the results. In previous works it was shown that the reduction of $KMnO_4$ in water by radiolysis [8] and in carbonate media by chemical method [4] resulting MnO_2 and $K_{0.5}Mn_2O_4.1.5H_2O$ respectively. Fattahi *et al.* have suggested that the final product is a mixture of Mn(IV) and Mn(III) while our XPS results have shown that there is only Mn(IV). As it is shown in Figure IV.14, the final product of oxidation reaction is mainly manganese with oxygen bridge Mn-O-Mn (B.E = 529.7 eV) as described elsewhere [9]. The different products from oxidation and reduction reactions can be attributed to low kinetic steps of oxidation reaction thus less time for manganese to reacts with ligands before stabilization. Finally, we can notice that characterization of the solids, obtained during the final step of the reduction/oxidation processes, have confirmed that the final products by γ and He^{2+} radiolysis are identical and identified as a more or less hydrated tetravalent Mn(IV) oxide.

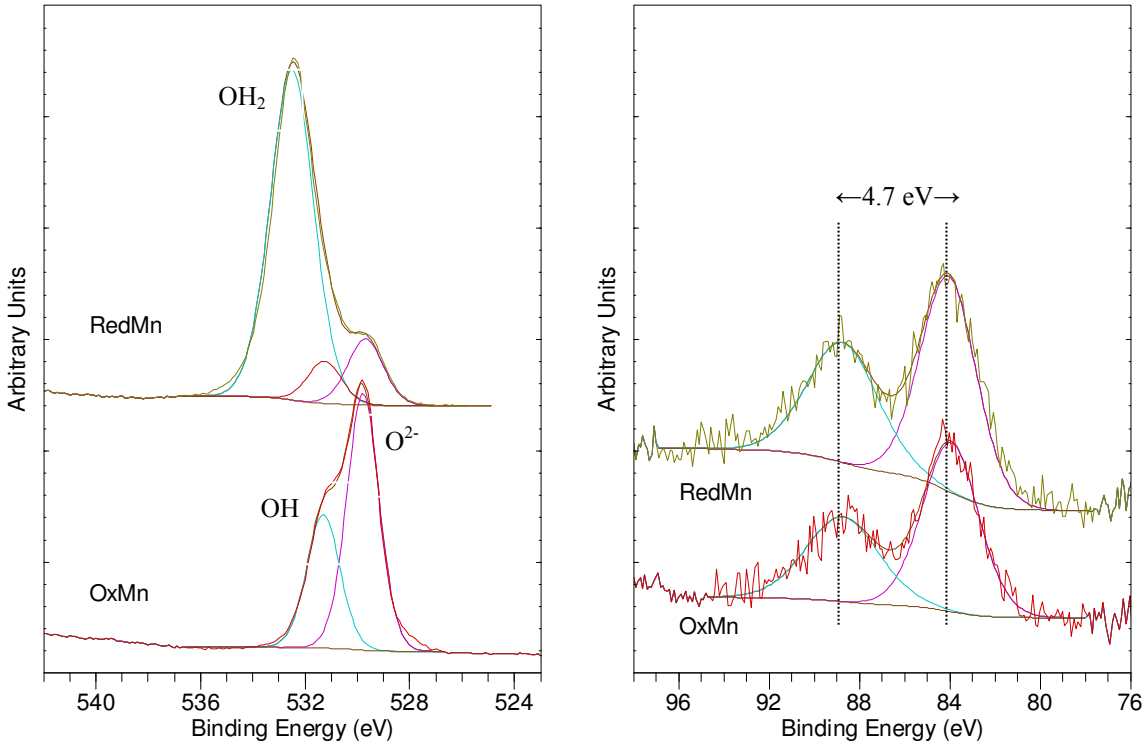

Figure IV.14: *O_{1s}(Left) and Mn_{3s}(Right) XPS spectra of final radiolysis products for RedMn and OxMn samples.*

***Table IV.1**: Fitting Parameters and Binding Energies for the O_{1s} and Mn_{3s} XPS measurements for Reduced and Oxidized Mn samples (see Figure IV.14).*

Spectra	Peak	BindingEnergy (eV)		FWHM (eV)	L/G ratio (%)
		RedMn	OxMn		
O_{1s}	O^{2-}	529.7 ± 0.1	529.7 ± 0.1	1.5 ± 0.1	30
	OH	531.3 ± 0.1	531.3 ± 0.1	1.5 ± 0.1	30
	OH_2	532.5 ± 0.1	×	1.9 ± 0.2	30
Mn_{3s}	(1)	84.0 ± 0.1	84.0 ± 0.1	2.9 ± 0.3	30
	(2)	88.7 ± 0.1	88.7 ± 0.1	3.8 ± 0.3	30

C. Overview of Mn speciation under γ-ray and He^{2+} radiolysis in highly concentrated carbonate solution

The experimental results determined during this work can be summarized by:

- The final step of both oxidation and reduction processes of Mn in highly concentrated carbonate solutions under He^{2+} and γ-ray irradiation gives the same solid precipitation (more or less hydrated tetravalent Mn(IV) oxide).
- During the reduction process Mn(VII) is the start species and the Mn(IV) is the final one. Then, it can be acceptable to assume that the intermediate species is Mn(V) identified by the two isobestic points. So, the reduction process of Mn under irradiation can be described as in Figure IV.15.
- Concerning the radiolytic yield of H_2, the reduction process of Mn(VII) consumes $e^-_{(aq)}$ and $H^\bullet$ through the indirect radiolysis; thus the $G(H_2)$ is lower than for the oxidation reaction. We assume that a catalytic effect can occur at the Mn(IV) oxide surface. Therefore, as Mn(II) is oxidized rapidly to Mn(IV), the H_2 production is higher than for the reduction of Mn(VII). However, this is a hypothesis and must be validated by further studies.

- Finally, with the kinetic difference for the reduction rate between He^{2+} and γ-ray radiolysis, we propose that the mechanisms of reduction implies mainly radical species and not molecular ones whereas for the oxidation process no conclusive results can be deduced. For the oxidation process we can suggest that the radical or molecular species contribution to the oxidation of the Mn(II) in Mn(IV) with Mn(III) as not detectable as intermediate species.
- The precipitation of Mn(IV) is due to the polymerization of Mn(IV) solution species and the heterogeneous energy deposition, during He^{2+} irradiation, can enhance this polymerization.
- All the radiolytic yields and absorption coefficients values obtained during this work have been summarized in Table IV.2.

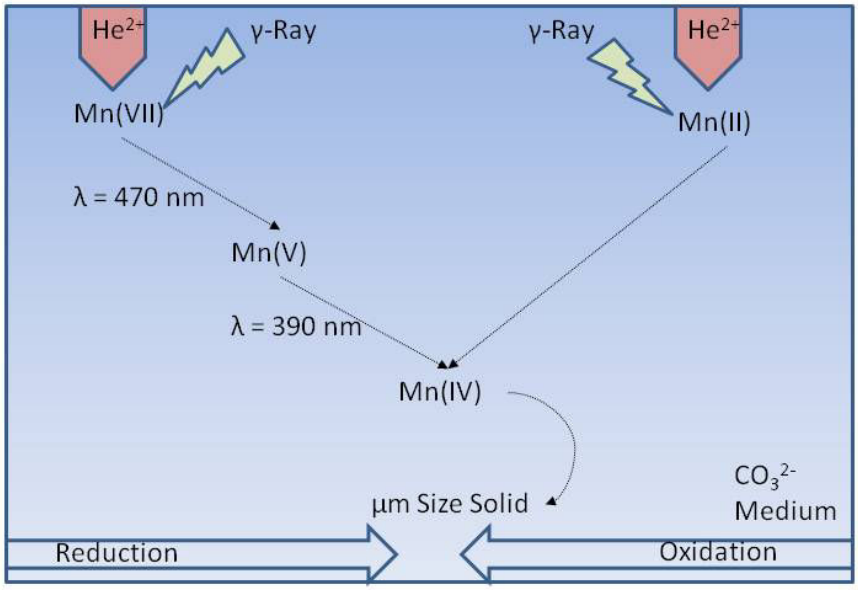

Figure IV.15: *Reduction/Oxidation Processes of Mn under He^{2+} and γ-ray irradiation with [Mn] = 5 x 10^{-4} mol.l^{-1}, [K_2CO_3] = 5 mol.l^{-1} + [$KHCO_3$] = 0.5 mol.l^{-1}, γ-Ray Dose = 9 kGy, He^{2+} particle Dose = 11.4 kGy.*

Table IV.2: *Radiolytic yields of Mn(VII) decay, of Mn(V) formation, of H_2 production and absorption coefficient values associated.*

$G(H_2)/mol.J^{-1} \times 10^{-8}$				
Ion Beam	RedMn	OxMn	Carbonate	Water
γ-Ray	1.3 ± 0.3	2.2 ± 0.5	1.4 ± 0.3	2.5 ± 0.3
γ-Ray (HDR)	0.32 ± 0.3	0.83 ± 0.3	not measured	not measured
He^{2+} Particle	2.7 ± 0.5	3.8 ± 0.8	2.8 ± 0.6	6.0 ± 0.6

$G(Mn(VII))/mol.J^{-1} \times 10^{-8}$		$G(Mn(V))/mol.J^{-1} \times 10^{-8}$
Ion Beam	Decay	Formation
γ-Ray (HDR)	10.7	10.0
He^{2+} Particle	3.0	×

Absorption coefficient/ $l.mol^{-1}.cm^{-1}$		
Species	521 nm	309 nm
Mn(VII)	2282	1840
Mn(V)	×	6900

LDR = low dose rate

HDR = high dose rate

n.b: Absorption coefficient of Mn species are calculated in concentrated carbonate solution (5 $mol.l^{-1}$)

References

1. Buxton, G.V., N.D. Wood, and S. Dyster, *Ionisation constants of ˙OH and HO˙2 in aqueous solution up to 200 °C. A pulse radiolysis study.* J. Chem. Soc., Faraday 1988. **84**: p. 1113-1121.
2. miao, J.-L., et al., *The scavenging reactions of nitrogen dioxide radical and carbonate radical by tea polyphenol derivatives: a pulse radiolysis study.* Radiation Physics and Chemistry, 2001. **60**: p. 163-168.
3. Crumière, F., et al., *LET Effects on the Hydrogen Production induced by the Radiolysis of pure Water.* Radiation Physics and Chemistry, 2013. **82**(0): p. 74-79.
4. Fattahi, M., et al., *Studies on aqueous soluble carbonato complexes of Mn^{II}, Mn^{III} and Mn^{IV}: Oxidation-Reduction relationships.* Acta Chemica Scandinavica, 1999. **53**: p. 1063-1068.
5. Costa, C., et al., *Chemical Dosimetry during Alpha Irradiation: A Specific System for UV-Vis in situ Measurement* American Journal of Analytical Chemistry, 2012. **3**: p. 6-11.
6. Toupin, M., T. Brousse, and D. Bélanger, *Charge Storage Mechanism of MnO2 Electrode Used in Aqueous Electrochemical Capacitor.* Chemistry of Materials, 2004. **16**: p. 3184-3190.
7. Chigane, M. and M. Ishikawa, *Manganese Oxide Thin Film Preparation by Potentiostatic Electrolyses and Electrochromism.* Journal of The Electrochemical Society, 2000. **147**(6): p. 2246-2251.
8. Puspalata, R., et al., *Gamma radiation induced formation and characterization of the nano-oxides of manganese.* Radiation Physics and Chemistry, 2013. **85**: p. 152-160.
9. Toupin, M., T. Brousse, and D. Bélanger, *Charge Storage Mechanism of MnO_2 Electrode Used in Aqueous Electrochemical Capacitor.* Chemistry of Materials, 2004. **16**(16): p. 3184-3190.

Chapter V: Speciation of technetium in concentrated carbonate solution under irradiation

In this chapter, the reduction reactions of technetium species with oxidation state of +VII (TcO_4^-) in highly concentrated carbonate solution (5 $mol.l^{-1}$) under irradiation are described. After the determination of the absorption bands and the characterization of the species by electrochemistry, the reduction of Tc(VII) by γ-ray and He^{2+} radiolysis are performed. Moreover, the carbonate complex of technetium is obtained by the chemical reaction of technetium ammonium chloride with hydrogen carbonate. Some parts of studies in this chapter have done by collaboration: (i) DFT simulation to check the stability of the final structure determined by EXAFS fitting (Jêrome Roques at IPN Orsay), (ii) Chemical reaction of $[NH_4]TcCl_6$ with HCO_3^- (Frederic Poineau, UNLV, USA) and (iii) EXAFS spectroscopy (Pier-Lorenzo Solary at SOLEIL Synchrotron). This chapter brings new data for the fundamental study concerning the solubility of technetium carbonate complex and its structure. Moreover this chapter answers to the scientific question about monomeric or polymeric form of technetium carbonate complex.

A. Oxidation/reduction of homologous of Tc (Mn and Re) in concentrated carbonate solution under irradiation

As technetium is a radioelement and its manipulation needs special regulation first the oxidation/reduction of manganese and rhenium in carbonate solution under irradiation (γ and He^{2+}) are attempted and discussed. It is important to notice that redox potential of technetium is between manganese and rhenium. Then these experiments are followed by γ-ray and He^{2+} irradiations of Tc(VII) in carbonate solution.

A.1. Oxidation/reduction of Mn in concentrated carbonate solution under irradiation

Chapter IV has brought results about the speciation and behavior of different oxidation states of manganese under γ and He^{2+} irradiation. The obtained data have shown that Mn(VII) and Mn(II) are reduced and oxidized respectively in concentrated carbonate solution under irradiation. The results have shown that carbonate concentration plays an important role on speciation of manganese and in solution with carbonate concentration lower than 2 $mol.l^{-1}$, the final product is MnO_2. It was observed that the final oxidation and also reduction reactions product have oxidation state of +IV. Moreover, it was determined that the γ radiolysis has higher efficiency for the reduction process than He^{2+} radiolysis due to its radical mechanism.

A.2. Oxidation/reduction of Re in concentrated carbonate solution under irradiation

Re(III), under $ReCl_3$ form, is irradiated in carbonate solution (5 $mol.l^{-1}$) by γ rays. The red-brown solution is oxidized to transparent solution of Re(VII). Figure V.1 shows the measurement *vs.* the irradiation time of UV-Vis spectra for γ-ray radiolysis experiment of Re(III) in carbonate solution. The Re(III) species has an absorption band at 543 nm while the Re(VII) absorbs only at 230 nm. Re(VII), under perrehnnetate species (ReO_4^-), is irradiated also in the same solution by γ-rays but it seems not been reduced. It is due to the redox potential of rhenium in comparison with the redox potential of $e^-_{(aq)}$ or $H^\bullet$ in presences of $CO_3^{\bullet-}$ ($E_{(ReO4-/ReO2)}$ = +510 V). The concentration of produced hydrogen is measured by μ-GC to know if this reducing agent is implied in the reduction process. With the density of solution (d = 1.54 g/cm^{-3}) the $G(H_2)$ values are measured for oxidation of Re(III) and irradiated solution of non-reduced Re(VII) in carbonate solution are 1.0 ± 0.3 × 10^{-8} $mol.J^{-1}$ and 2.9 ± 0.3 × 10^{-8} $mol.J^{-1}$.

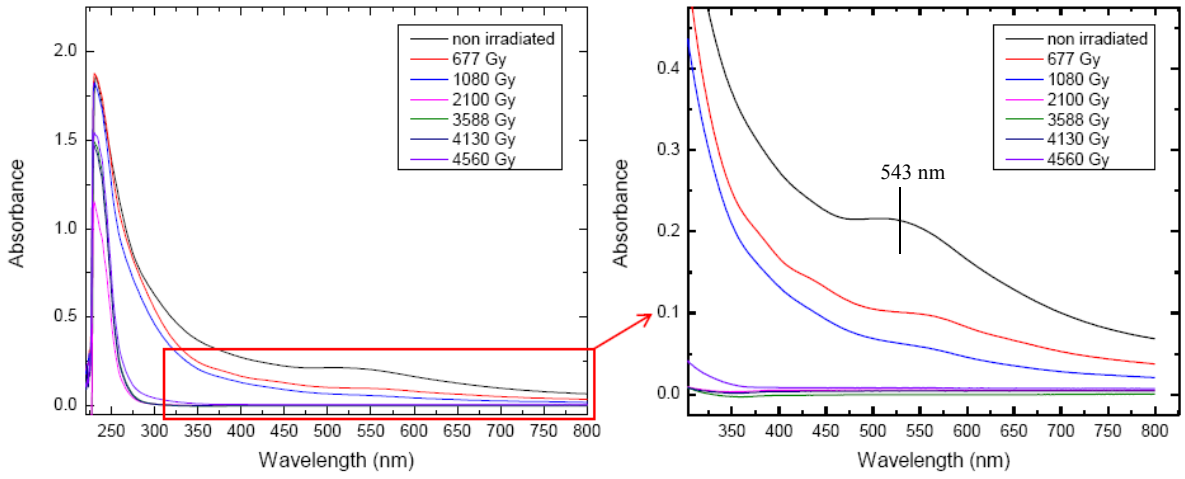

Figure V.1: *UV-Vis spectra of γ irradiation of Re(III) with concentration of 5 × 10^{-4} $mol.l^{-1}$ in carbonate solution(($[CO_3^{2-}]$ = 5 $mol.l^{-1}$ and $[HCO_3^-]$ = 0.5 $mol.l^{-1}$)). Dose rate: 3 $Gy.min^{-1}$. $\lambda_{Re(III)}$ = 543 nm.*

The formate ion is able to scavenge the hydroxyl radical ten-fold times faster than carbonate. Thus, by adding the formate ion to the carbonate solution, the concentration of $CO_3^{\bullet-}$ decreased significantly (the remaining $CO_3^{\bullet-}$ is formed through the direct effect). The formate ion with a concentration of 1 $mol.l^{-1}$ is added to the solution of $[ReO_4^-]$ = 5 × 10^{-4}

mol.l^{-1}, [CO_3^{2-}] = 5 mol.l^{-1} and [HCO_3^-] = 0.5 mol.l^{-1} and irradiated by γ rays. The transparent solution of Re(VII) is reduced to red solution of Re(IV) with an absorption band at 353 nm. Figure V.3 displays the UV-Vis spectra progress for the reduction of Re(VII) in carbonate solution in presence of formate under irradiation. The radiolytic yield of H_2 when there is non-reacting Re(VII) is three-fold higher than G(H_2) during the oxidation of Re(III). Figure V.2 shows the G(H_2) values for both Re(III) and Re(VII) radiolysis. In chapter IV, the radiolytic yield of H_2 for carbonate solution was calculated at $1.4 \pm 0.3 \times 10^{-8}$ mol.J^{-1}. Then, it can be concluded that there are several reactions that result catalytic effect on H_2 production and understanding them need complementary studies.

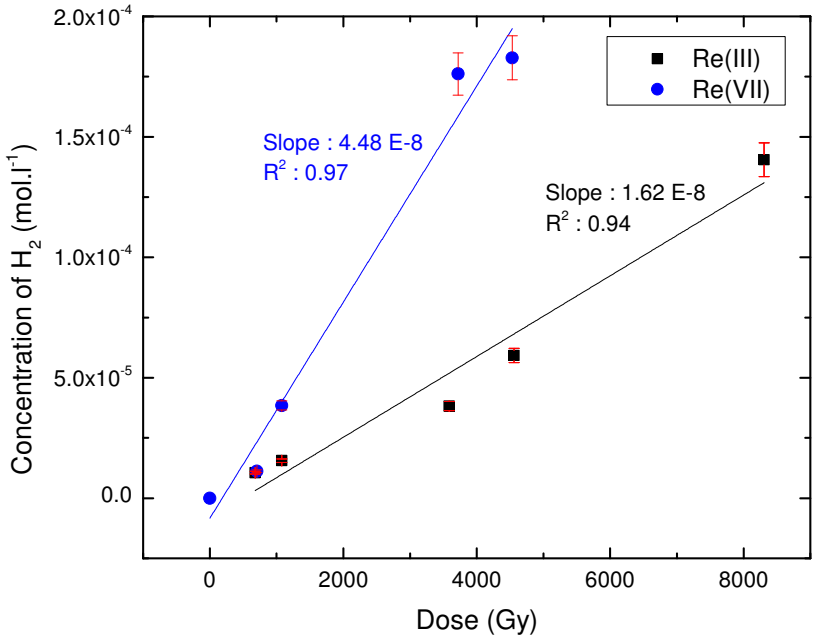

Figure V.2: Concentration of produced hydrogen for γ irradiation of Re(III) and Re(VII) in carbonate solution. Dose rate: 3 Gy.min^{-1}. [CO_3^{2-}] = 5 mol.l^{-1} and [HCO_3^-] = 0.5 mol.l^{-1}.

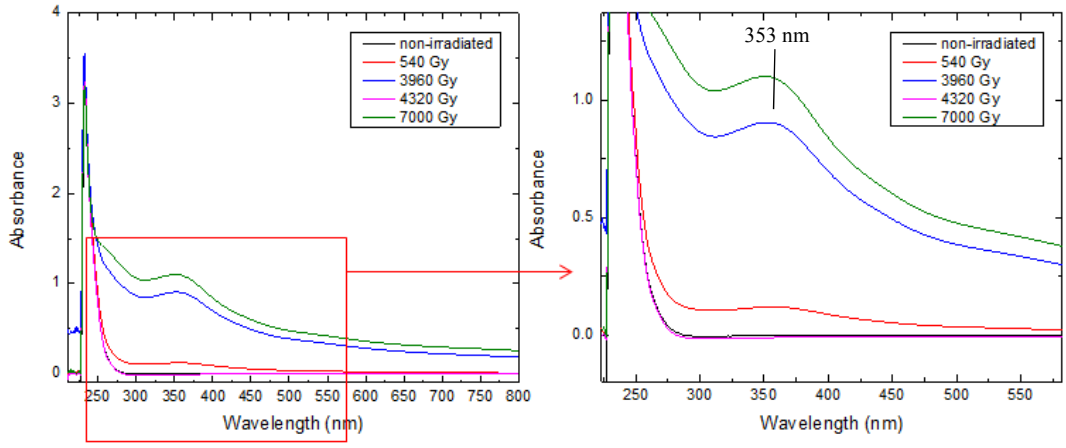

Figure V.3: *UV-Vis spectra for reduction of Re(VII) in carbonate solution ($[CO_3^{2-}]$ = 5 mol.l^{-1} and $[HCO_3^-]$ = 0.5 mol.l^{-1}) and [CO2-] = 1 mol.l^{-1} by γ radiolysis. $\lambda_{Re(IV)}$ = 353 nm. D.R = 3 Gy.min^{-1}.*

At the conclusion of this part, the rhenium species is oxidized easily and rapidly in carbonate solution under irradiation. Concerning the reduction process of Re(VII), the concentration of $CO_3^{\bullet-}$ must be decreased and the formate ion is a good candidate to achieve this goal.

Table V.1*: G(H_2) for γ irradiated solutions of Re(III) and non-reduced Re(VII) in carbonate solution. Dose rate: 3Gy.min^{-1}.*

G(H_2) × 10^{-8} mol.J^{-1}	
Re(III)	1.0 ± 0.3
Non-reduced Re(VII)	2.9 ± 0.3

B. Speciation of the Tc(IV) complex in carbonate solution

Before to carry out the radiolysis experiments, the structure and spectra of Tc(IV) complex is defined by using electrochemistry and chemical reaction in order to interpret radiolysis data easily and understand the radiolysis mechanism.

B.1. Chemical speciation of the Tc(IV) complex in carbonate media

$[NH_4]TcCl_6$ is dissolved in $KHCO_3$ solution. The concentration of $[NH_4]TcCl_6$ and $KHCO_3$ are 10^{-3} mol.l^{-1} and 2 mol.l^{-1} respectively. The violet solution of technetium chloride moves to a pink solution with absorption at 515 nm. Figure V.4 shows the UV-Vis absorption spectrum of the pink solution.

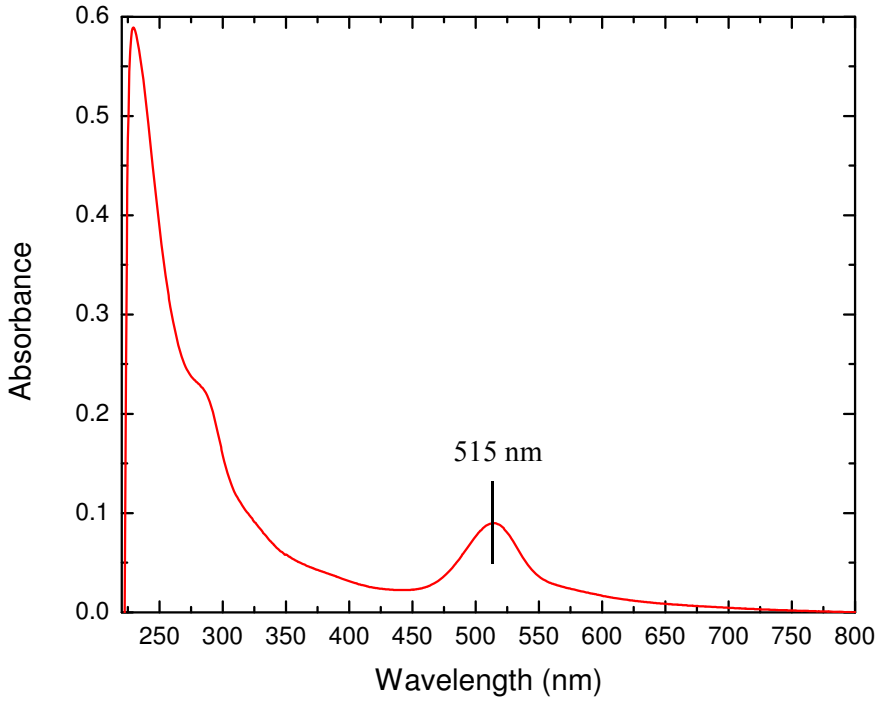

Figure V.4: UV-Vis spectrum of obtained pink solution by dissolving $[NH_4]TcCl_6$ in $[KHCO_3]$ = 2 mol.l^{-1}. $\lambda_{product}$ = 515 nm.

B.2. Structural characterization of Tc(IV) complex by EXAFS spectroscopy and DFT simulations

For structural definition the EXAFS spectroscopy is used. As explained before this technique is based on fitting the experimental spectra with theoretical spectra that come from DFT simulation. In this study, Arthemis is used as the software for fitting. In this software the experimental spectra is imported and after the theoretical spectra imported to the software.

The theoretical spectra provide different kinds of scattering and a combination of different scattering must be selected for fitting with experimental spectra. Interpreting EXAFS data takes lots of times because there are lots of scattering and their different combination should be tested. It is possible to test all the scattering combination but do not find a good fit because the theoretical spectra come from a wrong structure. The XANES spectrum of the pink solution shows that the oxidation state of this solution is +IV. In order to fit the EXAFS spectrum, the stability of different structures are tested by DFT simulations (these structures are presented in appendix). Simulation results have shown that only one structure is stable thermodynamically ($(OH)_2(CO_3)_2Tc\text{-}O_2\text{-}Tc(CO_3)_2(OH)_2$) (Figure V.6). The EXAFS spectra fits have been performed with Arthemis software. Fitting is based on different scattering and in order to do that different scattering of theoretical simulation are chosen to be compared with experimental spectra. The fitting result approves that the structure of pink solution is in good agreement with the simulation result. Figures V.5 and Table V.2 summarize the EXAFS fitting results.

Table V.2: *Results of EXAFS spectra fits for the technetium carbonate complex obtained by dissolution of $[NH_4]TcCl_6$ in the solution of $KHCO_3$ with concentration of 2 mol.l^{-1}.*

Scattering	C.N	R (Å)	σ^2 (Å^2)
Tc-O	4	2.03	0.009
Tc-O	2	2.51	0.0064
Tc-Tc	1	2.32	0.0054
Tc-C	2	3.12	0.00335
Tc-O	8	3.89	0.0042

$S_0^2 = 1$, fit in R space, $K_w = 3$, R-factor = 0.0002 and reduced $\chi^2 = 1.47$

C.N: number of neighboring at distance R

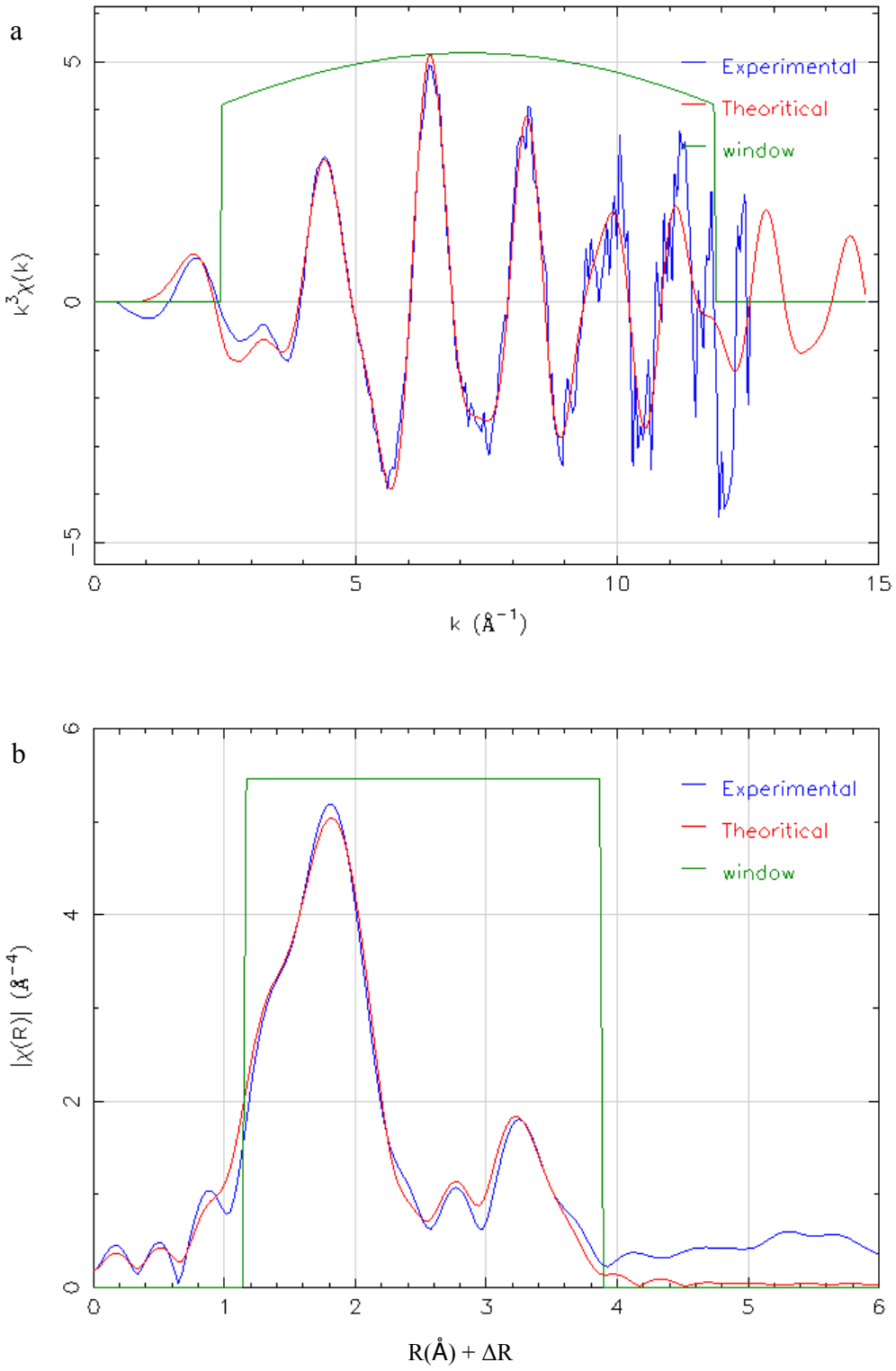

Figure V.5: *a) Fit of k^3- EXAFS spectra of Tc-Carbonate. k = 2.9-11.45 Å^{-1} Kaiser-Bessel (dk = 1) . ΔE_0= -7.13 eV. Fit in red and Experimental data in blue, b) Fit of the Fourier Transform of the k^3- EXAFS spectra of Tc-Carbonate. R-range = 1.15-3.89 Fit in red and Experimental data in blue.*

EXAFS results, shown in Table V.2, indicate the coordination of 6 for technetium with an oxidation state of +IV. The first two scattering, shown in Table V.2, confirm the DFT simulation which O atoms are located at different distance from Tc. There are four O atoms with the same distance from Tc that related to Tc-OH and Tc-OCO_2 bonds. The two Tc atoms are attached each other by two O atoms. These two O atoms do not have the same distance from Tc atom. One of them has 0.25 Å lower distances (distance for two O atoms between Tc atoms: 2.13 Å and 1.78 Å).

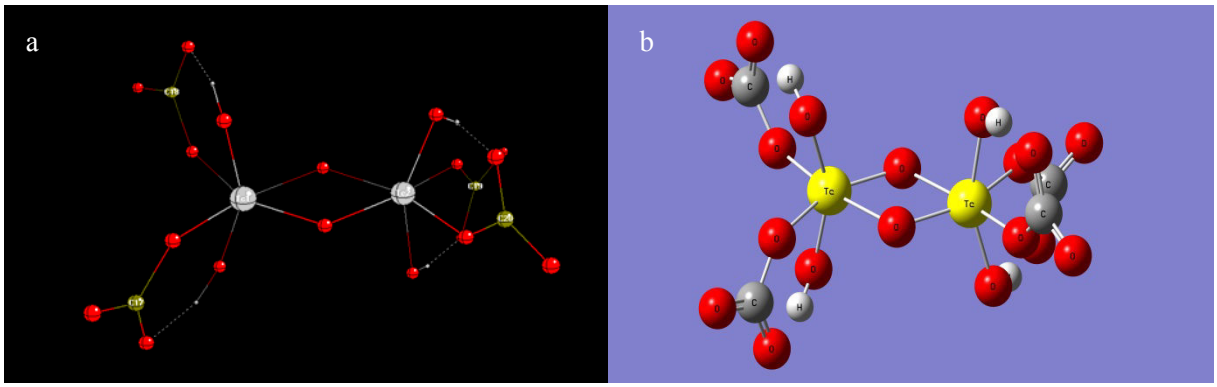

Figure V.6: *a)Calculated structure by DFT simulation of the technetium carbonate complex; Technetium, oxygen, carbon and hydrogen atoms are in gray, red, green and white colors; hydrogen bonds are showing in dotted mode. Its formula is* $Tc_2(\mu\text{-}O)_2(CO_3)_4(OH)_4$*, b) Another view of complex that is shown in part a, the both parts are showing exactly the same complex and their difference is the way of showing.*

As summary, technetium chloride with the oxidation state of +IV in the solution of $KHCO_3$ with concentration of 2 $mol.l^{-1}$ tends to be polymerized (forming dimer) and then form carbonate, hydroxyl complex with coordination of 6 for technetium. No alteration is observed for the oxidation state of technetium and stays at +IV. The carbonate complex of Tc(IV) has the formula $Tc_2(\mu\text{-}O)_2(CO_3)_4(OH)_4$.

B.3. Electrochemical reduction of Tc(VII) in carbonate solution

Pertechnetate (TcO_4^-) as Tc(VII) with a concentration of 5×10^{-4} $mol.l^{-1}$ is reduced by electrochemistry (reduction potential, E = 0.78 V [1]) in highly concentrated solution ($[CO_3^{2-}]$ = 5 $mol.l^{-1}$ and $[HCO_3^-]$ = 0.5 $mol.l^{-1}$). The transparent solution of Tc(VII) became the pink solution of Tc(IV). The UV-Vis absorption (Figure V.7) indicates that the obtained Tc(IV) has the same chemical compound as one obtained in section B.1.

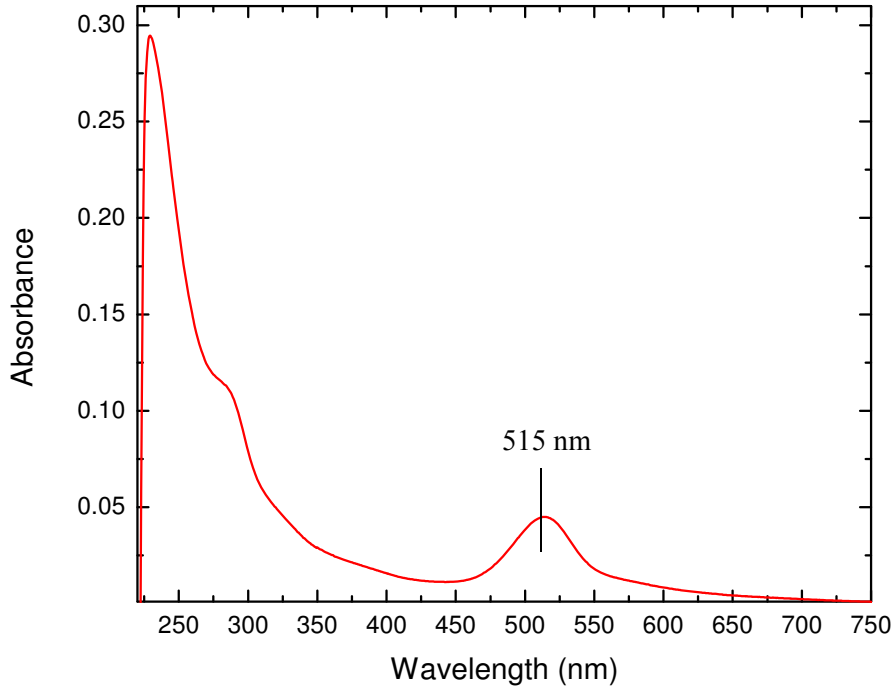

Figure V.7: *UV-Vis spectrum of obtained pink solution by electrochemical reduction of TcO_4^- in highly concentrated carbonate solution ($[CO_3^{2-}]$ = 5 mol.l^{-1} and $[HCO_3^-]$ = 0.5 mol.l^{-1}. E = 0.78 V. λTc(IV) = 515 nm.*

The work electrode, used for reduction, is composed by a platinum plate with dimension of 30 mm × 10 mm. The obtained pink solution of carbonate, hydroxyl technetium complex seems not to be more reduced and shows stability against reduction. In a previous study [2], the reduction of pertechnetate in the same solution, by using a very big work electrode, has induced the reduction of Tc(VII) to Tc(III) with an absorption band at 630 nm. Then, the Tc(III) species obtained is re-oxidized to the pink solution of Tc(IV) with an absorption at 515 nm in contact with air (re-oxidation duration is 15 hours). The EXAFS fit has revealed that the carbonate hydroxyl complex of Tc(IV) is a dimer. Thus, it can be concluded that onto the small work electrode the reduced technetium is localized and polymerized at the oxidation state of +IV. Moreover, this complex cannot be reduced to the Tc(III) species. However, a very big work electrode does not localize the reduced technetium, does not polymerize the Tc(IV) and can reduce this complex to a Tc(III) species. As the complex has one $Tc_2(\mu\text{-}O)_2$ center, the concentration of the complex at the end of reduction is half of the initial concentration of Tc(VII) before reduction. So, the concentration of complex

can be calculated at the end of the reaction and is equal to 2.5×10^{-4} mol.l^{-1}. Finally, with the complex concentration and its absorption band, the absorption coefficient can be calculated at 200 l.mol^{-1}.cm^{-1}.

In order to summarize the electrochemical reduction of Tc(VII), if the reduced technetium are localized, when the Tc(VII) is reduced to Tc(IV) polymerized and forms the carbonate hydroxyl complex if not the single Tc(IV) is reduced to Tc(III).

C. Speciation of the Tc(IV) complex in carbonate solution under irradiation

In this part the speciation of Tc(IV) complex in carbonate solution under γ and He^{2+} irradiations is presented and discussed.

C.1. Speciation of the Tc(IV) complex in carbonate solution under γ irradiation

Pertechnetate (TcO_4^-), as Tc(VII) species, with a concentration of 5×10^{-4} mol.l^{-1} is added to the carbonate solution (5 mol.l^{-1}). Tc(VII) has not been reduced under irradiation due to its redox potential in presence of carbonate radical as a powerful oxidant. As it was observed for Re(VII), it was reduced in carbonate solution under irradiation by adding formate. Thus, the formate ion is added to the carbonate solution in order to reduce Tc(VII). In a first step, the formate added with the concentration of 1 mol.l^{-1} to the carbonate solution (5 mol.l^{-1}) and Tc(VII) is reduced to the pink solution associated to the Tc(IV) complex. The oxidation state of +IV is identified by XANES spectroscopy (Figure V.8). Figure V.9 shows the UV-Vis spectra during the reduction process of Tc(VII) in carbonate solution by γ radiolysis.

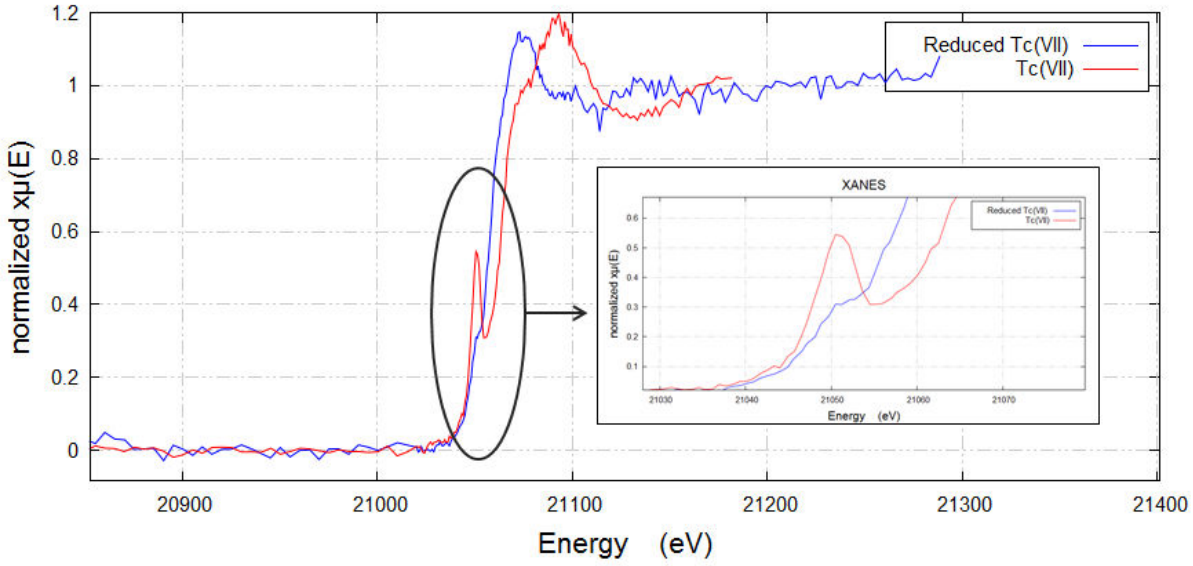

Figure V.8: *XANES spectra of Tc(VII) in red and reduced Tc in blue. γ radiolysis of Tc(VII) in the solution of carbonate ($[CO_3^{2-}]$ = 5 mol.l^{-1} and $[HCO_3^-]$ = 0.5 mol.l^{-1}) and $[CO_2^-]$ =1 mol.l^{-1}. D.R: 3 Gy.min^{-1}.*

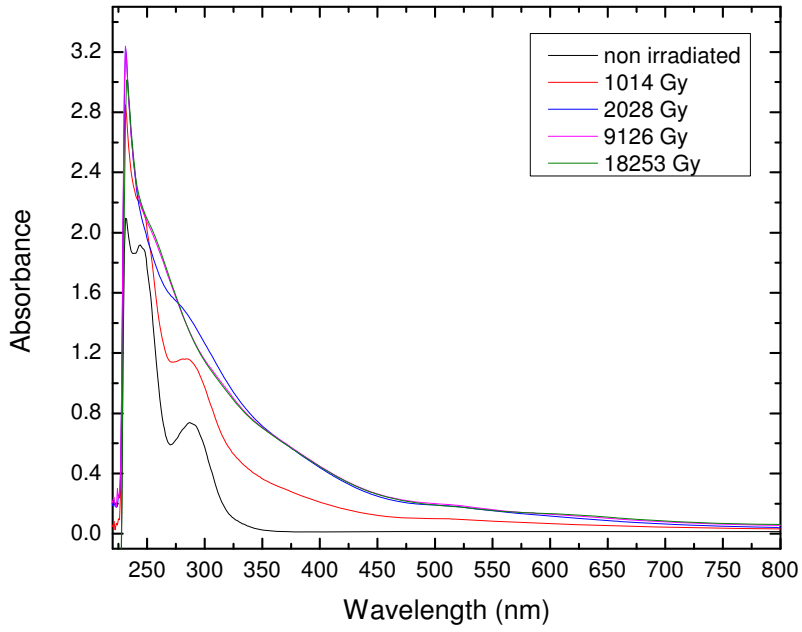

Figure V.9: *UV-Vis spectra of γ radiolysis of Tc(VII) in the solution of carbonate ($[CO_3^{2-}]$ = 5 mol.l^{-1} and $[HCO_3^-]$ = 0.5 mol.l^{-1}) and* $[CO_2^-]$ =1 mol.l^{-1}. *D.R: 3 Gy.min^{-1}.*

The progress *vs.* the irradiation time of the spectra indicates that Tc(VI) and Tc(V) are unstable or they reduced rapidly through radiolysis or disproportionation to Tc(IV). Therefore, it can be concluded that Tc(VII) is reduced directly to Tc(IV). The UV-Vis spectrum of final product is different from those obtained by electrochemical and chemical synthesis of technetium carbonate hydroxyl complex. It implies that the final product of γ radiolysis has a different structure. The same radiolysis experiment is carried out but with a formate concentration of 0.7 $mol.l^{-1}$ in order to prevent the direct effect of the formate radiolysis. Figure V.10 presents the UV-Vis spectra of this experiment.

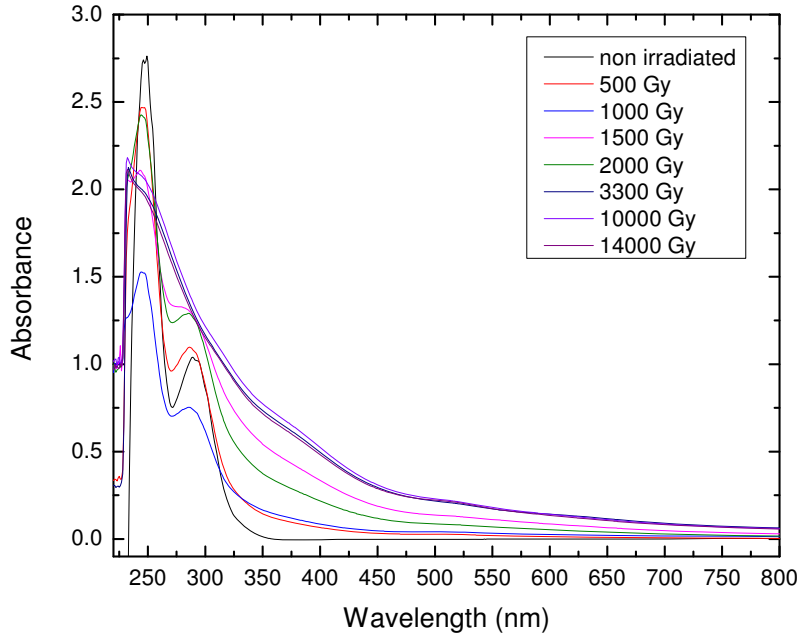

Figure V.10: *UV-Vis spectra of γ irradiation of Tc(VII) in the solution of carbonate ($[CO_3^{2-}]$ = 5 $mol.l^{-1}$ and $[HCO_3^-]$ = 0.5 $mol.l^{-1}$) and $[CO_2^-]$ = 0.7 $mol.l^{-1}$. D.R : 3 Gy.min-1.*

When the formate concentration is higher, the reduction is faster.

The hydrogen concentration determined during the radiolysis experiment of Tc(VII) in carbonate solution with formate concentration of 0.7 $mol.l^{-1,}$ is measured by μ-GC (Figure V.11). The high density of the solution (1.54 $g.cm^{-3}$) has been taken into account for the $G(H_2)$ calculation ($1.46 \pm 0.3 \times 10^{-8}$ $mol.J^{-1}$) and this value is close to the $G(H_2)$ for the carbonate solution without Tc ($1.4 \pm 0.3 \times 10^{-8}$ $mol.J^{-1}$). Considering this data and the $G(H_2)$ determined for the radiolytic reduction of Mn(VII) in carbonate solution ($1.3 \pm 0.3 \times 10^{-8}$

mol.J^{-1}); we can conclude that the formate radical ($CO_2^{\bullet-}$) is involved in the reduction process of Tc(VII). Thus, lower $e^-_{(aq)}$ is consumed in the reduction of Tc(VII) than the reduction of Mn(VII) one. The $G(H_2)$ value determined for the γ radiolysis experiment of pure water is 2.5 ± 0.3 mol.J^{-1} [3] which is around two-fold higher than the obtained $G(H_2)$ for reduction of Tc(VII) in concentrated carbonate solution under γ-ray irradiation. So we can conclude of this fact that Tc(VII) is reduced mostly by $e^-_{(aq)}$ and partly by the formate radicals. Therefore, the reduction mechanism of Tc(VII) can be supposed as below, however it should be confirmed by pulse radiolysis experiment:

$$Tc(VII) + e^-_{(aq)}/CO_2^{\bullet-} \rightarrow Tc(VI) \qquad (V\text{-}1)$$

$$Tc(VI) + e^-_{(aq)}/CO_2^{\bullet-} \rightarrow Tc(V) \qquad (V\text{-}2)$$

$$Tc(V) + e^-_{(aq)}/CO_2^{\bullet-} \rightarrow Tc(IV) \qquad (V\text{-}3)$$

Lukens *et al.* [4] have discussed the mechanisms of TcO_4^- reduction by e^- and of disproportionation. The rate constant for disproportionation of Tc(VI) and Tc(V) are determined:

$$2Tc(VI) \rightarrow Tc(VII) + Tc(V) \qquad k = 1.5 \times 10^5 \text{ l.mol}^{-1}.\text{s}^{-1} \qquad (V\text{-}4)\ [4]$$

$$2Tc(V) \rightarrow Tc(VI) + Tc(IV) \qquad k = 2.4 \times 10^3 \text{ l.mol}^{-1}.\text{s}^{-1} \qquad (V\text{-}5)\ [4]$$

These rates constants are low. Moreover, without having the radiolytic yield of formation of Tc(IV), it is not possible to verify if there is any disproportionation in reduction mechanism or not.

The pink final solution sample does not present ESR signal; it implies that the oxidation state of final product can be +IV because Tc(IV) is not a paramagnetic species. However the oxidation state of +IV for the final products have been confirmed by XANES spectroscopy (figure V.8) performed onto the SOLEIL synchrotron (MARS beamline). The EXAFS spectroscopy is carried out on the final product of reduction of Tc(VII) in carbonate solution with concentration of 5 mol.l^{-1} and formate 1 mol.l^{-1} but the fitting has not been completed yet (fitting is a long process which is based on obtained theoretical spectra from theoretical models) but by EXAFS the existence of $Tc_2(\mu\text{-}O)_2$ center is revealed.

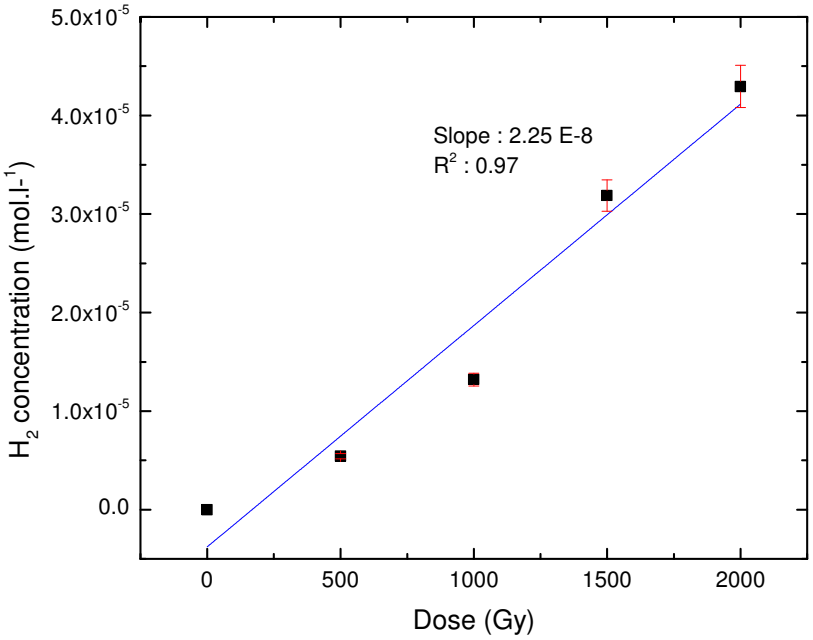

Figure V.11: *Hydrogen concentration as a function of absorbed dose for γ radiolysis of Tc(VII) with* $[CO_3^{2-}] = 5$ *mol.l*$^{-1}$, $[HCO_3^-] = 0.5$ *mol.l*$^{-1}$ *and* $[HCO_2^-] = 0.7$ *mol.l*$^{-1}$. *D.R: 3 Gy.min*$^{-1}$.

C.2. Carbonate concentration effect

Another radiolysis experiment is carried out under γ-ray irradiation of Tc(VII) with concentration of 5×10^{-4} mol.l^{-1} in solution with carbonate concentration of 10^{-2} mol.l^{-1} , bicarbonate 10^{-3} mol.l^{-1} and formate 10^{-2} mol.l^{-1} in order to study the effect of carbonate concentration on formation of technetium complexes. The UV-Vis spectra (Figure V.12) have shown that the final product of radiolysis is the very fine particles of TcO_2. It indicates that carbonate plays role as ligand only at high concentrations.

C.3. Formate effect on complexation

In order to study the effect of formate on complexation of technetium, the Tc(VII) is irradiated with γ rays in the solution of formate with concentration of 1 mol.l^{-1} but without carbonate. Figure V.13 shows the UV-Vis spectrum for final products of this experiment. The measurements check that, in the formate concentration used here (1 mol.l^{-1}), this ion is playing on speciation of final product.

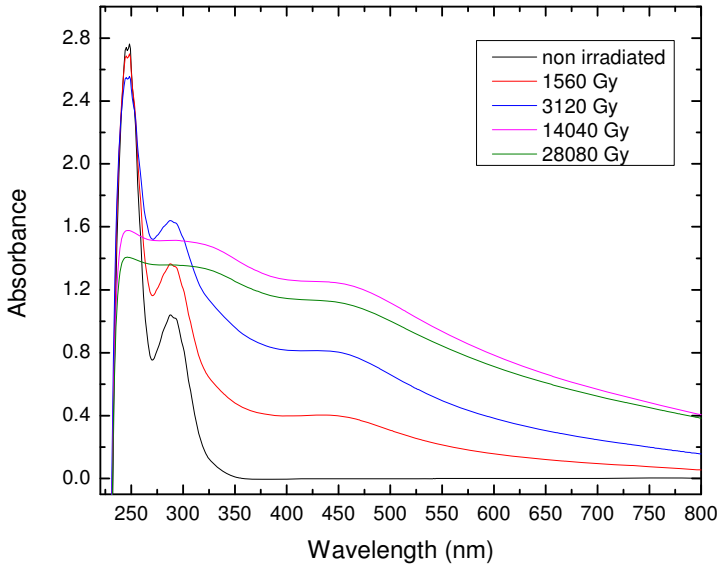

Figure V.12: *UV-Vis spectra of γ radiolysis of Tc(VII) with concentration of 5 × 10^{-4} mol.l^{-1} in solution with carbonate ([CO_3^{2-}] = 10^{-2} mol.l^{-1} and [HCO_3^-] = 10^{-3} mol.l^{-1}) and [CO_2^-] = 10^{-3} mol.l^{-1}.*

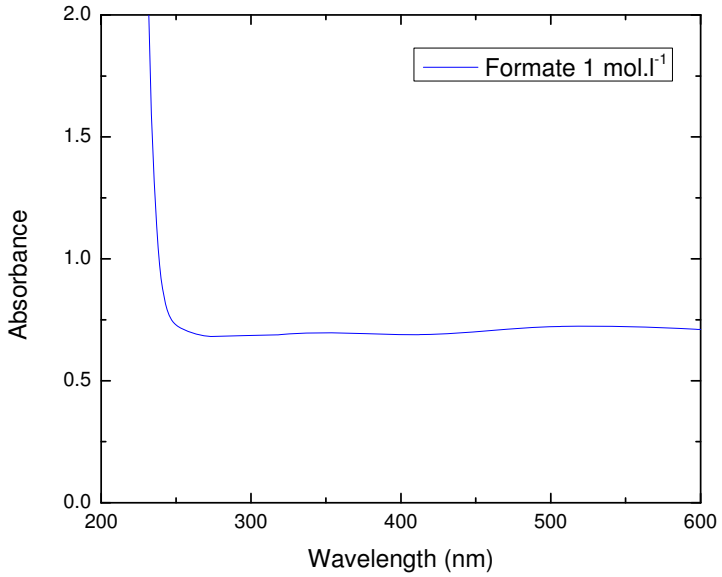

Figure V.13: *UV-Vis spectrum for final products of Tc(VII) radiolysis in formate solution.*

To summarize this part, Tc(VII) cannot be reduced in carbonate solution under irradiation unless adding formate. The final oxidation state of reduced technetium by γ radiolysis is +IV. The final product has the $Tc_2(\mu\text{-}O)_2$ center. Reduction of Tc(VII) in the solutions with carbonate concentrations lower than 1 $mol.l^{-1}$ forms only TcO_2 solid as final product.

C.4. Speciation of Tc(VII) under He^{2+} irradiation in carbonate solution

Tc(VII) with a concentration of 5×10^{-4} $mol.l^{-1}$ is irradiated in carbonate solution with concentration of 5 $mol.l^{-1}$ and formate 0.7 $mol.l^{-1}$ with a dose rate of 1000 $Gy.min^{-1}$ (dose rate is measured with super Fricke method). Figure V.14 presents the UV-Vis spectra for He^{2+} radiolysis of Tc(VII) in carbonate solution. The spectra indicate that the Tc(VII) is reduced to Tc(IV) with $Tc_2(\mu\text{-}O)_2$ center and it should has the same structure like reduced Tc(VII) by electrochemistry ($Tc_2(\mu\text{-}O)_2(CO_3)_4(OH)_4$). XANES spectroscopy approved the oxidation state of +IV for final product (Figure V.14). The final product is silent toward ESR spectroscopy and it is another confirmation of oxidation state +IV. The produced H_2 is measured by μ-GC with and without presence of formate. The results (Figure V.16) shows when the Tc(VII) is reduced, the $G(H_2)$ is lower. $G(H_2)$ for reduced and non-reduced Tc(VII) are 4.0×10^{-8} $mol.J^{-1}$ and 5.27×10^{-8} $mol.l^{-1}$ respectively. If we compare these results with $G(H_2)$ of water under He^{2+} irradiation ($6.0 \pm 0.6 \times 10^{-8}$ $mol.J^{-1}$) [3], we can conclude that the reduction reaction of Tc(VII) implies a radical mechanism. The results also show without presence of formate Tc(VII) participates in some reactions resulting catalytic role for H_2 production.

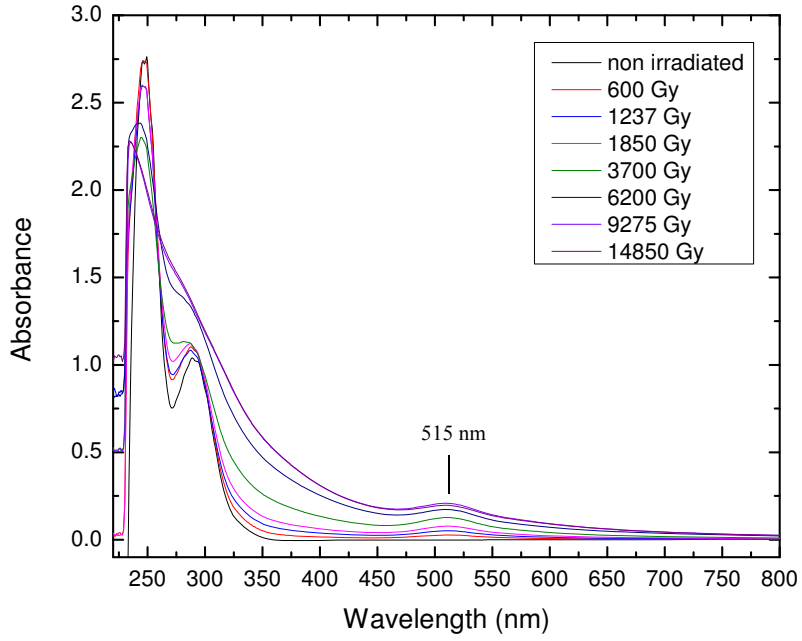

Figure V.14: *UV-Vis spectra of He^{2+} radiolysis of [Tc(VII)] = of 5 × 10^{-4} mol.l^{-1} in carbonate solution ([CO_3^{2-}] = 5 mol.l^{-1} and [HCO_3^-] = 0.5 mol.l^{-1}) and [CO_2^-] = 0.7 mol.l^{-1}. λ = 515 nm. D.R: 1000 $Gy.^{-1}$.*

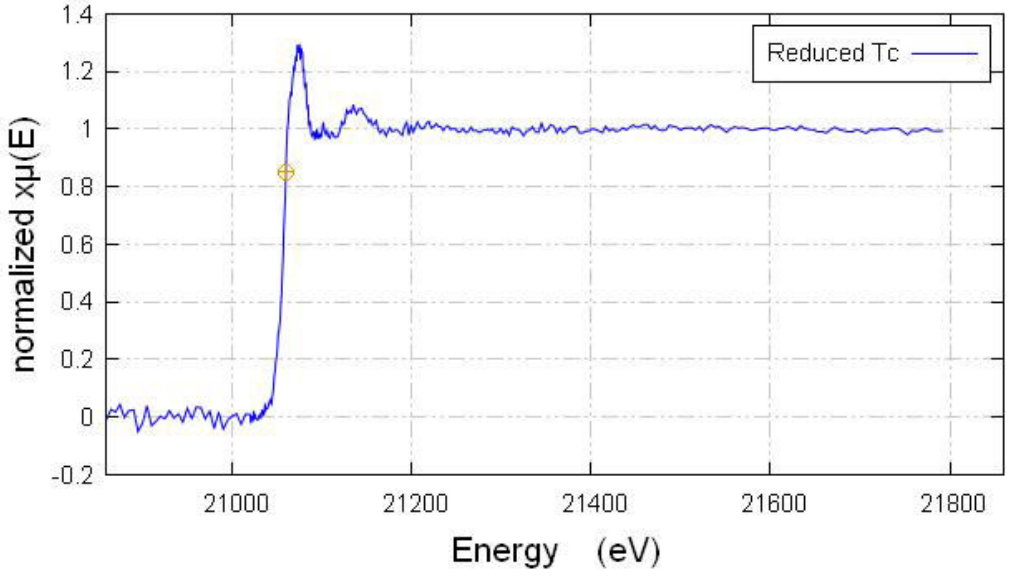

Figure V.15: *XANES spectrum of reduced technetium in carbonate solution (5 mol.l^{-1}) under He^{2+} irradiation. The spectrum shows oxidation state of +IV for reduced technetium.*

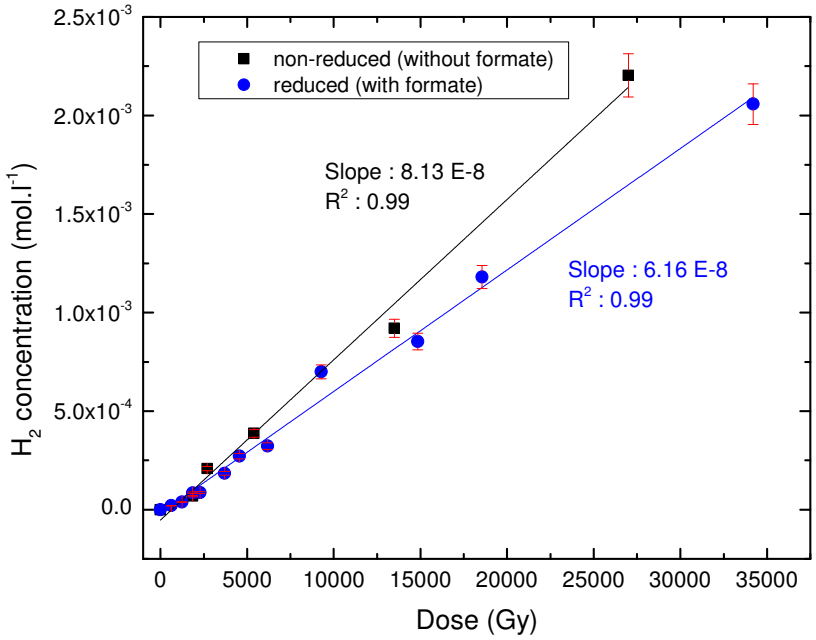

***Figure V.16**: Hydrogen concentration as a function of absorbed dose for He^{2+} radiolysis of Tc(VII) in carbonate ($[CO_3^{2-}]$ = 5 mol.l^{-1} and $[HCO_3^-]$ = 0.5 mol.l^{-1}) and $[CO_2^-]$ = 0.7 mol.l^{-1} solution. D.R: 1000 Gy.min^{-1}.*

The UV-Vis spectra of final product seems similar to the $Tc_2(\mu\text{-}O)_2$ center product obtained by electrochemistry with a nuance. Then, the same absorption coefficient is used for the obtained product by He^{2+} radiolysis at 515 nm. Figure V.17 displays the concentration of $Tc_2(\mu\text{-}O)_2$ center product as a function of absorbed dose. The $G(Tc_2(\mu\text{-}O)_2)$ values is 2.45×10^{-8} mol.J^{-1}.

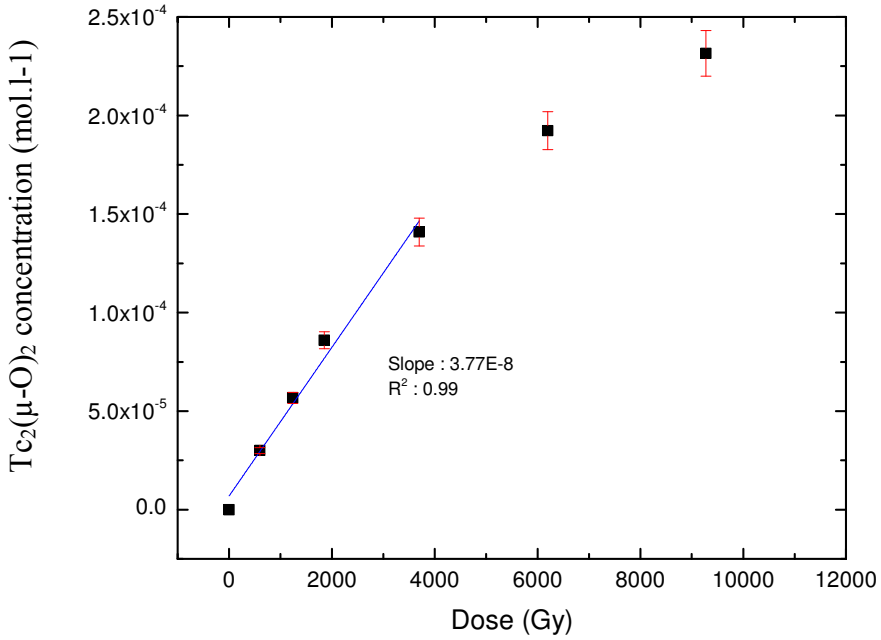

Figure V.17: *Concentration of obtained $Tc_2(\mu\text{-}O)_2$ center product by He^{2+} radiolysis as a function of dose. D.R: 1000 Gy.min^{-1}.*

EXAFS spectroscopy is carried out to determine the structure of the obtained $Tc_2(\mu\text{-}O)_2$ center product by He^{2+} radiolysis. Figure V.18 and Table V.3 show the results for the fitting step of EXAFS. The fitting results shows that the obtained complex by He^{2+} radiolysis has the same structure than the obtained complex by electrochemistry and chemical synthesis (Figure V.6) except OH groups are replaced by H_2O thus its formula is $Tc_2(\mu\text{-}O)_2(CO_3)_4(H_2O)_4$. This structural difference is due to the reduction mechanism because in radiolysis there are different types of radicals ($CO_2^{\bullet -}$, $e^-_{(aq)}$, $H^\bullet$, $CO_3^{\bullet -}$). The fitting result have shown, in contrary to obtained complex by electrochemistry and chemical method, the distance of two O atoms in μ bond are the same. Moreover, all the deduced radiolytic yields under He^{2+} irradiation are presented in Tables V.4.

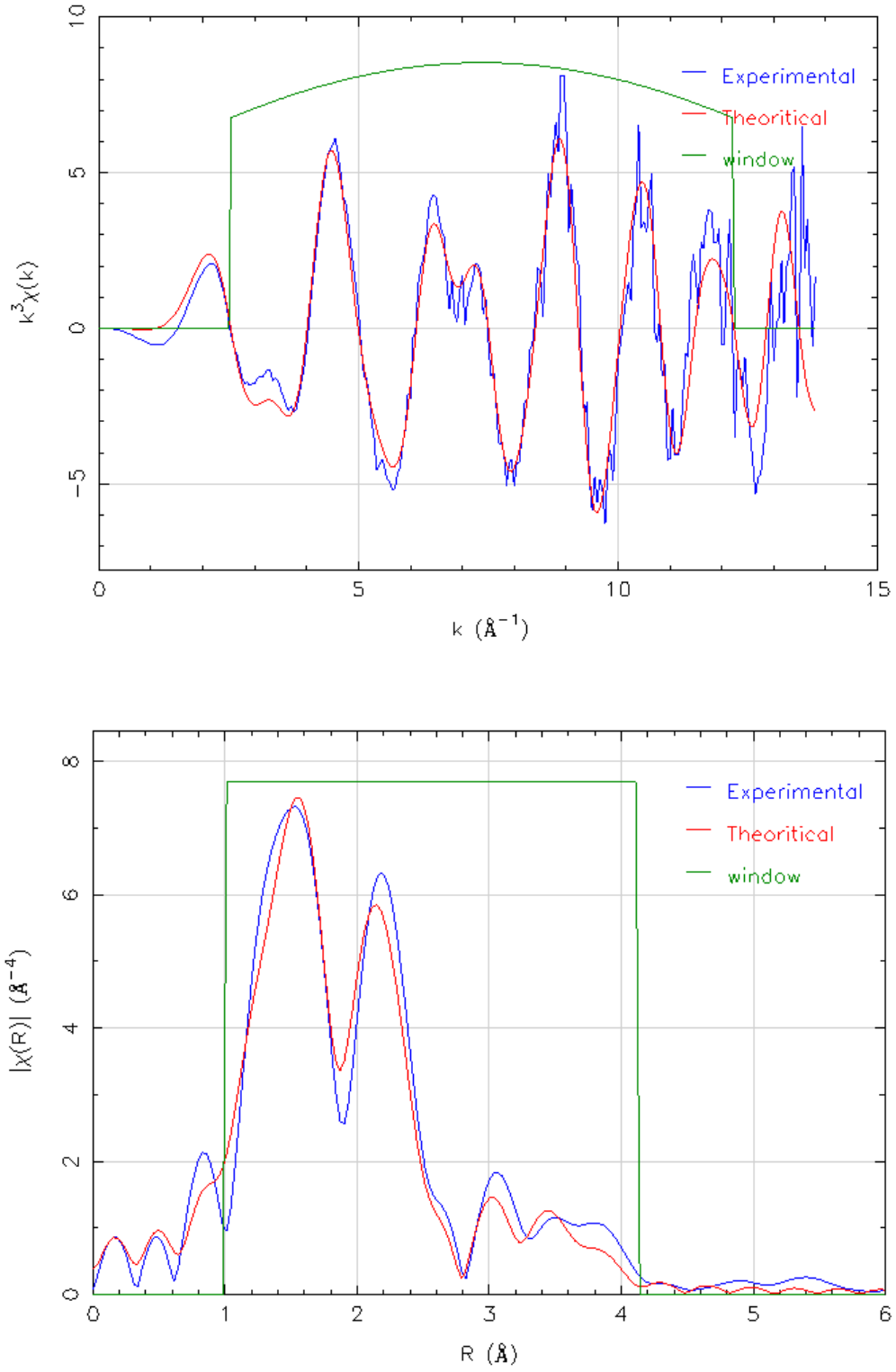

Figure V.18: *a) Fit of k^3- EXAFS spectra of Tc-Carbonate. k = 2.9-11.45 Å-1 Kaiser-Bessel (dk = 1). ΔE_0= -2.96 eV. Fit in red and Experimental data in blue, b) Fit of the Fourier Transform of the k^3- EXAFS spectra of Tc-Carbonate. R-range = 1.00-4.11 Fit in red and Experimental data in blue.*

Table V.3: *Results of fitting of experimental and theoretical EXAFS spectra of technetium carbonate complex obtained by He^{2+} radiolysis of Tc(VII) in carbonate solution*

Scattering	C.N	R (Å)	σ^2 (Å^2)
Tc-O	6	2.00	0.0067
Tc-Tc	1	2.51	0.0024
Tc-C	2	3.09	0.0062
Tc-O	10	3.94	0.0096

$S_0^2 = 1$, fit in R space, $K_w = 3$, R-factor = 0.0018 and reduced $\chi^2 = 1.47$

Table V.4: *Radiolytic yield of H_2 and Tc(IV) in* carbonate ($[CO_3^{2-}] = 5$ mol.l^{-1} and $[HCO_3^-] = 0.5$ mol.l^{-1}) and $[CO_2^-] = 0.7$ mol.l^{-1} solution *under He^{2+} irradiation. D.R: 1000 Gy.min^{-1}.*

	G(H_2)/mol.J^{-1} × 10^{-8}	
Ionizing beam	Reduced Tc(VII)	Non-Reduced Tc(VII)
He^{2+} Particle	4.0 ± 0.5	5.27 ± 0.8

	G(Tc(IV))/mol.J^{-1} × 10^{-8}
Irradiation	$[CO_2^-] = 0.7$ mol.l^{-1}
He^{2+} Particle	2.45

D. Overview of the Tc speciation under γ/He^{2+} irradiation in carbonate solution

Experimental results determined during this study can be summarized by:

- The final oxidation state of reduction of Tc(VII) in highly concentrated carbonate solutions is +IV.

- Tc(VI) and Tc(V) are not observed during the reduction thus it can be said that Tc(VII) reduced directly to Tc(IV).
- Concerning the radiolytic yield of H_2, the $G(H_2)$ in He^{2+} radiolysis is higher than in γ radiolysis. Moreover non-reduced technetium and also rhenium show catalytic reactions activity for hydrogen production in concentrated carbonate solutions.
- The higher concentration of formate, the faster reduction.
- Finally EXAFS reveals the final structure of $Tc_2(\mu\text{-}O)_2$ center product. There is small difference between final product of radiolysis ($Tc_2(\mu\text{-}O)_2(CO_3)_4(H_2O)_4$) and electrochemical reduction ($Tc_2(\mu\text{-}O)_2(CO_3)_4(OH)_4$).
- All the obtained radiolytic yields in this chapter are presented in Table V. 5.

Table V.5*: Obtained radiolytic yields concerning the Tc species in this study*

	$G(H_2)/mol.J^{-1} \times 10^{-8}$			
Ion Beam	Reduced Tc(VII)	Non-Reduced Tc(VII)	Re(III)	Re(VII)
γ-Ray D.R: 3 $Gy.min^{-1}$	1.46 ± 0.3	×	1.0 ± 0.3	2.9 ± 0.3
He^{2+} Particle D.R: 1000 $Gy.min^{-1}$	4.0 ± 0.5	5.27 ± 0.8	×	×

$G(Tc(IV))/mol.J^{-1} \times 10^{-8}$	
Ion Beam	$[CO_2^-] = 0.7$ $mol.l^{-1}$
He^{2+} Particle	2.45

The chapter V is devoted to the reduction of technetium in carbonate solution under irradiation. Before to carry out the radiolysis of Tc(VII), the Re(VII) was irradiated in carbonate solution and the results have shown that the rhenium cannot be reduced in carbonate solution because of its redox potential and existence of carbonate radical as a too strong oxidant. Thus, in order to be able to reduce Re(VII) in carbonate solution under irradiation, the formate (CO_2^-) is added to the solution because this ion can scavenge the

hydroxyl radical faster than carbonate; without formate the radiolysis of carbonate results a mixture of reducing and oxidant agents. The final product of reduction of Re(VII) is monomer. It was observed that also Tc(VII) cannot be reduced in carbonate solution under irradiation if the formate is not added for reduction of Tc(VII). The radiolytic yield of hydrogen of γ radiolysis is lower than He^{2+} radiolysis which indicates that reduction of Tc(VII) in carbonate solution has a radical mechanism. Moreover, the $G(H_2)$ for radiolysis of Tc(VII) measured in carbonate solution with and without formate. When the Tc(VII) is not reduced the radiolytic yield of hydrogen is higher due to the catalytic reactions. The UV-Vis spectra have shown that the Tc(VII) is reduced directly to Tc(IV). The oxidation state of final product was obtained by XANES spectroscopy. The final product has $Tc_2(\mu\text{-}O)_2$ center. This complex shows its stability toward more irradiation. The exact structure of $Tc_2(\mu\text{-}O)_2$ carbonate complex was defined by using EXAFS spectroscopy. Moreover Tc(VII) is reduced in carbonate solutions with different concentrations range between 2-5 $mol.l^{-1}$ (in this range $Tc_2(\mu\text{-}O)_2$ carbonate complex can be obtained) and the results have shown when the carbonate concentration is higher the $Tc_2(\mu\text{-}O)_2$ carbonate complex has higher resistance against re-oxidation in contact with air. Also Tc(VII) is reduced in pure concentrated formate solutions and the UV-Vis spectra have shown that the formate or formate radicals participate in speciation of technetium. The results of radiolysis of Tc(VII) in carbonate solution are compared with obtained data from electrochemical reduction of Tc(VII) in carbonate solution and chemical synthesis of $Tc_2(\mu\text{-}O)_2$ carbonate complex in chapter V.

Concerning scientific problems and lack of fundamental knowledge on chemistry of technetium, this study revealed some parts of technetium chemistry for the first time:

- The carbonate complex of Tc(IV) has dimeric form not monomeric one while before in literature it was suggested monomeric forms.
- This study shows that carbonate complex of Tc(IV) is soluble at concentration of 5×10^{-4} $mol.l^{-1}$ while in literature its solubility was suggested around 10^{-7} $mol.l^{-1}$.
- The exact structure of carbonate complex of Tc(IV) is defined in this study ($(Tc_2(\mu\text{-}O)_2(CO_3)_4(H_2O)_4)$ and $(Tc_2(\mu\text{-}O)_2(CO_3)_4(OH)_4)$).
- The absorption coefficient of carbonate complex of Tc(IV) with an absorption at 515 nm is 200 $l.mol^{-1}.cm^{-1}$.

References

1. Vanysek, P., *Electrochemical Series*. 2002, CRC Press LLC.
2. BenSaid, K., *Contribitun a l'etude des réactions d'oxydoréduction et à la speciation du technétium en milieu chloré et carbonaté*. 1999, Université de Nantes.
3. Essehli, R., et al., *H_2 production by γ and He ions water radiolysis, effect of presence TiO_2 nanoparticles.* International Journal of Hydrogen Energy, 2011. **36**(22): p. 14342-14348.
4. Lukens, W.W., et al., *Radiolysis of TcO_4^- in Alkaline, Nitrate Solutions: Reduction by NO_3^{2-}.* The Journal of Physical Chemistry A, 2001. **105**(41): p. 9611-9615.
5. Vichot, L., et al., *XAS study of technetium(IV) polymer formation in mixed sulphate/chloride media.* Radiochimica Acta, 2002. **90**: p. 575-579.
6. Sundrehagen, E., *Polymer formation and hydrolysation of 99Tc(IV).* The International Journal of Applied Radiation and Isotopes, 1979. **30**(12): p. 739-742.

General Conclusion

This work is a fundamental study and its aim is the investigation of oxidation/reduction reactions and speciation of technetium in highly concentrated carbonate solution under irradiation. γ-ray and He^{2+} radiolysis processes are applied in order to have different LET and energy particles to understand phenomena and determine the mechanisms of reactions. As the technetium is a radioelement and needs special regulation for experiments, thus the manganese and rhenium are chosen as the homologous of technetium because the redox potential of technetium is between of them. Different types of irradiation experiments where are involved: (i) He^{2+} ion beam with high energy (64 MeV), γ-ray with high dose rate (^{60}Co source) and γ-ray with low dose rate (^{137}Cs Source). Moreover, electron pico-second pulse radiolysis is carried out on carbonate solutions with different concentration to determine the formation and the decay kinetics of carbonate radical. These kinetics data are useful to propose mechanisms of oxidation/reduction reactions. The schematic of applications of different types of irradiation sources that used in this study is shown below:

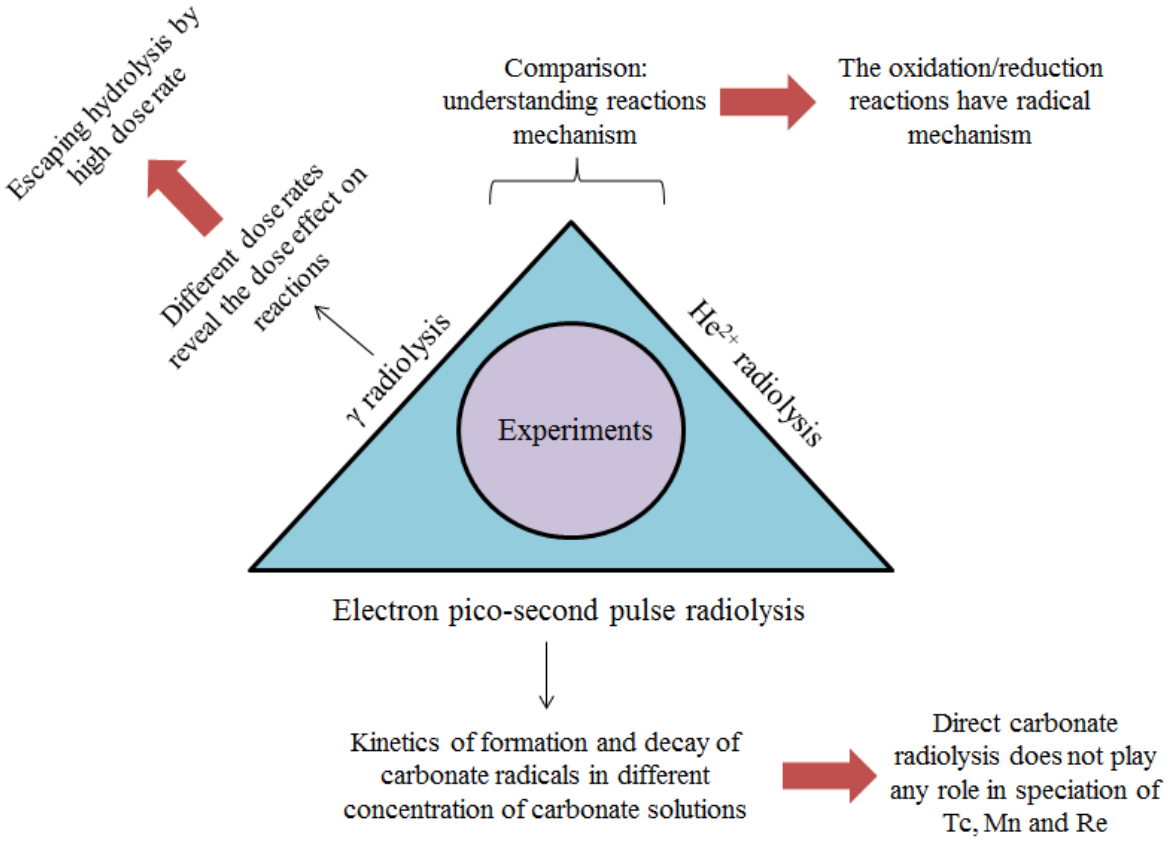

Figure VI.1*: Different types of irradiation experiments used during this study and results associated*

In the chapter I of this study, the chemistry of technetium and its impact into the nuclear waste management is described. It was well explained that technetium with a high half-life must be stabilized by changing its oxidation state and complexation reaction. Due to existence of ionizing radiation in the nuclear waste, the stabilization experiments must be studied under irradiation. Also the chemical properties of manganese are described. Moreover, the radiolysis and in particularly the radiolysis of carbonate solutions is detailed.

The chapter II described irradiation sources that used in this study. They involve γ source (^{60}Co and ^{137}Cs), ARRONAX cyclotron for He^{2+} irradiation and ELYSE for electron pico-second pulse radiolysis. A variety of analytical methods have been used during this study for qualitative and quantitative analysis. All of them are described in this chapter with their application for this study.

The chapter III presents the pulse radiolysis experiment of concentrated carbonate solutions. In literature there was only pulse radiolysis data of diluted carbonate solutions whereas this work deals with the concentrated carbonate solutions. Thus, the kinetics of formation and decay of carbonate radical in different concentrations of highly concentrated carbonate solution were investigated. To achieve this key topic, the electron pico-second pulse radiolysis in ELYSE was used. The obtained data have shown that the carbonate radical is produced through direct and indirect radiolysis in concentrated carbonate solutions. However, as the decay of carbonate radical is too fast, the obtained carbonate radical through direct effect decays with a lifetime around 2 ns. That is the reason why, it is considered that those carbonate radicals, involved in the oxidation/reduction reactions, comes from indirect effect. As a conclusion, it was determined that the direct radiolysis of carbonate has no impact on the oxidation/reduction reactions of Tc, Mn and Re. The obtained data have shown that when the radiolytic yield of carbonate radical in carbonate solution with a concentration of 5 $mol.l^{-1}$ is much higher than carbonate solutions with concentrations of 3 $mol.l^{-1}$ and 2 $mol.l^{-1}$. These results could be due to the dimerization of carbonate radical that has absorbs light in the same region but with higher absorption coefficient. The carbonate shifts the absorption band of solvated electron to 600 nm, where exactly carbonate radical absorbs light. Therefore different types of electron scavenger are tested to scavenge the solvated electron in order to obtain the spectrum of carbonate radical. Among all the electron scavengers tested, only nitrate ion (NO_3^-) is available for these experiments.

The chapter IV presents the reduction of Mn(VII) and the oxidation of Mn(II) in carbonate solution with concentration of 5 $mol.l^{-1}$. In order to obtain the best experimental conditions (carbonate and Mn concentration, atmosphere), electrochemistry was performed firstly. After calibration of the absorption band and characterization of the species by electrochemistry, the γ-ray and He^{2+} radiolysis experiments were performed. The data have shown that to prevent the synthesis of MnO_2, the concentration of carbonate should be higher than 2 $mol.l^{-1}$. So, Ar purged is used in all experiments to prevent the re-oxidation of formed species by air. The result have shown that the final products of reduction of Mn(VII) and oxidation of Mn(II) in highly concentrated carbonate solution have oxidation state of +IV. The radiolytic yield of produced H_2 was measured for both oxidation and reduction reactions. The obtained $G(H_2)$ are higher in He^{2+} radiolysis in comparison to γ radiolysis which implies the oxidation/reduction reactions presents a radical mechanism. Also it was observed that the radiolytic yield of hydrogen in oxidation reaction is higher than reduction that may imply the catalytic role of manganese in hydrogen production. The radiolytic yield hydrogen in carbonate solution in absence of manganese obtained and compared with water. The radiolytic yield of formation and decay of manganese at different oxidation states in reduction of Mn(VII) were calculated by obtained data. From these calculations the mechanism of reduction of Mn(VII) to Mn(IV) is provided in this chapter which indicates that reduction of Mn(VII) occurs through radiolysis and disproportionation. Mn(V) is a stable intermediate species and its spectrum is shown. The produced Mn(IV) can be soluble at the beginning but it precipitate due to hydrolysis and it is faster in higher dose rate radiolysis and localized radiolysis. The analytical methods revealed that the final products of both oxidation and reduction are amorphous. The obtained products through oxidation and reduction have a tetravalent oxide structure but they differ from each other by hydration. Moreover it was observed in this set-up that the manganese stabilizes at oxidation state of +IV.

The chapter V presented firstly the oxidation/reduction reactions of Re(III) and Re(VII) in highly concentrated carbonate solutions under irradiation. Rhenium is oxidized easily in carbonate solution under irradiation but due to its redox potential it cannot be reduced in presence of carbonate radical as a strong oxidant. As formate scavenge hydroxyl radical faster than carbonate thus it was added to carbonate solution in order to reduce Re(VII) in highly concentrated carbonate solution. After rhenium the reduction of Tc(VII) in highly concentrated carbonate solution by electrochemistry and under irradiation were carried out. It was observed that technetium like rhenium cannot be reduced in concentrated

carbonate solutions under irradiation due to its redox potential. Again the formate is added to carbonate solution in order to reduce Tc(VII). The final product of reduction of Tc(VII) has the oxidation state of +IV in both γ and He^{2+} radiolysis. Their oxidation state was obtained by using XANES spectroscopy. The Tc(VII) is reduced directly to Tc(IV). From measured radiolytic yield of hydrogen, it was made the evidence that non-reacting technetium plays a catalytic role for H_2 production. The final product of Tc(VII) reduction is a mixture of $Tc_2(\mu\text{-}O)_2$ center complex and TcO_2. When the reduction is faster (by higher dose rate or higher concentration of formate), the concentration of TcO_2 is higher in final product. The synthesized $Tc_2(\mu\text{-}O)_2$ center complex from He^{2+} irradiation and electrochemical reduction have the same UV-Vis spectra. The exact structure of this $Tc_2(\mu\text{-}O)_2$ center complex is defined by EXAFS spectroscopy, and it has the coordination of 6 with the formula $Tc_2(\mu\text{-}O)_2(CO_3)_4(OH)_4$. The obtained experimental EXAFS spectrum is in good agreement with obtained theoretical EXAFS spectrum from DFT simulation. The effect of formate was studied and at used concentrations it has no impact on speciation of Tc(IV) complex. Moreover the effect of carbonate concentration was investigated and it was observed that in the carbonate solutions with concentrations lower than 2 $mol.l^{-1}$, the final product of reduction is TcO_2. However, in carbonate solutions with concentrations higher than 2 $mol.l^{-1}$, the stability of $Tc_2(\mu\text{-}O)_2(CO_3)_4(OH)_4$ against re-oxidation by contacting with air has direct relation with carbonate concentration. The comparison of data from chapter III and IV with chapter V implies that manganese and rhenium are good homologous for study oxidation/reduction of technetium in highly concentrated carbonate solution under irradiation.

These obtained data from this study cannot be used only in the fundamental research. Concerning the nuclear waste, the concentration of carbonate is around 10^{-3} $mol.l^{-1}$ (maximum 10^{-2} $mol.l^{-1}$) and due to the reducing media the technetium exists as TcO_2. Concerning nuclear medicine, Tc(IV) carbonate complex can be studied for targeting of organs.

There are several perspectives concerning this study. Measuring the solubility of $Tc_2(\mu\text{-}O)_2(CO_3)_4(OH)_4$ complex. This study has shown that this complex at concentration of 5×10^{-4} $mol.l^{-1}$ is soluble but the higher concentrations must be examined. In this study a mechanism suggested for oxidation/reduction of each metal but for determination the exact mechanism of oxidation/reduction reactions of Mn, Tc and Re in highly concentrated carbonate solution under irradiation, the pulse radiolysis should be carrying out. For application in nuclear science the chemical reactivity and chemical reactions of $Tc_2(\mu\text{-}O)_2(CO_3)_4(OH)_4$ should be studied. As it was observed, the formate concentration has a high

impact on ratio of final products then, study the reduction of Tc(VII) and Re(VII) in highly concentrated carbonate solution under irradiation with a variety of formate concentration (in this study formate was used at 1 and 0.7 $mol.l^{-1}$) can be useful for the synthesize of Tc(IV) carbonate complex without TcO_2 as impurity. Carrying out EXAFS spectroscopy for structure definition of final product of reduction of Re(VII) can reveals if rhenium and technetium form the same complex and if Re can be really considered as Tc homologous. Carrying out He^{2+} pulse radiolysis on carbonate solutions in order to compare the mechanism with electron pulse radiolysis will be useful to understand the fundamental processes. Finally, the radiolysis of carbonate results species such as formate, involving in chemical speciation. Study their formation and quantifying carbonate radiolysis products such as acetate, formate and oxalate must be extensively investigated.

Appendixes

Appendix 1: Other Analytical Methods

RAMAN spectroscopy

Raman spectroscopy used in this study for investigation the oxidation state of final products of oxidation/reduction of manganese. The Raman spectra were recorded using an iHR550 spectrometer purchased from HORIBA Jobin–Yvon Company and equipped with two optical fibers with diameter of 100 μm and length of 20 m. The detector is a charged coupled device (CCD) cooled by Peltier effect (203 K). The samples were excited using a He/Ne Laser emitting a red beam at 632.8 nm with a power of 14 mW when coming out of the optical fiber. A near infra-red 100X Mitutoyo lens was used to focus the laser beam on the samples. The lens has a diameter of 24.6 mm and a working distance of 12 mm from the sample. The spectral range studied was between 100 and 900 cm^{-1}. The Raman backscattering is collected through the same objective and dispersed by 1200 groves/mm gratings to reach 5 cm^{-1} spectral resolution. The wavenumber accuracy has been checked and was better than 0.5 cm^{-1}.

FT-IR

Shimadzu Fourier Transform Infrared Spectrophotometer model FT-IR-8400 used for this study. A maximum resolution of 0.85cm-1, the FT-IR-8400 achieves the best signal-to-noise ratio in its price-class by 20,000:1 or better (peak-to-peak, 4cm-1 resolution, averaged over 1 minute). Designed with the user in mind, this instrument can be operated using an ordinary desktop or a laptop PC. Highly precise control of the moving mirror is required to stabilize the interferogram of the FT-IR instrument. The FT-IR-8400 includes the patented FJS system – very smooth and precise moving mirror unit and the dynamic alignment system to optimize and stabilize the interferometer unit. FTIR-8400S requires only a short stabilization time and is very secure.

EPR spectroscopy

For studying the oxidation states of used metals and their reactions mechanism, electron paired resonance spectroscopy (EPR) used. The Bruker EMX EPR spectrometer is a

research grade scientific instrument that used in this study. This machine is capable for routine measurments, as well as sophisticated and advanced experiments by proper accessories. The modular design makes the spectrometer easy to upgrade or expand. The characteristics of this instruments are:

- 18 bit center field resolution, corresponding to a precision of <60 mG
- 18 bit signal digitization
- Up to 128,000 points for sweep axis
- Full freedom in magnetic field sweep from 100 mG up to the maximum field
- Independent of conversion time, large and small signals can be detected at once with one gain setting
- Sequential detection of 1st and 2nd harmonic (or 0° and 90° modulation phase)
- Sensitivity up to 1200:1 (International Weak-Pitch Protocol)
- Easy upgrade to multi-frequency CW-EPR from L-band to Q-band
- Range of accessories and dedicated resonators
- Devoted Instruments

Appendix 2: Solvated Electron Spectrum

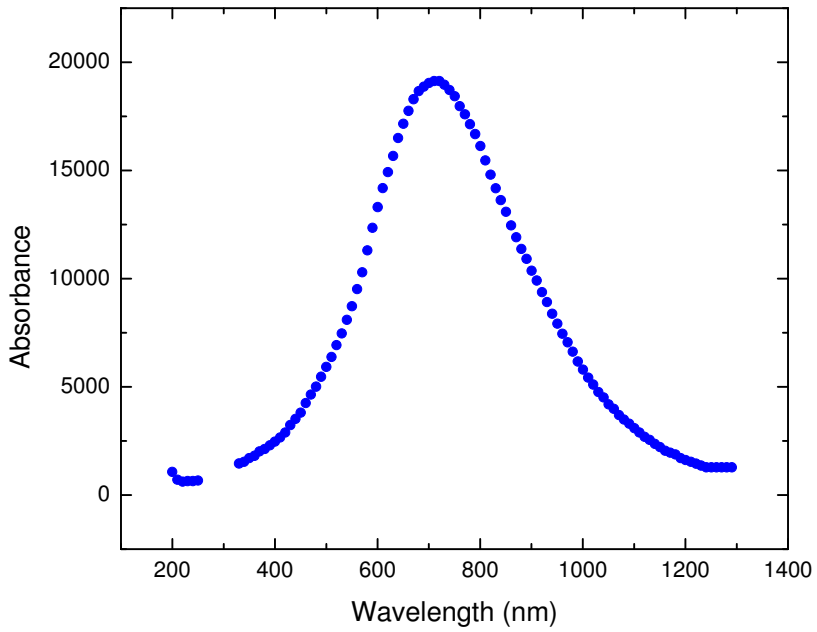

Figure App2.1: Solvated electron spectrum

In electron picosecond pulse radiolysis of carbonate solutions at each solution the concentration of solvated electron is calculated from absorption at 780 nm. By having absorption coefficient of solvated electron and using Beer-Lambert law the spectrum of solvated electron is deduced. It should be noted that the shift of solvated electron spectrum must be taken in account. Figure App.2.1 is showing the standard spectrum of solvated electron.

Appendix 3: DFT Simulation for EXAFS Spectroscopy

The suggested structures in this study were optimized by using density functional theory (DFT). The calculations were done at Institute de Physique Nucléaire d'Orsay (IPN Orsay) by Jérôme Roque. The Gaussian 09 was used as the software. To achieve appropriate representation of atomic orbitals, the double base zeta Dunning-Hazinaga (Dλ5V) was chosen for the oxygen and hydrogen atoms. In this study, we used the pseudo-potential SDS ECPs (Stuttgart / Dresden effective core potentials) for the core of the atom of Tc. The effect of solvation was partly taken into account using the polarizable continuum model CPCM (Conductor Polarized Continuum Model) implemented in the Gaussian 09 software. Optimized theoretical models are then constructed using the Moldraw software, introducing the values of the atomic coordinates of all atoms contained in a sphere radius determined around the central atom. The FEFF file obtained by Moldraw for fitting EXAFS spectra in Arthemis software. The suggested structures for DFT simulation shown below:

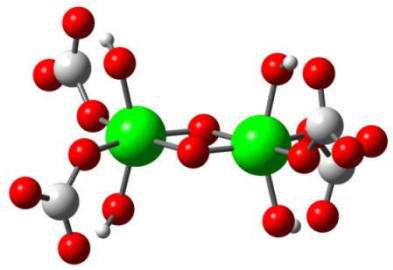	Structure n1: $(CO_3^{2-})_2$ $(OH^-)_2$ $(Tc^{4+})_2$ $(OH^-)_2$ $(CO_3^{2-})_2$
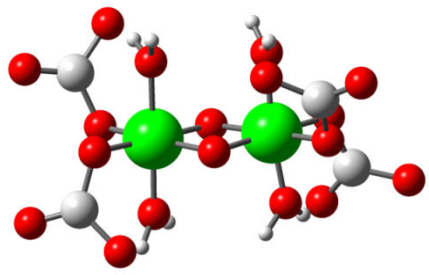	Structure n2: $(CO_3^{2-})_2(H_2O)_2(Tc^{4+})_2$ $(H_2O)_2(CO_3^{2-})_2$
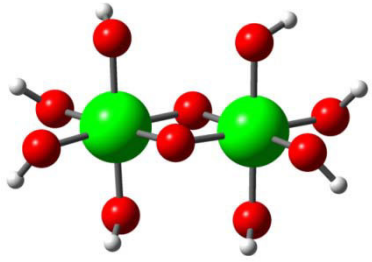	Structure n3: $(OH^-)_4$ $(Tc^{4+})_2$ $(OH^-)_4$

Thèse de Doctorat

Mohammad GHALEI

Etude de la spéciation du Tc et de ses homologues Mn et Re sous irradiation γ et He2+ en milieu carbonate hautement concentré

Study of the speciation of Tc and its homologous Mn and Re in concentrated carbonate solution under γ and He2+ irradiation

Résumé

Ce projet s'inscrit dans le cadre d'une étude fondamentale liée à l'oxydation et la réduction de ces éléments sous irradiation γ et He^{2+}. $^{+}$. Tout d'abord la technique d'électrochimie a été utilisée pour la réduction du Mn (VII) afin d'obtenir les meilleures conditions expérimentales. Car les expériences étant réalisées sous irradiation ainsi les radicaux carbonate qui sont produits par radiolyse jouent un rôle important dans les réactions. La cinétique de formation et la décroissance des radicaux carbonate dans les solutions de carbonate concentrées ont été étudiés par radiolyse pulsée β pico-seconde. Après la réduction du Mn (VII) et l'oxydation du Mn (II) dans une solution de carbonate ($[CO_3^{2-}]$ = 5 $mol.l^{-1}$) sont réalisées sous irradiation γ et He^{2+}. Par des données obtenues pour H_2 produit, les spectres UV-Vis et structure finale, les mécanismes de la réaction sont discutés. Re (III) est oxydé facilement dans une solution de carbonate concentré sous irradiation (γ et He2 +) mais Re (VII) ne peut être réduite à moins que l'addition de formiate afin d'empêcher la formation de radicaux carbonate. De la même façon, Tc (VII) ne peut être réduit dans les solutions concentrées de carbonate sous irradiation (γ et He^{2+}) sans ajout de formiate. L'état d'oxydation du produit final de la réduction de Tc(VII) a été déterminée par spectroscopie XANES et est de + IV. En outre, la structure finale du produit final a été déterminée par spectroscopie EXAFS. Le mécanisme de la réaction, le rendement radiolytique de décroissance et la formation du Tc et l'effet de concentration du carbonate sur la produit final de la réduction du Tc (VII) sous irradiation sont discutés.

Mots clés

technétium, manganèse, rhénium, carbonate, radiolyse γ et He^{2+}, radiolyse pulse β pico-second

Abstrac

This project is one part of the fundamental study and deals with the oxidation/reduction reactions and speciation of technetium and its homologous manganese and rhenium in highly concentrated carbonate solutions under γ and He^{2+} irradiation. Firstly the electrochemistry experiment is carried out for the reduction of Mn(VII) in order to obtain the best experimental conditions. As the experiments are performed under irradiation, the carbonate radicals, which are produced by radiolysis, play an important role in the reactions. The formation and decay kinetics of the carbonate radicals in concentrated carbonate solutions were studied by electron pico-second pulse radiolysis. The reduction of Mn(VII) and the oxidation of Mn(II) experiments in carbonate solution ($[CO_3^{2-}]$ = 5 $mol.l^{-1}$) are carried out under γ and He^{2+} irradiation. By the obtained data from the produced H_2, UV-Vis spectra and the final structure determination, the mechanisms of the reaction are discussed. Re(III) is oxidized easily in concentrated carbonate solution under irradiation (γ and He^{2+}) but Re(VII) cannot be reduced unless addition of formate in order to prevent carbonate radical formation. Also Tc(VII) cannot be reduced in concentrated carbonate solutions under irradiation (γ and He^{2+}) without formate addition. The oxidation state of the final product of reduction of Tc(VII) was determined by XANES spectroscopy and is +IV. Moreover, the final structure of the product was determined by EXAFS spectroscopy. The mechanisms of reaction, decay and formation radiolytic yield of Tc and also the effect of concentration of carbonate on final product of reduction of Tc(VII) under irradiation are discussed.

Key Words

technetium, manganese, rhenium, carbonate, γ and He^{2+} radiolysis, electron pico-second pulse radiolysis